DOCTORAL THESIS

Prediction of risk of an event using sensor signals, with application to the prevention of driving accidents due to drowsiness

Author: Pouyan Ebrahimbabaie
Supervisor: Professor Jacques G. Verly

A thesis submitted in partial fulfillment of the requirements for the degree of Doctor of Philosophy in Engineering Sciences

November 2020
Department of Electrical Engineering and Computer Science
Faculty of Applied Sciences
University of Liège
Liège, Belgium

Abstract

The drowsy state is an intermediate state between alert wakefulness and sleep. Drowsiness is a major cause of accidents in many areas of human activity, and transportation is probably the single most important source of drowsiness-related accidents. It is thus paramount to continuously, and in real-time, monitor the level of drowsiness (LoD) of a driver, and to devise in-car safety systems to help prevent related accidents.

For road vehicles, it is useful to distinguish between three categories of drowsiness monitoring in-vehicle systems, respectively monitoring the car behavior, the driver behavior, and the driver physiology. The systems in the last category are the only ones that can truly measure the state of drowsiness of a person. These systems are the only ones of interest in the context of this thesis.

The handful of existing drowsiness monitoring systems based on the physiology of the monitored individual generally use data acquired in a window of time that is a few (tens of) seconds long and extends up to close to the present time. This means that the LoD values produced do not correspond to the present time, but to a time in the recent past, which can be, say, 20 or 30 seconds in the past. When one realizes that it only takes two (2) seconds for a typical vehicle to leave its driving lane and possibly hit a nearby fixed or moving obstacle, one immediately realizes the interest and importance of estimating, at the present time, what the LoD will be even in a time as short as two (2) seconds in the future. Of course, it is also very useful to make LoD-related predictions farther into the future. Hence, prediction is crucial for operational, real-time drowsiness monitoring systems.

We examined the two prediction frameworks of random process (RP) models and machine learning (ML) techniques. However, we ultimately reached the conclusion that the use of RP models was more feasible to make LoD-related predictions.

Given their nature, LoD signals must be viewed as realizations of RPs. Within the context of RPs, predicting the (unknown) future values (FVs) of such signals, as well as related events, based upon data available up to close to the present time

requires one to have a model of the underlying RP. It is intuitively clear that this model will preferably need to be updated as time progresses. Of course, independently of any drowsiness monitoring system, it is also intellectually interesting to try to further understand what biological and physiological process underlie the evolution in time of LoD signals, and, more generally, of drowsiness.

The RP models that often come to mind in a wide variety of applications are the AR, MA, ARMA, and ARIMA RP models, where "AR" stands for "autoregressive", "MA" for "moving average", and "I" for "integrated". We examine the application of these conventional RP models to LoD signals, and we find that these signals can be properly modeled by AR(I)MA RP models. However, we also point out that these conventional RP models are quite heavy to deal with, and require human intervention in the process of building the RP models; it follows that they are not suitable for real-time applications.

Our search for better RP models in the context of drowsiness monitoring led us to examine the geometric Brownian motion (GBM) RP model. This RP model is frequently used in finance and led to two Nobel prizes in Economic Sciences, i.e., to Professor Paul Samuelson (MIT) in 1970, and to Professor Robert Merton and Professor Myron Scholes (Stanford and MIT) in 1997. However, the GBM RP model is generally unknown in other important domains, such as in engineering.

Using a carefully planned and executed protocol, and a validated drowsiness monitoring system, we collected discrete-time signals that represent the evolution of the LoD of 30 individuals at three progressively increasing levels of sleep deprivation over three days, thus resulting in 90 validated LoD signals.

We showed that GBM is a valid choice of RP model for modeling all 90 LoD signals, thus without a single exception. Of course, the GBM RP model corresponding to each of the 90 signals is characterized by a set of parameters specific to this signal.

We stress that a given GBM RP model can model a signal/realization with a trend that is mostly either growing, or steady-state, or decreasing (and only one such trend). The fact that the 90 signals examined are relatively short (9.2 or 14 minutes) explains why a single (i.e., fixed) GBM RP model has a chance to model them successfully. As already alluded to, for longer signals (say, of 1 or more hours), it is critical to adapt the GBM model with time. We studied the question of adaptation from several points of view, and we suggested a pragmatic approach consisting in using a sliding time window and recomputing the parameters of the model using the sample in each successive window.

Besides the modeling of LoD (and PERCLOS) signals via the GBM RP model (either fixed or adaptive), we developed in detail methods of predictions (of futures values and other statistical parameters), and we applied them to a number of the

signals available to us.

We compared the prediction accuracy of the GBM RP model with the conventional RP models. We observed that the GBM RP model provides the same accuracy as the best conventional RP models, but with a computation time reduced by a factor of 1,000.

We developed several drowsiness-prediction systems, and we considered and evaluated in detail one of them (based on the concept of survival probability).

In conclusion, the time-adaptive GBM RP model appears to be particularly well suited for modeling LoD signals and related signals such as the PERCLOS signals, and its application in drowsiness monitoring systems could lead to the development of operational systems with far greater capabilities of preventing accidents due to falling asleep at the wheel and, thus, of saving human lives.

Acknowledgments

First and foremost, I would like to express my sincere gratitude to my supervisor Prof. Jacques G. Verly for his continuous support of my PhD studies and research, for his patience, motivation, enthusiasm, and immense knowledge. His guidance helped me in my research and my personal life. I enjoyed every single second of working with him, and I could not have imagined having a better advisor. I will be forever grateful to him for having given me the opportunity to realize my thesis under his supervision.

Besides my advisor, I would like to thank the other members of my thesis committee, namely, Prof. Maarten Arnst, Dr. Clémentine François, Dr. Quentin Massoz, Prof. Jean-Michel Redoute, and Prof. Louis Wehenkel for accepting to be on the jury of this PhD thesis and for providing several valuable comments on some first drafts of this document.

I wish to thank particularly Dr. Clémentine François, for many years on our research team, for providing the level-of-drowsiness signals used in this thesis. She played a significant role in their acquisition, as part of her own PhD thesis work.

My sincere thanks goes to my friends and colleagues from the University of Liège, including, Quentin, Artem, Evgeny, Elizaveta, Marie, Sampath, Andreas, Kirill, Sude, Justinas, Yuan, Irien, and Stephan.

Last but not the least, I would like to thank my mother Nasrin, my father Houshang, and my brother Pedram, for their unconditional love and support.

Contents

List of acronyms

APA	American Psychiatric Association
AR	AutoRegressive
ARIMA	AutoRegressive Integrated Moving Average
ARMA	AutoRegressive Moving Average
ASP	Average Sleep Propensity
BJ method	Box-Jenkins method
BM	Brownian Motion
CDC	Centers for Disease Control and Prevention
CDF	Cumulative Density Function
DT	Discrete Time
ECG	ElectroCardioGram
EDS	Excessive Daytime Sleepiness
EEG	ElectroEncephaloGram
EMG	ElectroMyoGram
EOG	ElectroOculoGram
ESS	Epworth Sleepiness Scale
FHT	First Hitting Time
FIR	Finite Impulse Response
FoS	First-order Stationary

FV	Future Value
GBM	Geometric Brownian Motion
IIR	Infinite Impulse Response
IR	InfraRed
JVT	Johns Test of Vigilance
KSS	Karolinska Sleepiness Scale
LoD	Level of Drowsiness
LR	Log-Ratio
MA	Moving Average
MSLT	Multiple Sleep Latency Test
MWT	Maintenance of Wakefulness Test
NHTSA	National Highway Traffic Safety Administration
NTSB	National Transportation Safety Board
OOG	OptoOculoGraphy
OSLER	Oxford Sleep Resistance
PDF	Probability Density Function
POG	PhotoOculoGraphy
Process C	Circadian process
Process S	Homeostatic process
PSG	PolySomnoGraphy
PVT	Psychomotor Vigilance Test
Q-Q	Quantile-Quantile
RP	Random Process
RV	Random Variable

SA	Survival Analysis
SDE	Stochastic Differential Equation
SL	Sleep Latency
SoS	Second-order Stationary
SP	Survival Probability
SSS	Stanford Sleepiness Scale
ST	Sleep Threshold
SWGN	Standard White Gaussian Noise
S-W test	Shapiro-Wilk test
WN	White Noise
WP	Wiener Process
WT	Wakefulness Threshold

Chapter 1

Introduction

1.1 Context

Drowsiness is a major cause of accidents in many areas of human activity (whether personal or professional), and transportation is probably the single most important source of drowsiness-related accidents. For example, one third (1/3) of fatal accidents on highways in France are reported due to the driver falling asleep at the wheel [6].

The large number of such driving accidents is due to the combined sheer number of road vehicles and the fact that, until recently, car manufacturers and safety authorities have taken no drastic, effective actions to prevent these accidents (even though they are generally preventable). Any driver—whether healthy or suffering from some sleep pathology—may become the victim of such an accident. These accidents typically result in severe injuries, deaths, and/or loss of property.

It is thus critical to monitor a driver's level of drowsiness (LoD), and to devise in-car safety systems to help prevent drowsiness-related accidents. In 2019, the European Union (EU) Parliament adopted rules requiring life-saving technologies in vehicles. Starting in May 2022, all road vehicles sold in the EU will need to be fitted with safety systems including for drowsiness monitoring and intelligent speed assistance [44].

For road vehicles, it is useful to distinguish between three categories of in-vehicle systems for monitoring drowsiness, namely systems monitoring the car behavior (e.g., lane crossing), systems monitoring the driver behavior (e.g., steering wheel motion), and systems monitoring the driver physiology. The systems in the first category do not work when lane-separating ("white") lines are not present or are covered, e.g., by snow, and have difficulties in curving roads. The systems

in the first two categories are specific to road vehicles and not transferable to air, water, and space vehicles. The systems in the last category are the only ones that can truly measure the state of drowsiness of a person, and they are application independent and "universal". They can also be used outside the domain of transportation.

To the best of our knowledge, the handful of existing drowsiness monitoring systems based on the physiology of the monitored person use data acquired in a time window that is a few (tens of) seconds long and extends up to close to the present time. This means that the LoD values that these systems produce do not even correspond to the present time, but to a time in the recent past, which can be, say, 20 or 30 seconds in the past.

When one realizes that it only takes two (2) seconds for a vehicle moving at 96 km/h (60 mph) to leave its driving lane and possibly hit a nearby obstacle, one immediately understands the interest and importance of estimating, at the present time, what the LoD will be even in two (2) seconds [26]. Of course, it is also very useful to make LoD-related predictions farther into the future. Hence, prediction is crucial for operational, real-time drowsiness monitoring systems.

1.2 Goals of thesis

All significant drowsiness monitoring systems that reasonably claim to estimate and produce the LoD of an operator in real-time do, in fact, produce an LoD that is representative of the recent past and not of the present time. Even if this LoD did somehow correspond to the present time, it might be too late to take proper action to avoid an accident. Therefore, there is an imperative need to estimate how the LoD will evolve past the present time, and to make various types of predictions based on the past evolution of the LoD with time. These LoD-related predictions can take several forms, such as predicting future values (FVs) of the LoD, e.g., to anticipate the crossing of a reference (danger) level, or computing other quantities indicating a probability or risk of some event (happening). While this event might be "leaving the driving lane", one may wish to define other types of events that are intrinsically linked to the evolution of the LoD of a person, and not to a specific application such as driving.

The main goals of this thesis are as follows:

1. Design a system to predict, at the present time ("now"), the future evolution of the level of drowsiness (LoD) of a subject (e.g., a driver) based upon a number of "measurements" taken (in some way) from this subject, preferably

non-invasively, which means, in the present context, without having to attach sensors (such as electrodes) to the subject.

2. Design other systems to produce other types of LoD-related predictions, e.g., the probability of some event (happening) or the time until the LoD crosses a reference (danger) level.

3. Provide an interpretable mathematical model for the evolution of drowsiness in time. Indeed, being able to show that the drowsiness of a person evolves according to a particular mathematical model would be a major contribution to basic science.

One should note that the problem of predicting FVs (of a signal) based upon past and present values is an important, classical problem of signal processing. Predicting FVs is absolutely essential in a number of applications, such as the compression of audio and video signals and the prediction of future stock prices. However, such predictions have not been investigated in the field of drowsiness monitoring. The main goal of the present thesis is to provide the missing link of prediction in the domain of technologies for drowsiness monitoring.

Figure 1.1 shows a typical drowsiness monitoring system and the position of the prediction subsystem in the processing chain. This subsystem is the main object of this thesis.

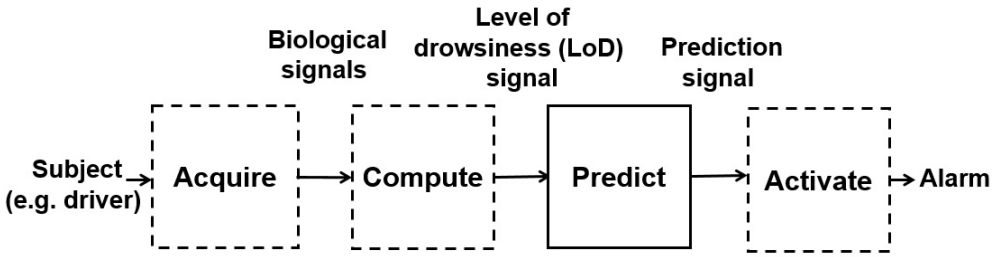

Figure 1.1: Block-diagram of a typical drowsiness monitoring system. The "predict" subsystem is the main object of this thesis.

1.3 Personal contributions

This thesis contains the following main personal contributions:

- Identify the need, in drowsiness monitoring, to make predictions related to the evolution of the level of drowsiness (LoD) in the future.

- Identify the need to have a model (of some sort) of the past evolution of this LoD to enable the making of predictions.
- Participate in the collection of data to produce LoD signals of subjects performing specific tasks.
- Identify two candidate frameworks for modeling LoD signals, namely random process (RP) models and machine learning (ML) techniques.
- Perform an intensive investigation of the applicability to LoD signals of two types of RP models, namely (1) the geometric Brownian motion (GBM) RP model and (2) conventional RP models, i.e., autoregressive (integrated) moving average (ARIMA) models.
- Discover that the GBM RP model appears to be an excellent tool to model the local evolution of LoD signals.
- Identify the need for locally adapting the RP model, and thus of the important GBM RP model.
- Push as far as possible a theoretical analysis of the question of adaptation of the GBM RP model, discover that the Îto-process model (which is more general than the GBM RP model), while going in the right direction, is not general enough for our modeling needs.
- Propose the pragmatic solution of locally adapting the GBM RP model using a sliding time window (butting against the present time) and estimating the model parameters based on the samples in this window.
- Explore ways of performing various types of predictions for RP models, both GBM and conventional.
- Get the idea of bringing in concept from survival analysis.
- Develop as much as possible three types of predictions for above RP models: future values (FVs) (of LoD signal), the first hitting time (FHT), and the survival probability (SP).
- Develop drowsiness-detection systems based on the idea of thresholding FV, FHT, or SP signal, fully develop such a system based on SP, and evaluate its performance.
- Participate in a confidential study with a Belgian company and a major car manufacturer.

- Present at several national and international conferences, and publish results in various forms.
- Obtain several patents, with some pending, on the modeling and prediction using the GBM RP model and the Îto-process model in the context of drowsiness monitoring.

The main results of this thesis were published in journals, conference proceedings, and patents. Several results were also presented at conferences. The list of our publications is given near the end of the thesis.

1.4 Brief descriptions of subsequent chapters

The topics addressed in the next ten chapters of the thesis are as follows:

- Chapter 2
  - motivates the work of the thesis by providing statistics on drowsiness-related accidents;
  - describes the tightly-coupled phenomena of sleep and drowsiness, the biological mechanism of sleep, and sleep disorders;
  - provides a clear definition of drowsiness, and explains the difference with fatigue;
  - gives the main clinical methods for characterizing drowsiness, both subjective and objective;
  - gives the main methods for characterizing drowsiness in operational settings;
  - describes the system we used to produce signals characterizing the level of drowsiness.
- Chapter 3
  - describes why prediction is absolutely necessary;
  - provides detailed information about the main frameworks to produce LoD-related predictions;
  - presents different types of LoD-related predictions;
  - explains how to select an appropriate framework to produce LoD-related predictions.

- Chapter 4
  - explains why LoD signals must be treated as realizations of an underlying RP;
  - provides the precise definition of a RP;
  - presents the conventional RP models and the geometric Brownian motion (GBM) RP model, which is the cornerstone of this thesis.
- Chapter 5
  - describes how to use conventional RP models to produce different types of predictions;
  - presents a method called the Box-Jenkins method to select an appropriate conventional RP model for a given signal;
  - addresses the main weaknesses of the Box-Jenkins method.
- Chapter 6
  - describes how to use the GBM RP model to produce different types of predictions, i.e., future values (FVs), first hitting time (FHT), and survival probability (SP);
  - presents the methodology that is typically used to determine whether the GBM RP model is a valid RP model for a given signal;
  - explains how to estimate the parameters of a GBM RP model;
  - provides a list of the advantages of the GBM RP model over conventional RP models.
- Chapter 7
  - provides an introduction to the laboratory-based experiments used in this thesis;
  - describes the general characteristics of the participants, applied protocols, measurements setup, and drowsiness monitoring system used in our experiments.
- Chapter 8
  - explains the need for adapting the RP model with time to properly handle long signals;

- emphasizes the fact that the GBM RP model can model a trend that is either growing, steady-state, or decaying (but not all at once), with the consequence that the model must be adapted to deal with long periods of time, such as for long drives;
- pushes as far possible, based upon the state of our knowledge, the theory of adaptation of the GBM RP model;
- addresses the question of whether a contiguous portion of a signal/realization that is GBM is also GBM;
- provides a pragmatic method for adapting the GBM RP model using a sliding time-window.

- Chapter 9
  - describes the modeling results obtained from the experimental data (i.e., from laboratory-based experiments);
  - illustrates the application of the methodology (presented in Chapter 6) to data obtained from laboratory-based experiments;
  - illustrates the modeling of LoD signals using the GBM RP model;
  - illustrates the modeling of LoD signals using the conventional RP models;
  - illustrates the adaptation with time of the GBM RP model.
- Chapter 10
  - illustrates the non-adaptive prediction of FVs of an LoD signal using the GBM RP model;
  - quantifies the performance of non-adaptive prediction of FVs (of a signal) using both the GBM RP model and conventional RP models, this in terms of prediction accuracy and computation speed;
  - illustrates the computation of the FHT and SP using a GBM RP model that adapts at each time step;
  - describes drowsiness-detection systems built by applying a threshold to FVs, the FHT, and the SP;
  - indicates how the detection of these systems can be characterized;
  - describes in detail a drowsiness-detection system based on SP and describes its performance in terms of ROC curves.
- Chapter 11
  - summarizes the thesis and provides a perspective for possible future researches.

1.5 Remark

Throughout the thesis, we often use the gender-neutral terms ”he”, ”him”, and ”his”, which thus include the corresponding ”she”, ”her”, and ”her”.

Chapter 2

Drowsiness: medical basis and characterization systems

This chapter describes (1) the medical basis of drowsiness and (2) systems to characterize this drowsiness. Section 2.1 provides an introduction to drowsiness and drowsiness-related accidents. Section 2.2 describes the mechanisms of sleep and drowsiness. Section 2.3 provides an overview of the clinical methods used for characterizing drowsiness. Section 2.4 describes the methods used for characterizing drowsiness in operational settings. Section 2.5 presents the system used to produce level-of-drowsiness data in our laboratory-based studies. Section 2.6 gives the basic motivation for making predictions in the context of drowsiness. Section 2.7 concludes this chapter.

2.1 Introduction

The drowsy state is an intermediate state between alert wakefulness and sleep [1, 53, 54, 55]. Drowsiness is a major cause of accidents in many areas of human activity (whether personal or professional), and transportation is probably the single most important source of drowsiness-related accidents.

According to one study in France, one third (1/3) of fatal accidents on highways are reported to be due to the driver falling asleep at the wheel [6].

Another study in the United States (US) shows that drowsy driving between 2009 and 2013 led to an estimated 21% of crashes resulting in death and to an estimated 13% of crashes causing severe injury [66].

In 2013, in the US, the "National Highway Traffic Safety Administration (NHTSA)" estimated that drowsy driving was responsible for 72,000 crashes, 44,000 injuries,

and 800 deaths [78]. However, according to the "Centers for Disease Control and Prevention (CDC)," these numbers are underestimated, and drowsiness leads to nearly 6,000 fatal crashes every year [17].

Furthermore, the risk of drowsy driving is more important for those who work during the night, e.g., police officers and firefighters. In the US, about 15% of workers, i.e., over 15 million people, work the night shift or rotating shift schedules [68].

Drowsiness in police officers has been reported "to significantly increase the number of errors, safety violations, injuries, and falling asleep while driving" [70]. According to one study in the US, "28.5% of police officers surveyed reported falling asleep while driving at least once a month" [70].

Despite the large number of drowsiness-related accidents, drowsy driving is often referred to as a preventable public health issue [68]. It is thus paramount to monitor the level of drowsiness (LoD) of a driver and to devise in-car safety systems that can help prevent often-catastrophic accidents due to drowsiness.

In the next section, we provide an overview of sleep and drowsiness, which are intertwined topics.

2.2 Sleep and drowsiness

Sleep is a biological imperative that appears to be evolutionarily preserved under the influence of the natural selection process operating across species [43]. As a consequence of the shared evolutionary history between humans and other species, sleep became a biological imperative for humans [43].

Sleep is essential for the human body to maintain good functioning and health. In fact, sleep of sufficient duration, continuity, and intensity (depth) is necessary to promote high levels of attention and cognitive performance during the wake period, and to prevent physiological changes with adverse health outcomes in general [43, 38].

The need to sleep increases with the duration of wakefulness and dissipates with time spent asleep [88]. Drowsiness is the intermediate state between (1) wakefulness and (2) sleep. In the same vein as hunger and thirst are the instincts that drive us to eat and drink, drowsiness is the instinct that drives us to sleep [38]. Therefore, drowsiness and sleep are inextricably intertwined topics.

This section comprises three subsections. The first two subsections provide a reasonably comprehensive overview of the sleep mechanism and sleep disorders, and the third subsection provides a theoretical introduction to drowsiness.

2.2.1 Sleep mechanism

It is generally agreed that our sleep-wake pattern and our alertness level during wakefulness can be explained by a two-process model. The two processes of the model are (1) the homeostatic process (denoted by S), which corresponds to the drive for sleep that increases as we stay awake and decreases when we sleep, and (2) the circadian processes (denoted by C), which corresponds to the internal oscillatory rhythm that has a period of about 24 hours and can be reset by the environmental light [33, 43].

One should note that this two-process model has probably been the most dominant model in the field of sleep over the past 30 years, in part because the concepts of the model are easy to apply to a broad range of questions in sleep research [25].

In subsequent subsections, we first introduce the homeostatic and circadian processes, and we then explain how these two processes work together.

2.2.1.1 Circadian process

The drive for sleep increases as we stay awake and decreases when we sleep. When the drive for sleep reaches a certain threshold level, it triggers sleep. This threshold level fluctuates periodically in a 24h cycle, i.e., it has circadian fluctuations. In the context of the two-process model, this fluctuating threshold level is called the sleep threshold (denoted by ST). In the same vein as the sleep threshold, the wakefulness threshold (denoted by WT) is defined as a fluctuating threshold level that triggers wakefulness. The circadian fluctuations of the sleep and wakefulness thresholds are controlled by a biological clock. This mechanism is called the circadian process or simply process C [46].

The circadian fluctuations of the sleep and wakefulness thresholds (i.e., ST and WT) are shown in Figure 2.1 [46].

The circadian process is endogenous (i.e., internally generated), and consists in self-sustaining oscillations. Therefore, the circadian process continues periodically even in the absence of periodic external time cues, such as sunlight and darkness, or sleep and wakefulness.

In humans, many other physiological processes, such as body temperature, renal and cardiac function, and hormone secretion also vary according to a circadian process [29].

The circadian process is present at all levels of biological complexity from unicellular organisms to humans. The reason for this is that the origin of life on Earth, behavior, and physiology have been shaped by the rotation of our planet around its axis. Consequently, a biological circadian timing system evolved and

enabled species to anticipate daily environmental changes rather than just reacting to them [25, 29].

2.2.1.2 Homeostatic process

The future sleep is affected by the duration of the current wakefulness. After prolonged wakefulness due, e.g., to staying up all night, there is an increase in the desire for sleep during the following day. The longer the duration of continuous wakefulness before sleep onset (i.e., the duration of sleep deprivation) is, the greater the sleep propensity is [46, 38].

In human, sleep propensity or sleep pressure caused by prolonged wakefulness is called the homeostatic process, or simply process S [46].

To illustrate the evolution with time of the level of process S, we consider three cases over two full days (Day 1, Night 1, Day 2, Night 2):

1. Baseline case: each day, subject stays awake for 16 hours (Day 1 and Day 2) and sleeps 8 hours (Night 1 and Night 2).
2. 2-h nap case: same as baseline case, except for a 2-h nap around 6 pm on Day 1.
3. Sleep deprivation case: same as baseline case, except that subject is prevented from sleeping during Night 1.

Figure 2.1 shows the evolution of the level of process S over the two full days of interest for the three above cases [25].

2.2.1.3 Two-process model

The two-process model of sleep regulation was proposed by Borbély and Dann in 1982 [9, 10]. This model is essential to understanding the relationship between the sleep-wake cycle and the biological-clock system in humans.

In the two-process model, as already described in Section 2.2.1.2, process S represents sleep homeostasis or sleep debt, which increases during waking and decreases during sleep, within a range that oscillates with a periodicity that is entrained by the circadian process (i.e., process C).

When S reaches the wakefulness threshold WT, it triggers wakefulness, and when S reaches the sleep threshold ST, it triggers sleep. The most important interactions between the two processes occur at the moments where S reaches the sleep threshold ST, transitioning from wakefulness to sleep, or the wakefulness threshold WT, transitioning from sleep to wakefulness.

A simplified representation of the two-process model of sleep regulation, for the three cases mentioned in Section 2.2.1.2 within a two-day period, is shown in Figure 2.1.

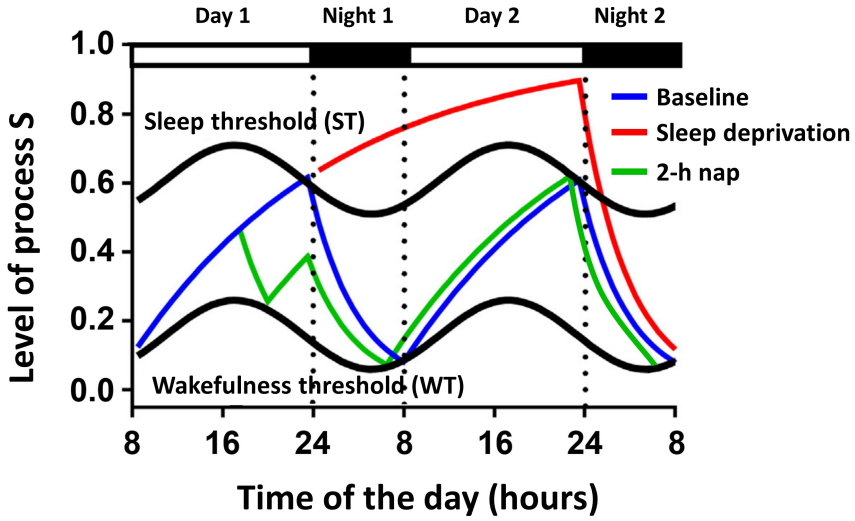

Figure 2.1: The graph shows the evolution of the level of process S as a function of time over two full days divided in four successive parts, i.e., Day 1, Night 1, Day 2, Night 2, for three cases described in the text, and respectively corresponding to the baseline, 2-h nap, and sleep deprivation cases. The circadian fluctuations of the sleep threshold (ST) and wakefulness threshold (WT) are shown over the period of interest. This figure is strongly inspired from Figure 2 in [25].

2.2.2 Sleep disorders

As already alluded to, sleep of sufficient duration, continuity, and depth is essential for the human body to maintain good functioning and good health. According to the "American Psychiatric Association (APA)", any problem associated with the quality, timing, and amount of sleep, is considered to be a sleep disorder [5]. In fact, sleep disorders can severely affect the cognitive performance of an individual during the wake period, and, consequently, his safety and quality of life. One should note that sleep disorders are linked to both physiological and emotional problems [5].

In subsequent subsections, we provide a brief introduction to some common sleep disorders.

2.2.2.1 Insomnia

Insomnia involves problems getting to sleep or staying asleep. According to the APA, insomnia is the most common sleep disorder. Indeed, roughly one-third of adults report some symptoms of insomnia. Furthermore, an estimated 40-50 percent of individuals with insomnia also suffer from some other mental disorders [5].

Problems in getting to sleep are more common among young adults and problems in staying asleep are more common among middle-age and older adults. Some common treatments for improving quality of sleep are as follows:

- relaxation techniques before bedtime,
- herbs and dietary supplements, and
- melatonin supplements.

2.2.2.2 Excessive Daytime Sleepiness (EDS)

A person who has excessive daytime sleepiness (EDS) feels drowsy, i.e., affected by drowsiness (as defined in upcoming Section 2.2.3) everyday, and this symptom often interferes with his work, study, and daily activities. Although people with this condition often complain of "fatigue" and of a general lack of energy, EDS is different from fatigue, which is characterized by low energy and the need to rest but not necessarily to sleep. EDS is also different from depression. Indeed, a person suffering from depression may have a reduced desire to do normal activities, even the ones he used to like [23, 38].

EDS is a common sleep disorder. Indeed, about 20% of the population can be classified as suffering from EDS.

Common causes are as follows:

- poor sleep habits,
- another sleep disorder, e.g., obstructive sleep apnea (described later),
- side effects from certain medications, and
- other underlying medical conditions.

For most people suffering from EDS, changing their sleep habits and their sleep environments improves their conditions. For some people suffering from this condition, further medical tests and/or sleep studies are required [23].

2.2.2.3 Obstructive sleep apnea

A person with obstructive sleep apnea has repeated periods of breathing problems during sleep causing snoring or pauses in breathing. This interrupted sleep causes sleepiness during daytime. Sleep apnea is diagnosed with a clinical sleep study using as polysomnography (PSG) [5].

Sleep apnea affects about 2% to 15% of middle-age adults and more than 20% of older adults. The main risk factors for sleep apnea are as follows:

- obesity,
- male gender, and
- family history of sleep apnea.

2.2.2.4 Narcolepsy

Narcolepsy is a chronic sleep disorder, the exact cause of which is unknown. It is characterized by excessive and overwhelming daytime sleepiness, even after adequate nighttime sleep. A person with narcolepsy is likely to become drowsy (as defined later in Section 2.2.3) or to fall asleep, often at inappropriate times and places. The sleep attacks may occur with or without warning, and may be irresistible [81].

Other classic symptoms of narcolepsy are as follows:

- Cataplexy: sudden episodes of loss of muscle function, where this loss may vary from slight weakness to complete body collapse.
- Sleep paralysis: temporary inability to talk or move when falling asleep or waking up, where this inability may last from a few seconds to several minutes.
- Hypnagogic hallucinations: vivid, often frightening, dream-like experiences that occur while falling asleep.

Sleep paralysis and hypnagogic hallucinations can also occur in people who do not have narcolepsy. Narcolepsy affects 0.04% of the population, but it is estimated that less than 25% of affected people are diagnosed.

Narcolepsy is often misdiagnosed as being related to depression, epilepsy, and the side effects of medications [81].

2.2.3 Drowsiness

As already indicated, drowsiness and sleep are intertwined topics. In fact, drowsiness is a physiological necessity that drives us to sleep [38].

Below, we first provide a precise definition of drowsiness, and we then clarify the major differences between drowsiness and fatigue.

2.2.3.1 Definition of drowsiness

In the context of the work described in this thesis, it is of the utmost importance to provide a precise definition of drowsiness. One of the most precise and recent definitions of drowsiness is the one proposed by Q. Massoz [72]:

> "Drowsiness is defined as the state of being drowsy, that is, having a difficulty of staying awake, a strong inclination toward falling asleep. Here follow the main characteristics of drowsiness:
>
> - it is an intermediate state between fully awake and asleep;
> - it is experienced at a continuous level that varies in time;
> - it is characterized by physiological changes, and by impairments of both cognitive performance, and psychomotor performance."

One should note that, there is confusion among such terms as "sleepiness", "drowsiness", "somnolence", and "fatigue" [55, p. 3]. In fact, the first three terms, i.e., "sleepiness", "drowsiness", and "somnolence" are synonyms and can be used interchangeably [72, 38]. But, as already indicated in Section 2.2.2.2, "fatigue" is significantly different from "drowsiness". Below, we clarify the key difference between "drowsiness" and "fatigue".

2.2.3.2 Difference between drowsiness and fatigue

Concerning "fatigue", one must distinguish physiological or muscular fatigue from psychological or mental fatigue. Here, we talk about psychological/mental fatigue.

Psychological fatigue is defined as the "subjective experience of tiredness and a disinclination to continue performing the current task" [14, 55]. Fatigue is associated with the duration of a continuous task and the available time for rest (but not necessarily for sleep).

Clearly, the two concepts, i.e., "drowsiness" and "fatigue" have arisen from different disciplines. "Fatigue" came from the psychology of work and performance, whereas "drowsiness" came from the study of sleep [55, p. 6].

In a nutshell, fatigue refers to a feeling of tiredness or exhaustion due to performing a continuous task, whereas drowsiness refers to a physiological state between alertness and sleep.

2.3 Clinical methods for characterizing drowsiness

We provide a brief introduction to the clinical methods for characterizing drowsiness. For further details about each method, one can refer to [38].

Figure 2.2 shows a hierarchy of the clinical methods. The figure shows that the clinical methods for characterizing drowsiness fall into two broad categories: (1) subjective methods, which are mainly based on questionnaires and refer to self-reported measurements, and (2) objective methods, which are mainly based either on performance measures or on physiological measures [38, 72, 55].

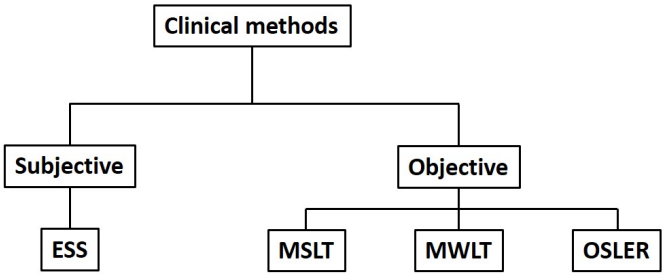

Figure 2.2: Hierarchy of clinical methods for characterizing drowsiness. This figure is strongly inspired from Figure 2.2 in [38].

We now successively describe each of the two broad categories of methods, i.e., subjective and objective methods.

2.3.1 Subjective methods

The subjective methods are mainly based on questionnaires, which evaluate the sleep propensity based on the answers of the respondent.

Below, we provide an overview of the most common subjective method to evaluate sleep propensity in a clinical setting, i.e., the Epworth Sleepiness Scale (ESS).

2.3.1.1 Epworth Sleepiness Scale (ESS)

The Epworth Sleepiness Scale (ESS) test asks the respondent to score on a 4-point scale (0-3) his usual chances of having "dozed off" or "fallen asleep" while engaged in eight different activities such as sitting and reading, watching TV, sitting and talking to someone, etc. These activities vary widely in their somnificity; e.g., a specific person falls asleep more easily when he is watching TV than when he is sitting and talking to someone [38, 56].

The total ESS score gives an estimate of "average sleep propensity (ASP)" of a person in his daily life [56].

The interpretation of the ESS scores is given in Table 2.1.

Epworth Sleepiness Scale (ESS)	
Score	Interpretation
0-5	Lower normal daytime sleepiness
6-10	Higher normal daytime sleepiness
11-12	Mild excessive daytime sleepiness
13-15	Moderate excessive daytime sleepiness
16-24	Severe excessive daytime sleepiness

Table 2.1: Interpretations of the scores of the Epworth Sleepiness Scale (ESS) [38, 56].

The ESS is highly reliable to evaluate the general (average) sleep propensity of a person. However, one should note that, since the ESS test is taken at one specific point in the time, typically in a clinical setting, the ESS score does not represent the true state of drowsiness of a person at any later time, e.g., in real-time during driving. [38, 56].

2.3.2 Objective methods

The objective methods determine the sleep propensity based either on performance measures or on physiological measures.

Below, we provide overviews of the most common objective methods to evaluate sleep propensity in a clinical setting.

2.3.2.1 Multiple Sleep Latency Test (MSLT)

The Multiple Sleep Latency Test (MSLT) is designed to measure how fast one person falls asleep in a dark and quiet environment during the day. MSLT is

a standard tool to diagnose different sleep disorders such as narcolepsy. The test relies upon the idea that the drowsier a person is, the faster this person falls asleep.

The MSLT is administrated during daytime and consists of four to five sessions, with each session called a "nap". Naps are separated by 2-h breaks. During each nap, the subject lies quietly in bed and tries to fall asleep. The test measures the time between "lights out" (with eyes closed) and the moment when the subject falls asleep. In any case, the subject is awaken after 20 minutes [38].

The mean of the measured times for all four or five naps is called the sleep latency (SL). The interpretation of SL is presented in Table 2.2.

Multiple Sleep Latency Test (MSLT)	
SL (min)	Interpretation
SL<5	Severe drowsiness
5<SL<10	Moderate drowsiness
SL>10	Normal drowsiness

Table 2.2: States of drowsiness based on the value of sleep latency (SL) [38].

The moment when the individual falls asleep is determined from polysomnography (PSG) recordings. For further details about PSG and MSLT, one can refer to [38].

2.3.2.2 Maintenance of Wakefulness Test (MWT)

The Maintenance of Wakefulness Test (MWT) is designed to measure drowsiness during the day. It is also a reliable diagnostic tool to identify EDS for legal considerations, such as reinstating a driver's license. Similar to MSLT, MWT also relies upon the idea that the drowsier a person is, the faster this person falls asleep.

The test is administrated during daytime and consists of four sessions that are separated by 2-h breaks. For each session, the subject is asked to stay awake as long as possible. Each session ends when the subject falls asleep or after 40 minutes if he does not. During the test, the subject is isolated from outside factors that can affect his ability to fall asleep, e.g., the room should be quiet and dimly lit.

The mean of the durations between the start of the session and the moment the subject falls asleep is usually called the MWT SL.

In the same way as the MSLT, the moment when the individual falls asleep is determined from polysomnography (PSG) recordings.

The MWT latencies of less than 8 minutes may indicate an underlying sleep disorder such as EDS [38].

2.3.2.3 Oxford Sleep Resistance (OSLER) test

The Oxford Sleep Resistance (OSLER) test is very similar to the Maintenance of Wakefulness Test (MWT). The fundamental difference is that the OSLER test uses performance-based parameters to determine the moment when the individual falls asleep, whereas the MWT uses EEG-based parameters.

During the test, the individual is asked to lie down and to try to stay awake. He must respond to a light stimulus by touching a button. The light stimulus consists in a LED that flashes for one second every three seconds. To determine the SL for one 40 minutes session, the test measures the time before the occurrence of 7 consecutive flashes without any response (i.e., 21 seconds) [52].

There is good correlation between the results from the OSLER test and those of the MWT [38]. For further details about the OSLER test, one can refer to [38, 52].

2.4 Methods for characterizing drowsiness in operational settings

In this section, we provide an overview of the main methods for characterizing drowsiness in real-time (aka operational methods). We divide the operational methods into two broad categories: (1) subjective methods, which are mainly based on questionnaires, interviews, or self-reports from the subject, and (2) objective methods, which are based on the direct measurement of physiological parameters of the subject or on the performance of the subject while performing a task.

Figure 2.3 shows a hierarchy of the operational methods.

2.4.1 Subjective methods

Below, we present three main subjective methods for characterizing the drowsiness of a person in an operational setting.

2.4.1.1 Karolinska Sleepiness Scale (KSS)

The Karolinska Sleepiness Scale (KSS) test measures the subjective level of drowsiness at a particular time during the day [86]. The test asks the respondent to select,

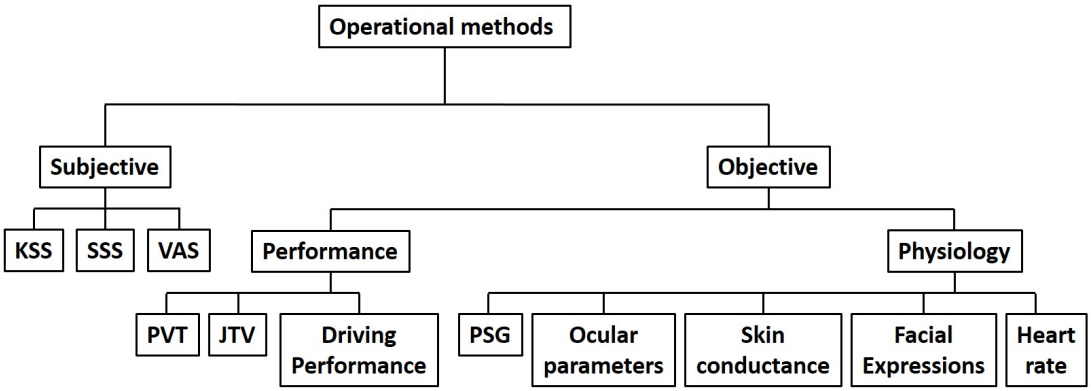

Figure 2.3: Hierarchy of operational methods for characterizing drowsiness. This figure is strongly inspired from Figure 2.3 in [38].

among nine drowsiness states (shown in Table 2.3), the one that best reflects his state of drowsiness in the last 10 minutes.

Karolinska Sleepiness Scale	
Rating	State
1	Extremely alert
2	Very alert
3	Alert
4	Rather alert
5	Neither alert nor sleepy
6	Some signs of sleepiness
7	Sleepy, but no effort to remain awake
8	Sleepy, some effort to stay awake
9	Very sleepy, great effort to stay awake, fighting sleep

Table 2.3: Nine-point Karolinska Sleepiness Scale (KSS) [86, 38].

Due to the simplicity of the test, it can be taken repeatedly without a major distraction to the respondent.

The KSS results are highly correlated with EEG features [86, 38, 57]. In part due to this correlation, the KSS is the most prevalent subjective scale in the drowsiness-related literature. However, the KSS test is not a reliable tool to diagnose sleep disorders [38].

2.4.1.2 Stanford Sleepiness Scale (SSS)

The Stanford Sleepiness Scale (SSS) is very similar to the KSS. The main difference is that SSS uses a seven-point scale for characterizing drowsiness.

The SSS drowsiness states are shown in Table 2.4.

Stanford Sleepiness Scale	
Rating	State
1	Feeling active, vital, alert, or wide awake
2	Functioning at high levels, but not at a peak; able to concentrate
3	Awake, but relaxed; responsive but not fully alert
4	Somewhat foggy, let down
5	Foggy; loosing interest in remaining awake; slowed down
6	Sleepy, woozy, fighting sleep; prefer to lie down
7	No longer fighting sleep, sleep onset soon; have dream-like thoughts

Table 2.4: Seven-point Stanford Sleepiness Scale (SSS) [38].

2.4.1.3 Visual Analog Scale (VAS)

The Visual Analog Scale (VAS) is a tool used to help a subject rate the intensity of certain sensations and feelings, such as pain, satisfaction, or drowsiness.

The VAS for drowsiness is a horizontal straight line segment with two ends, corresponding to "very alert" and "very drowsy". The subject is asked to mark a point on the scale/segment that reflects his level of drowsiness in the last few minutes. The position of the mark can then be converted into a number, e.g., from 0 to 10 [38].

2.4.2 Objective methods

Below, we provide an overview of the objective methods for charactering drowsiness in operational settings. These methods can be divided into two categories: (1) physiology-based methods, which are independent of the task performed by the subject, and (2) performance-based methods, which are dependent on this task.

2.4.2.1 Physiology-based methods

Below, we briefly introduce the five most common physiology-based methods for characterizing drowsiness in operational settings.

2.4.2.1.1 Polysomnography (PSG)

Polysomnography (PSG) is the gold standard for sleep studies. PSG simultaneously records, via the use of electrodes, several body activities such as from the brain (via the electroencephalogram (EEG)), the eye (via the electrooculogram (EOG)), the muscles (via the electromyogram (EMG)), and the cardiac activity (via the electrocardiogram (ECG)) [58, 87, 38].

PSG is considered to be the gold standard for diagnosing many different sleep disorders [87]. In addition to this, since the late 90s, PSG signals have been used to determine the state of drowsiness of an individual in "active situations" (i.e., not necessarily laying down with closed eyes) and at a given time [38].

The Karolinska Drowsiness Scale (KDS) and the Objective Sleepiness Scale (OSS) are the main PSG-based methods for characterizing drowsiness in active situations.

In the KDS, one divides PSG signals into successive windows of 20 seconds and one visually determines a (KDS) score. The KDS score for each 20-second window varies from 0 (fully alert) to 100 (very drowsy).

Similarly to the KDS, the OSS also divides PSG signals into successive windows of 20 seconds and one visually determines the scores. However, the OSS scores vary from 0 (fully alert) to 4 (very drowsy).

For further details about the KDS and OSS scoring methods, one can refer to [38].

2.4.2.1.2 Ocular parameters (OPs)

The eyes are windows into the brain [65]. The activity of the eyes and their surrounding features (such as the eyelids) are closely related to cognitive processes (such as attention, memory, and decision-making), alertness or drowsiness, and, in general, brain activity [38].

In this thesis, we use the term "ocular parameter (OP)" to denote a parameter that describes the state or dynamics of an eye and its surrounding area, including the eyelids.

To date, different OPs and their combinations have been proposed as reliable physiological markers of drowsiness [2, 27].

Among them, the PERCLOS (PERcentage of eye CLOSure) appears to have been the first OP to be widely recognized as a reliable measure for characterizing the level of drowsiness of a subject.

The PERCLOS is defined as percentage of time that the eye remains closed more than 80 (or 70) % [62, 27].

The definition of PERCLOS was established for the first time in 1994 during a driving simulator study [62, 27]. Since then, several other OPs, such as the duration of blinks and their frequency, have demonstrated promising efficiency in the characterization of drowsiness.

There are three main techniques for extracting OPs: (1) photooculography (POG), based on the acquisition and analysis of video images of the eye, (2) optooculography (OOG), based on the transmission of infrared (IR) pulses and on the analysis of the reflected signals, and (3) electrooculography (EOG), based on the measuring the corneo-retinal dipole potential of the eyeball [38].

2.4.2.1.3 Facial expressions

Several studies have explored the link between "facial expressions" and "drowsiness" [73, 77]. Recent advances in computer-vision algorithms provide the opportunity to monitor, in real-time, different drowsiness-related facial expressions, such as yawn, lip stretch, and eye blink. These facial expressions can be used for characterizing drowsiness, in real-time and non-invasively, in operational settings.

For further details about the link between facial expressions and drowsiness, one can refer to [72, 73, 77]

2.4.2.1.4 Skin conductance

The skin conductance—aka electrodermal activity (EDA)—is used to quantify the sweat gland activity and changes in the sympathetic nervous system. The EDA can be measured by two electrodes placed on the surface of the skin (typically on the palm or fingertips). Several studies propose EDA as a physiological marker of drowsiness [83, 38].

2.4.2.1.5 Heart rate (HR)

The heart rate (HR) is another physiological marker of drowsiness. One can divide the HR frequency spectrum into two parts: (1) the low-frequency (LF) part in the range of $[0.04 - 0.15]$ Hz, and (2) the high-frequency (HF) part in the range of $[0.15 - 0.4]$ Hz. Some studies have shown that the ratio of (1) the power in the LF part to (2) the power in the HF part decreases when the duration of sleep deprivation increases [24, 38].

2.4.2.2 Performance-based methods

Below, we briefly introduce the three most common performance-based methods for characterizing drowsiness in operational settings.

2.4.2.2.1 Psychomotor Vigilance Test (PVT)

The Psychomotor Vigilance Test (PVT) is a computer-based test, which relies on the assumption that drowsiness increases the reaction time (RT). The PVT is a simple, popular, and very reliable test. The PVT takes 10 minutes and, during the test, the subject is instructed to respond to a visual stimulus—which is typically a yellow counter that appears on the screen at random time intervals, between 2 and 10 seconds—by pressing a button or clicking on a mouse.

The results of the PVT are the numbers of (1) omissions, which are defined as failures to respond, and (2) lapses, which are defined as RTs greater than 0.5 sec.

Many studies have clearly shown that the results of the PVT are very sensitive to sleep deprivation [45, 59, 38].

2.4.2.2.2 Johns Test of Vigilance (JTV)

The Johns Test of Vigilance (JTV) is a modified version of the PVT. The JVT takes from 10 to 15 minutes and, during the test, the subject is instructed to respond to a visual stimulus—which is a change in the shape of an object (for example three circles, three squares, or three diamonds)—by pushing a button that the subject holds in his hands.

The results of the JVT are based on the numbers of omissions and lapses (i.e., RT greater than 2 seconds) [38].

2.4.2.2.3 Driving performance

Several studies have explored the impact of drowsiness on driving parameters [82, 50]. The term "driving parameters" refers to parameters that reflect the performance of driver while he drives.

The main drowsiness-related driving parameters are as follows [38]:

- deviation of the vehicle position on the road, aka standard deviation of the lateral position (SDLP),
- variability of the steering wheel motion, and
- speed.

2.5 System used to produce level-of-drowsiness data for later experiments

It is useful to distinguish between three categories of in-vehicle drowsiness monitoring systems. These categories respectively correspond to monitoring the car behavior (e.g. lane crossing), the driver behavior (e.g. steering wheel motion), and the driver physiology [38].

Systems in the first category do not work when lane-separating ("white") lines are not present or are covered, e.g. by snow, and have difficulties in curving roads. Systems in the first two categories are specific to road vehicles and not transferable to air, water, and space vehicles. The systems in the last category are the only ones that can truly measure the state of drowsiness of a person; they are thus application independent and "universal". These are the systems of interest in the context of this thesis.

Within the third category of drowsiness monitoring systems (i.e., physiology-based drowsiness monitoring systems), we used a POG drowsiness monitoring system to collect data.

POG systems are of two types:

- they send impulses of light to the eye and analyze the returns from it (as is the case for the glasses commercialized by Optalert from Australia), or
- they illuminate the eye and analyze images thereof (as is the case for the "drowsimeter" commercialized by Phasya from Belgium).

In our research, we used a system of the second type.

Section 7.4 describes the technical details of the system used to produce level-of-drowsiness (LoD) data in our laboratory-based studies.

2.6 Basic motivation for need for prediction

All significant PSG and POG drowsiness monitoring systems that we know of are capable of producing an LoD in real-time (of course with a small processing and computation delay) based on past data, typically in a contiguous time window with duration of a few tens of seconds (generally 20 to 60 sec) extending up to the present. Therefore, for each such window, these systems produce an LoD that is more representative of the evolution of drowsiness over the duration of this window than of the drowsiness at the present time. In fact, it is more logical to say that

the produced LoD corresponds to the center of the window, which is, say, 10 to 30 sec in the past.

Knowing that it can take only 2 sec for a road vehicle—driving at 96 km/h (60 mph) and with a 4° drift angle—to hit a nearby object, these systems are thus not able to prevent all drowsiness-related accidents [30].

Therefore, there is an imperative need to estimate how the LoD will evolve past the present time, and to make LoD-related predictions.

In the next chapter, we explain in detail why prediction is absolutely needed, and we present different types of LoD-related predictions.

2.7 Conclusion

The drowsy state is an intermediate state between alert wakefulness and sleep. Drowsiness is a significant cause of accidents in many areas of human activity (whether personal or professional), and transportation is probably the single most important source of drowsiness-related accidents.

Drowsiness and sleep are inextricably intertwined topics. It is generally agreed that a two-process model can explain our sleep-wake pattern and our alertness level during wakefulness. The first process of the model is the homeostatic process (process S), which refers to the drive for sleep that increases as we stay awake and decreases when we sleep. The second process of the model is circadian process (process C), which refers to the internal oscillatory rhythm that runs about 24 hours and can be reset by the environmental light.

Drowsiness can be characterized via different methods in both clinical and operational settings.

For road vehicles, one can distinguish between three categories of in-vehicle drowsiness monitoring systems, respectively monitoring the car behavior (e.g. lane crossing), the driver behavior (e.g. steering wheel motion), and the driver physiology.

In our research, we used a drowsiness monitoring system from the third category, i.e., a physiology-based drowsiness monitoring system, furthermore based on the images of the eye.

We briefly addressed the need for predicting the future evolution of drowsiness, a topic further developed in the next chapter.

Chapter 3

Prediction

This chapter presents the two main frameworks to produce different types of predictions. Section 3.1 explains why prediction is absolutely necessary. Section 3.2 describes the general principle of prediction. Section 3.3 presents different types of predictions. Section 3.4 describes the first prediction framework, i.e., prediction using random process (RP) models. Section 3.5 describes the second prediction framework, i.e., prediction using machine learning (ML) techniques. Section 3.6 explains why the RP models framework is appropriate for our prediction problem. Section 3.7 concludes the chapter.

3.1 Introduction

In-vehicle drowsiness monitoring systems must be able—at a minimum—to evaluate the state of drowsiness of the operator continuously and near-instantaneously (a joint feature that we refer to here as "real-time"). Indeed, in the "National Transportation Safety Board (NTSB)" hearings of 21 October 2014, David F. Dinges indicated that, at 96 km/h (60 mph), it takes only two (2) seconds for a road vehicle to get out of its driving lane, possibly hitting other vehicles in nearby lanes or objects by the roadside [26]. Figure 3.1 illustrates this scenario.

As indicated in Section 2.6, all significant drowsiness monitoring systems that reasonably claim to estimate and produce the level-of-drowsiness (LoD) of an operator in real-time do, in fact, produce an LoD that is representative of the recent past and not of the present time. Even if this LoD did somehow correspond to the present time, it might be too late to take proper action to avoid an accident. Accordingly, it is absolutely necessary to estimate how the LoD will evolve past the present time and/or to make LoD-related predictions.

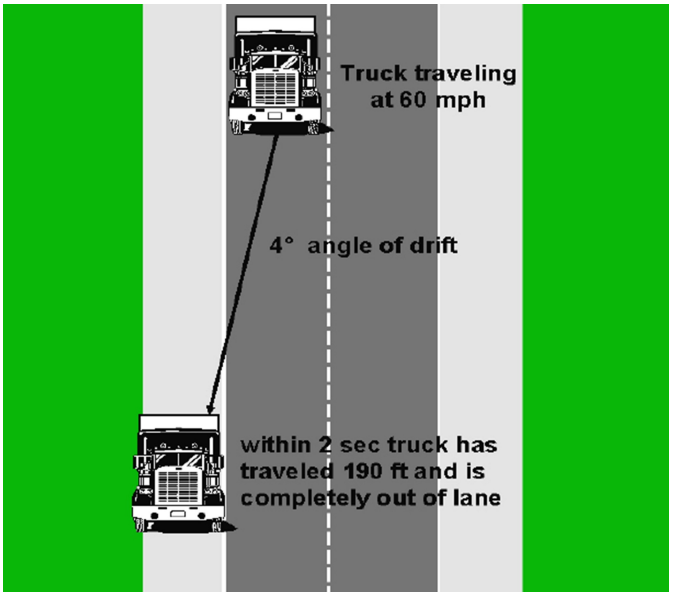

Figure 3.1: For a road vehicle, with a speed of 96 km/h (60 mph) and a drift angle of 4°, it takes only two (2) seconds to get out of its driving lane [26].

These LoD-related predictions can take several forms, such as predicting future values (FVs) of the LoD, e.g., to anticipate the crossing of a reference (danger) level, or computing other quantities indicating a probability or risk of some event (happening). While this event might be "leaving the driving lane", one may wish to define other types of events that are intrinsically linked to the LoD of a person, and not to a specific application such as driving.

In subsequent sections, we describe different types of predictions methods.

3.2 General principle of prediction in our work

Figure 3.2 provides a pictorial description of the general, common principle of all of our prediction methods for the two frameworks introduced in sections 3.4 and 3.5, i.e., for the methods based on RP models and the methods based on ML techniques.

The figure contains the graphs of two discrete-time (DT) signals (shown in the form of traditional lollipop diagrams), with their time axes aligned vertically.

The first graph shows—in a nutshell—what we call the measurement signal, often referred to simply as the signal, and denoted by x_n. Let us recall that the

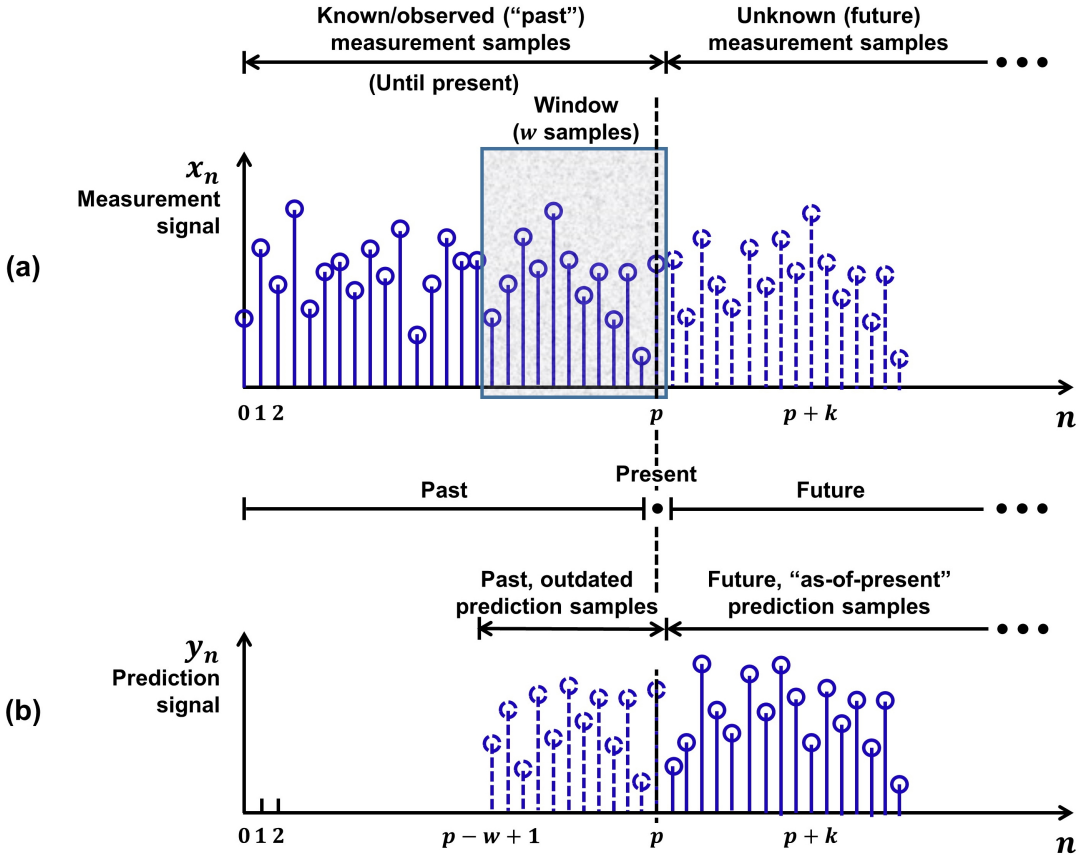

Figure 3.2: This figure illustrates the general principle of our prediction strategy. In all cases, we consider two main signals indexed by the discrete-time (DT) index n, i.e., (a) one input signal, called "measurement signal" and denoted by x_n, and (b) one output signal, called "prediction signal" and denoted by y_n. In accordance with our desire to produce, at the present time (i.e., now), predictions y_n for the future, we divide the time axis into past ($n < p$), present ($n = p$), and future ($n > p$); "past" refers to past and present. We produce/compute (values of) samples y_n in the future by using (values of) samples x_n from the past, or "past", possibly limited to a window. At each time step, the "position" of the present time p (and possible window) moves to the right by one unit. While we show all samples for both x_n and y_n, one should be aware that they only appear progressively during the experiment, i.e., as follows. For x_n, the samples are known only up to $n = p$. For y_n, at $n = p$, one can compute one or more future samples, in principle up to $+\infty$. Still for y_n, as the present time moves one step to the right, (1) all future sample will, in general, change, and (2) all past samples become frozen.

measurement signal is the signal available to us, and that one must view it as a particular realization of an underlying RP. The second graph shows what we call the prediction signal, denoted by y_n.

Both graphs are divided into three parts, i.e., the (signal) samples corresponding to the past, the present, and the future, respectively.

In examining, or working with, these graphs, it is convenient and useful to always take the present as the reference. In both graphs, the time index n corresponding to the present is denoted by p. Of course, as the wall-clock time progresses, the time index $(n =)p$ moves forward, i.e., to the right along the time axis.

For the (measurement) signal x_n, we know (i.e., have access to) the samples from the first sample at $n = 0$ until the present sample at $n = p$. Note that, whereas a DT signal varies in general from $-\infty$ to $+\infty$, we assume here that "things" start at $n = 0$. In graph (a), we refer to these samples as "known/observed ("past") measurement samples", where "past" (with quotes) means past and present.

In principle, all "past" samples, i.e., from 0 to p (or from 0 to $p - 1$) are available to us to make predictions for the future. In this regard, there are two main possibilities, i.e., we use either

1. all available samples, i.e., for $n \in [0, p]$ (or $n \in [0, p - 1]$), or
2. only the samples in a (continuous) window of adjustable width w running up to the present, i.e. for $n \in [p - w + 1, p]$ (or $n \in [p - w, p - 1]$).

Later in the thesis, we use the two possibilities above. The first possibility is attractive in a theoretical setting with few available samples, whereas the second is attractive (and almost a necessity) in a practical setting with many available samples. Looking ahead, we can already say that the use of a window allows the underlying model to adapt to the latest data, provided that the complexity of the model allows one to recompute it periodically, in the limit at each time step, i.e., from p to $p + 1$.

So far, we have introduced the "past" samples. Of course, at the present time $n = p$, the future samples of x_n are unknown. In graph (a), we refer to these samples as "unknown (future) measurement samples".

As indicated above, the present time p moves to the right in graph (a), together with the window, with wall-clock time. This means that the samples that are shown as unknown in graph (a) become, one sample at a time, known.

The above discussion can also be interpreted as follows. The measurement signal x_n extends from $-\infty$ (and, more specifically here, from 0) to $+\infty$ (and,

more realistically, to the end of the production of measurement samples). It is as though a wall-clock magician extended a curtain, attached on its right side at $+\infty$ (or, if appropriate, at the last meaningful value of n), step-by-step to the right, revealing, each time, the next so-far-unknown sample.

The above view is not far fetched. Indeed, once the experiment has ended, we have all samples "from $-\infty$ to $+\infty$", provided, of course, they have been recorded.

We point out that the application of interest to us corresponds to the case where x_n is an LoD signal. The signal x_n is either produced in a laboratory setting, or in an operational setting, typically a vehicle driving on a road.

This completes the description of the first graph and, thus, of the (measurement) signal x_n.

The second graph, i.e., graph (b) shows what we call the prediction signal. Later, we describe the main types of predictions. However, the present discussion is completely independent of the type of prediction used. In fact, one could even use several types of predictions simultaneously. We generally denote the prediction signal by y_n. (We would have denoted it by p_n, but we wish to reserve "p" for the value of n at the present time.) We now explain how this prediction is produced, at least at a very high and general level.

Using the "past" data of interest, either all samples, or the samples within the (moving) window, we assume here that we built a suitable model (based on RP models or ML techniques) and that this model allows us to carry out the desired prediction at any time beyond the present. To index a future sample we can use the index k relative to the present time, or the corresponding time index $n = p+k$, where k starts at 1 and increases up to the time $p + k$ where the last prediction should happen. One can thus write $k \in [1, k_e]$. Of course, one can also replace k_e by ∞ in some theoretical developments.

In practice, whether in a laboratory setting or in an operational setting, one can decide to consider a single k, or a few ks, or all possible ks in $[1, k_e]$ or $[1, \infty)$. Graph (b) shows a situation where we produce the desired predictions for all future time indices.

In graph (b), we refer to the past predictions as the "past, outdated prediction samples", and to the future predictions as the "future, as-of-present prediction samples". The past predictions are outdated because they have been replaced by "fresher" ones.

In regard to the last comment, it is critical to point out a major difference between the signals x_n and y_n (and, of course, their graphs). For the measurement signal, there is a single underlying x_n. Its samples appear progressively as the curtain is moved, one step at a time, to the right, by the wall-clock magician. For the prediction signal y_n, there is the possibility of changing all the future prediction

samples at each time step. Just to emphasize this point, all the "solid" lollipops in graph (b) will generally change at each time step (if one decide to compute all of them).

It is interesting to note that, for each present time p, the prediction y_p is fixed for ever, once the present time moves from p to $p+1$.

Therefore, we can use the above curtain analogy. At each time step, one can imagine the wall-clock magician moving the curtain by one step to the right, but with the curtain now attached on its left side to $-\infty$ (or to 0 if more appropriate) on the left side. In effect, this curtain now covers the prediction samples that have became frozen and dotted, effectively making them invisible.

In spite of the above discussion, the past, outdated prediction samples may have their use to evaluate the performance of the prediction system.

To conclude the analogy using the moving curtain, let us emphasize that, in graph (a), the curtain is on the right (say, attached to the ordinate axis at $+\infty$) and is progressively retracted to the right, whereas in graph (b), the curtain is on the left (attached at $-\infty$ or 0) is progressively extended also to the right.

3.3 Types of predictions

The principle of prediction described in the previous section is valid for all types of predictions presented below, and it may also apply to other types of predictions that might be imagined in the future.

In each case, it is sufficient (at least for the types that we have considered so far) to explain how, at the present time $n = p$, the value of sample of the prediction signal y_n is computed k steps later, i.e., at $n = p+k$. Said differently, for each type of prediction, we only need to explain how to compute y_{p+k} based on the model constructed above.

In this thesis, we focus on the following three types of predictions:

- Future values (FVs), i.e., $y_n \equiv \hat{x}_n$
- First hitting time (FHT)
- Survival probability (SP).

The first type of prediction (i.e., predicting FVs of signal x_n) is a straightforward concept. In contrast, the last two types of predictions (i.e., predicting the FHT and the SP) are more advanced and based upon concepts from the discipline in statistics called survival analysis (SA).

In the subsequent subsections, we first provide an overview of SA and its related concepts, and we then describe how to produce the last two types of predictions (i.e., predicting the FHT and the SP).

3.3.1 Review of key elements of survival analysis (SA)

Survival analysis (SA) is a collection of statistical methods used to address questions that have to do with whether and when an event of interest occurs [47].

Historically, the term "survival" comes from the insurance industry, in its development of methods for costing insurance premiums. The industry needed to know the average lifetime (or survival time) for each particular type of client [69].

However, most of the SA techniques have been developed and applied in relation to cancer clinical trials. In this domain, the survival time is often measured from the date of commencement of therapy until death [69].

Below, we briefly introduce the key elements of SA.

3.3.1.1 Follow-up

The term "follow-up" refers to the period of time between the beginning and the end of an experiment or study. The beginning of this period is often called the onset of follow-up. For example, it can corresponds to the beginning of a treatment.

3.3.1.2 Event

The term "event" refers to any experience that concerns, or may concern, an individual, e.g., death, graft failure, return of pain, pregnancy, and return to work.

Sometimes, we also refer to the term "event" as a "failure", because the event of interest usually is death, return of pain, or some other negative experience [60].

One should note that, in the theory of probability, an event is a well defined concept. It is a subset of the universal set (Ω), where Ω is the set that contains all possible results from an experiment.

Therefore, the term "event" used in SA has a meaning that is completely different from the term "event" used in the theory of probability.

Since SA is heavily based on the theory of probability, one should keep a clear distinction between these two drastically different uses of the term "event".

One has to be ready to encounter situations where, within the same development, the term "event" appears with both meanings.

3.3.1.3 Time to event

The time between the (1) onset of follow-up and (2) the event is called "time to event" or "survival time".

In SA, the time to event is treated as a random variable (RV). This RV is typically denoted by T, and is constrained to take only nonnegative values, i.e. $T \geqslant 0$. A background on RVs is found in [80].

3.3.1.4 Explanatory variables

The explanatory variables are the variables of interest that may affect the survival time. In the case of a person, examples of explanatory variables are the average number of cigarettes per day, the size of a tumor, the number of tumors, the age, the sex, and the dose of medication.

Each explanatory variable can remain constant in time, or vary with time, but during the follow-up, it must be known (ahead of time). In other words, each experimental variable must be a "deterministic" function of time [60].

3.3.1.5 Survival function

The survival function is a function of time denoted by $S(t)$ and defined as

$$S(t) \triangleq P(T > t) = 1 - F_T(t) = \int_t^\infty f_T(\alpha)\, d\alpha\,, \tag{3.1}$$

where $P(A)$ is the probability of the event A, in the traditional sense of the theory of probability, $F_T(t)$ is the cumulative distribution function (CDF) of RV T, and $f_T(t)$ is the probability density function (PDF) of RV T.

The survival function $S(t)$ gives, at time $t \geqslant 0$, the probability that a person survives longer than some specified time t, i.e., the probability that the RV T exceeds the specified time t [60].

The origin of time, i.e., $t = 0$ corresponds to the onset of follow-up.

The survival function $S(t)$ has the following main properties:

- it is a nonincreasing function of time;
- $S(0) = 1$, i.e., at the onset of follow-up, the survival probability is unity;
- $S(\infty) \triangleq \lim_{t\to\infty} S(t) = 0$, i.e., if the follow-up period increases without limit, ultimately nobody survives.

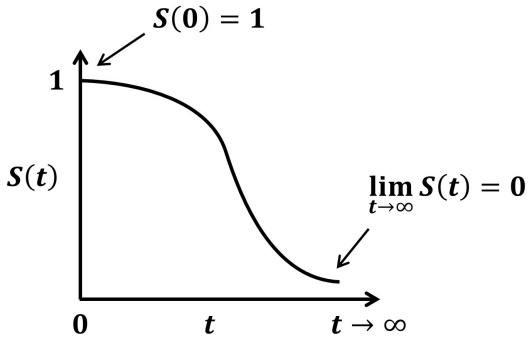

Figure 3.3: The graph shows the main properties of a typical survival function $S(t)$, i.e., $S(0) = 1$, nonincreasing, and $S(\infty) = 0$.

These properties are illustrated in Figure 3.3.

One often refers to the trace of a function $S(t)$ as a "survival curve".

Below, we use the term "population" to refer to the ensemble of persons considered in a particular study.

Survival curves often reveal valuable information about the possible effects of the explanatory variables on the population. For example, one can determine whether a treatment is effective or not by graphing, in the same system of coordinate axes, the survival curves obtained from the treatment group and the placebo group.

The typical survival curves for a treatment group and a placebo group are shown in Figure 3.4.

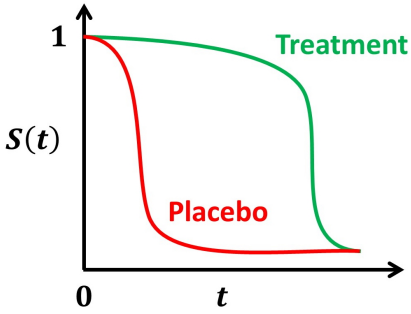

Figure 3.4: Typical survival curves for a treatment group and a placebo group.

The placebo group shows (1) a sharp drop in survival probabilities early in the follow-up and (2) a leveling-off thereafter. By contrast, the treatment group, shows (1) a very slow decrease in survival probabilities early in the follow-up and (2) a sharp drop later on.

3.3.1.6 Hazard function

The hazard function is denoted by $h(t)$ and defined as

$$h(t) = \lim_{\Delta t \to 0} \frac{P(t \leqslant T < t + \Delta t \,|\, T \geqslant t)}{\Delta t}\,, \tag{3.2}$$

where the numerator is the conditional probability that the event will occur in the interval $[t, t+\Delta t)$ given that it has not occurred before, and the denominator is the width of the interval. Dividing one by the other gives the rate of event occurrence per unit of time at time t. Taking the limit as the width of the interval goes down to zero gives the instantaneous rate of event occurrence at time t [84].

Using (3.1) and (3.2), one can show that the following relations exist between these key functions $S(t)$, $f_T(t)$, and $h(t)$ [84, 60]:

$$h(t) = \frac{f_T(t)}{S(t)}\,, \tag{3.3}$$

$$h(t) = -\frac{1}{S(t)}\frac{dS(t)}{dt}\,, \tag{3.4}$$

$$S(t) = \exp\left(-\int_0^t h(u)\,du\right)\,. \tag{3.5}$$

The last two relations show that if one knows either $S(t)$ or $h(t)$, one can get the other.

Similarly to the case of $S(t)$, one often refers to the trace of the function $h(t)$ as a "hazard curve".

The hazard curves reveal valuable information about how the risk of occurrence of an event varies with time for a particular population.

Figure 3.5 illustrates the most common shapes of hazard curves. All four illustrated hazard curves are simplified and conceptual. In all four cases, the event is death. Below, we briefly describe the situation depicted by each of the four subfigures, (a)-(d):

(a) This case corresponds to a group of healthy persons. Logically, the risk of death for any person in this group is constant with time. This translate into an $h(t)$ that is constant.

(b) This case corresponds to a group of leukemia patients not responding to treatment. Logically, the risk of death for any person in this group increases with time. This translate into an increasing $h(t)$.

(c) This case corresponds to a group of persons who are recovering from surgery. The risk of death after surgery usually decreases as the time after surgery increases. This translate into a decreasing $h(t)$.

(d) This case corresponds to a group of tuberculosis (TB) patients. Since the risk of death increases in the early stages of the sickness and then decreases, $h(t)$ first increases and then decreases.

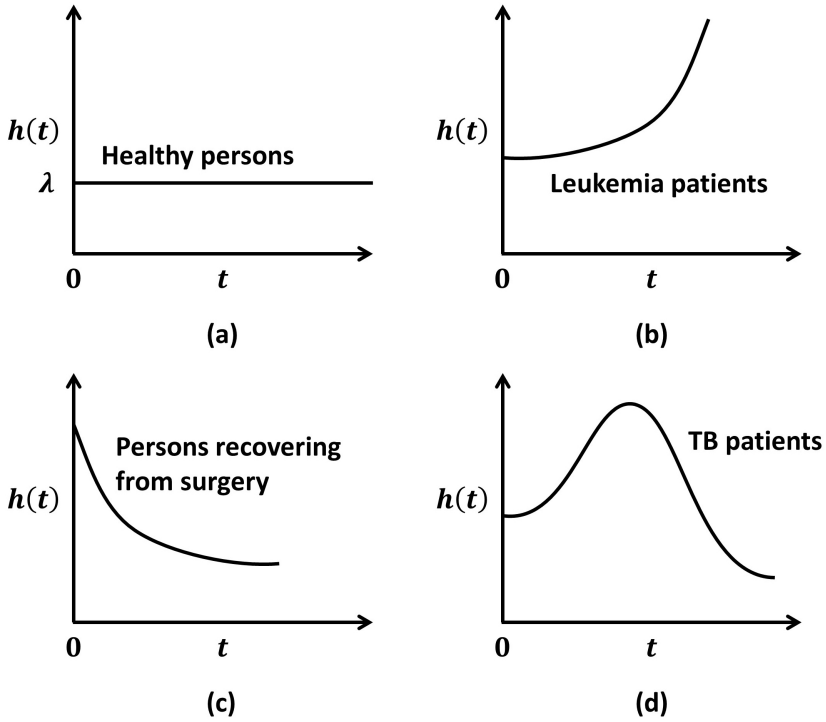

Figure 3.5: Conceptual hazard curves from different populations, i.e., (a) healthy persons, (b) leukemia patients, (c) persons recovering from surgery, and (d) tuberculosis (TB) patients [60].

3.3.1.7 Cox model

The Cox model, aka Cox proportional hazards (PH) regression model, is a regression model largely used in SA to estimate the hazard function $h(t)$ based on historical data.

The Cox model formula is given by

$$h(t, \underline{X}) = h_0(t)\, f(\underline{X})\,, \tag{3.6}$$

where $\underline{X} = (X_1, X_2, \cdots, X_p)$ is a vector of p explanatory variables, $f(\underline{X}) = \exp\left(\sum_{i=1}^{P} \beta_i X_i\right)$, and $h_0(t)$ is called the baseline hazard function.

A significant feature of the Cox model formula $h(\underline{X}, t)$ is that it is separable in t and $\underline{X}$ [60]. Indeed,

1. the baseline hazard function $h_0(t)$ only depends upon time, and
2. the function $f(\underline{X})$ depends only upon $\underline{X} = (X_1, X_2, \cdots, X_p)$.

We emphasize that $X_1, \cdots, X_p$ and, thus, $\underline{X}$ are time-independent, in contrast to $h_0(t)$.

For further details about the Cox model, one can refer to [60].

3.3.2 Casting prediction problem as a survival-analysis problem

We describe how to cast the prediction problem as an SA problem to produce two predictions of interest for us, i.e., the "first hitting time (FHT)" and the "survival probability (SP)", for a given real-valued signal.

Here—without loss of generality—we restrict our attention to DT signals.

As in all SA problems, a crucial step is to define the "event".

3.3.2.1 "Event" defined as first passage through some threshold level

For a real-valued signal, the event of interest is defined as the "first passage of the signal" through a specified threshold level.

Observe that the term "passage" is somewhat vague since it does not refer explicitly to the moment/time where this passage (or crossing) of the threshold (level) occurs.

Since the goal is to deal with the time at which the crossing occurs, it is better to talk about the "time of first passage of the signal" through the threshold.

In SA, this specific time is called the "first hitting time (FHT)". Below, we give a formal, mathematical definition of this important parameter.

Figure 3.6 shows the event for a signal x_n, and some specified threshold level α.

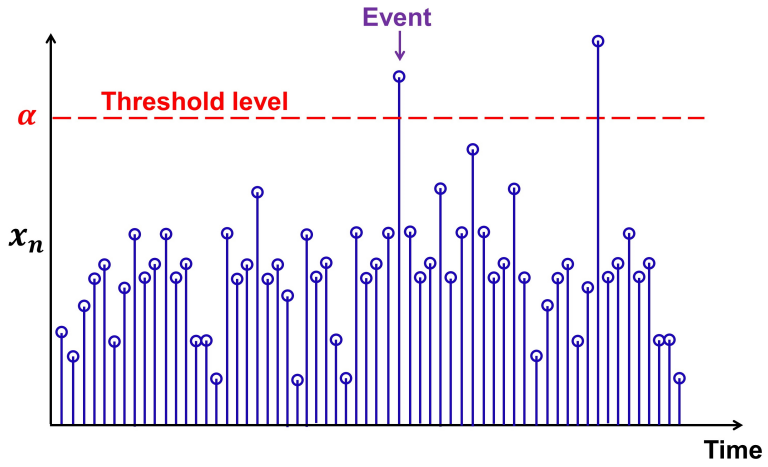

Figure 3.6: The figure illustrates the event of interest in our work, i.e., the "first passage" of the DT signal x_n through a specified threshold level α.

3.3.2.2 First hitting time (FHT)

For a real-valued signal x_n and some specified threshold level α, the first hitting time (FHT) is denoted by t_α and defined as

$$t_\alpha = (\inf \{n \geqslant 0 : x_n \geqslant \alpha\}) \, \Delta t \,, \tag{3.7}$$

where "inf" means infimum, and Δt is the sampling period.

Figure 3.7 shows the FHT t_α for a signal x_n and some specified threshold level α.

In the next two sections, we use the above concepts of event and FHT for a given signal to produce different types of predictions.

3.4 Prediction using random processes models

In this section, we first provide an overview of random processes (RP) models, and we then describe how to use RP models for the three types of predictions, i.e., predicting FVs, the FHT, and the SP.

3.4.1 Brief introduction to random processes (RPs)

Depending on the continuous or discrete nature of time, the RPs fall into one of the two broad categories of discrete-time (DT) RPs and continuous-time (CT)

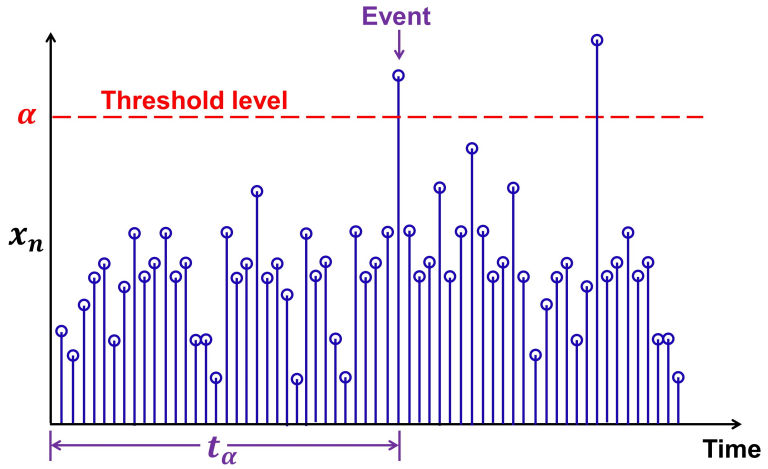

Figure 3.7: The figure illustrates the "first hitting time (FHT)", which is the time of "first passage" of a signal x_n through a specified threshold level α.

RPs.

A continuous-time (CT) random process (RP) $X_t(\omega)$ is a function of two variables, i.e., of the time $t \in [0, T]$ and of the outcome of the underlying random experiment $\omega \in \Omega$, where, $T \in \mathbb{R}$ and Ω is the set of all possible outcomes of the random experiment [19]. In probability theory, the set Ω is called the "sample space."

Consequently, the CT RP $X_t(\omega)$ is,

- for a fixed time t_0, a RV over Ω (i.e., $X_{t_0}(\omega)$, $\omega \in \Omega$), and,
- for a fixed outcome $\omega_0 \in \Omega$, a deterministic CT signal (i.e., $X_t(\omega_0)$, $t \in [0, T]$). This deterministic CT signal is called a realization of the CT RP $X_t(\omega)$.

Similarly to a CT RP, a discrete-time (DT) random process (RP) $X_n(\omega)$ is a function of two variables, i.e., of the time index $n \in \{0, 1, 2, \cdots, N-1\}$ and of the outcome of the underlying random experiment $\omega \in \Omega$, where $N \in \mathbb{N}$ and Ω is the sample space [48].

Consequently, the DT RP $X_n(\omega)$ is,

- for a fixed time index n_0, a RV over Ω (i.e., $X_{n_0}(\omega)$, $\omega \in \Omega$), and,
- for a fixed outcome $\omega_0 \in \Omega$, a deterministic DT signal (i.e., $X_n(\omega_0)$, $n \in \{0, 1, 2, \cdots, N-1\}$). This deterministic DT signal is called a realization of the DT RP $X_n(\omega)$.

Figure 3.8 illustrates the concept of a DT RP $X_n(\omega)$.

In the context of this thesis, we often omit the argument "ω", i.e., we use X_n instead of $X_n(\omega)$.

For further details about CT RPs and DT RPs, one can refer to Section 4.2.

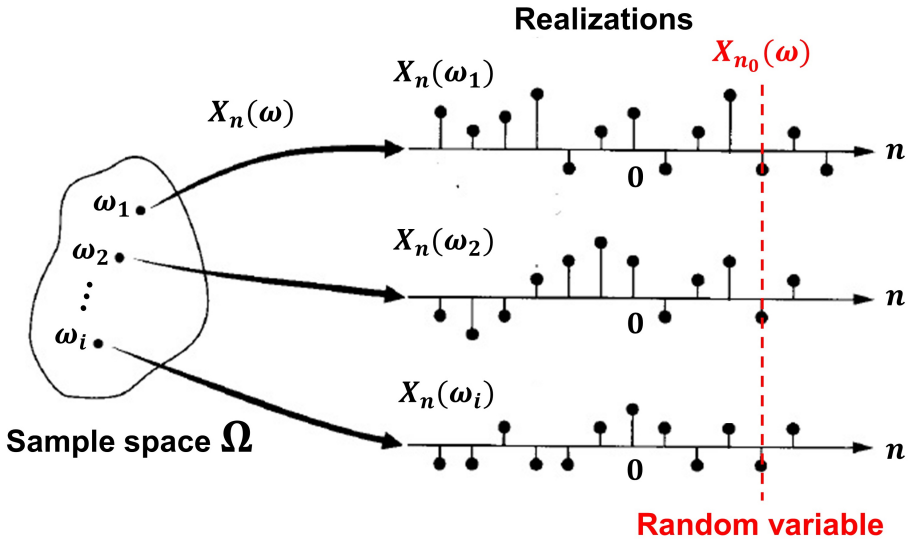

Figure 3.8: Graphical description of what a DT random process (RP) $X_n(\omega)$ is. At a fixed $\omega = \omega_1$, $X_n(\omega_1)$ is a deterministic DT signal, also called a realization, whereas, at a fixed $n = n_0$, $X_{n_0}(\omega)$ is a random variable (RV). The sample space Ω contains all possible outcomes ω of a random experiment. If a random experiment leads to an outcome ω_i, then $X_n(\omega_i)$ is the corresponding realization, i.e., deterministic DT signal. The RP $X_n(\omega)$ is simply the collection of the determinitic signals $X_n(\omega_i)$ for all possible ω_is in Ω [48].

3.4.2 Predicting future values of a signal using RP models

We address the problem of predicting FVs using RP models.

Consider the CT signal x_t shown in Figure 3.9. Suppose that we wish to predict its FVs based on its past values (aka historical values) up to the present time.

If FVs of the signal x_t can be predicted precisely from its past values, i.e., x_t is given by a closed-form formula, then the signal x_t is called a deterministic signal, and one can easily predict its FVs without any difficulty [19].

However, very often, the signals of interest for us are not deterministic. In this case, one should treat the given signal as a realization of an underlying RP, i.e.,

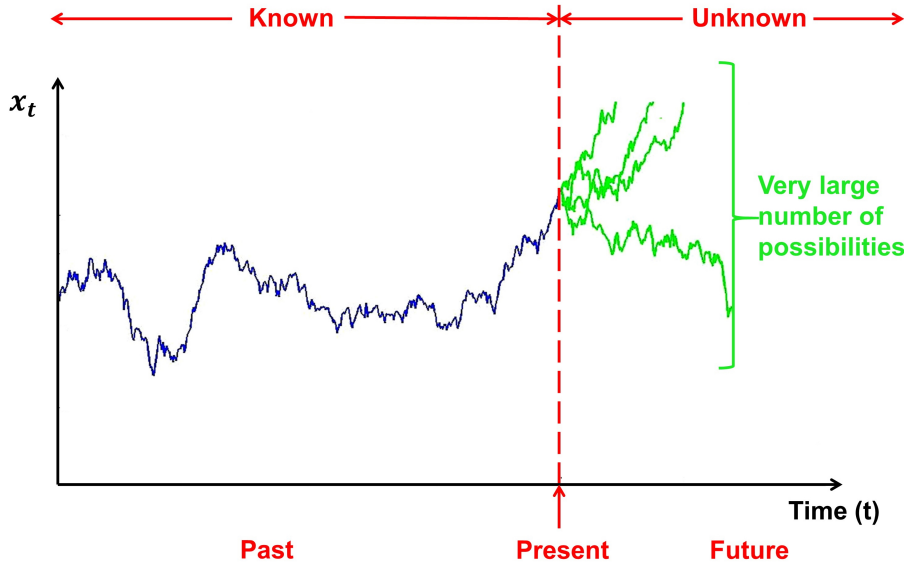

Figure 3.9: We wish to predict FVs of x_t based on its past values.

x_t must be treated as a realization of an underlying RP X_t [19].

Once one has identified an appropriate RP model for the underlying RP X_t corresponding to a given CT signal x_t, one can show that the "optimal" prediction from the present moment p, and for the forecasting horizon δt, is

$$\hat{x}_{p+\delta t} = E(X_{p+\delta t}|I)\,, \tag{3.8}$$

where $E(X)$ denotes the expected value of RV X, and I denotes all past values of x_t (which are "now" known), i.e., $I = \{x_t : t \in [0, p]\}$ [19]. Here, the term "optimal" is used in the sense that the mean square error (MSE) between the predicted value $\hat{x}_{p+\delta t}$ and the actual value $x_{p+\delta t}$ is minimized.

Similarly, once one has identified an appropriate RP model for the underlying RP X_n corresponding to a given DT signal x_n, one can show the "optimal" prediction from the present time index p, and for the forecasting horizon h is

$$\hat{x}_{p+h} = E(X_{p+h}|I)\,, \tag{3.9}$$

where I denotes all past values of x_n (which are "now" known), i.e., $I = \{x_n : n \in [0, p]\}$ [19].

In Chapter 4, we present different types of RP models, and, in Chapter 5, we describe how to select an appropriate RP model for a given signal and to predict FVs of this signal using this model.

3.4.3 Predicting "first hitting time" and "survival probability" using RP models

Once one has identified an appropriate CT RP model for the underlying RP X_t corresponding to a given CT signal x_t, one can estimate the first hitting time (FHT)—as defined in Section 3.3.2.2—for a threshold level α by

$$\hat{t}_\alpha \triangleq E(T_\alpha)\,, \tag{3.10}$$

where

$$T_\alpha \triangleq \inf\{t \geqslant 0 : X_t = \alpha\}\ . \tag{3.11}$$

It is useful to show that T_α, as defined by (3.11), is indeed a RV.

Consider the sample space Ω. For a particular outcome ω_0, the RP X_t "provides" a deterministic signal $X_t(\omega_0)$. One can then "easily" find the first instant where $X_t(\omega_0)$ crosses the threshold level α, we denote this instant by $T_\alpha(\omega_0)$.

Since the outcome ω_0 can take all values in Ω, $T_\alpha(\omega_0)$ is the realization for $\omega = \omega_0$ of some RV $T_\alpha(\omega)$ or, simply, T_α (since we indicated that one can drop the argument ω).

We thus conclude that the RHS of (3.11) indeed defines a RV.

Since T_α is a RV, it is legitimate to take its expected value on the RHS of (3.10).

In a similar way, once one identified an appropriate DT RP X_n, for a given DT signal x_n, one can estimate the FHT for a threshold level α by

$$\hat{t}_\alpha \triangleq E(T_\alpha)\,, \tag{3.12}$$

where

$$T_\alpha \triangleq (\inf\{n \geqslant 0 : X_n \geqslant \alpha\})\,\Delta t\,, \tag{3.13}$$

where Δt is the sampling period. This Δt is required to go back to "normal" wall-clock time.

Of course, the RVs defined by (3.11) and (3.13) are the time-to-event RV introduced in Section 3.3.1.3.

The survival function $S(t)$ is given by (3.1), i.e., it can be computed from the appropriate statistical characteristics of RV T_α, and in particular in terms of its CDF and PDF,

$$S(t) = P(T_\alpha > t)\,, \tag{3.14}$$

where $P(A)$ is the probability of the event A, in the traditional sense of the theory of probability.

The interpretation of $S(t)$ in (3.14) is important. Indeed, $S(t)$ gives the probability that all values of a given signal stay under the threshold level α for a duration of at least t from the onset of follow-up. This probability is often referred to as the survival probability (SP).

3.5 Prediction using machine learning techniques

Machine learning techniques—mainly neural networks (NNs)—can be used to automatically learn the temporal dependence structures for challenging prediction problems [15].

Machine learning may not be the best solution for all signal forecasting problems, but for those problems where the classical methods (i.e., prediction using RP models) fail, it can be considerd as an alternative [15].

Below, we first provide a brief introduction to machine learning, and we then present the main machine learning techniques used to produce the three types of predictions, i.e., predicting FVs, the FHT, and the SP.

3.5.1 Brief introduction to machine learning (ML)

Machine learning (ML) is a technology using algorithms that allow software applications to become more accurate in predicting outcomes without being explicitly programmed [79]. ML algorithms use historical data as input to predict new output values.

ML successfully performs many different tasks in our daily life or research areas. However, despite the success of ML in a broad range of tasks including advertising, movie recommendations, book recommendations, mortgage qualification, face recognition, forecasting, and many others, there is some mistrust about the results that ML provides [42]. Because the complex ML algorithms cannot provide insights into their behavior and internal processes, they are usually considered as uninterpretable "black boxes", which have also been shown to be easily fooled in many different conditions [42].

ML consists of many different branches and sub-branches. One of these sub-branches deals with neural networks (NNs), which is largely used to produce different types of predictions.

NNs consists of a collection of algorithms used to automatically learn arbitrary complex mapping from input to output (and, more generally, from several inputs

to several outputs).

3.5.2 Predicting future values of a signal using ML techniques

As just alluded to, NNs can be used to predict FVs of a signal. A NN can be viewed as being a non-linear system connecting a set of inputs to a set of outputs. In the context of prediction, the "output" can be the value of a signal to be forecasted and the "inputs" can be the past (i.e., lagged) values of the signal.

The connections between inputs and outputs of a NN are typically made via one or more hidden layers of connected "neurons" or "nodes", that define the structure, or architecture, of the NN. This architecture (i.e., number of neurons and hidden layers) depends on the type of variations of the signal. In general, one hidden layer is large enough for linear variations [19].

A typical NN with three inputs and one hidden layer of two neurons is shown in Figure 3.10.

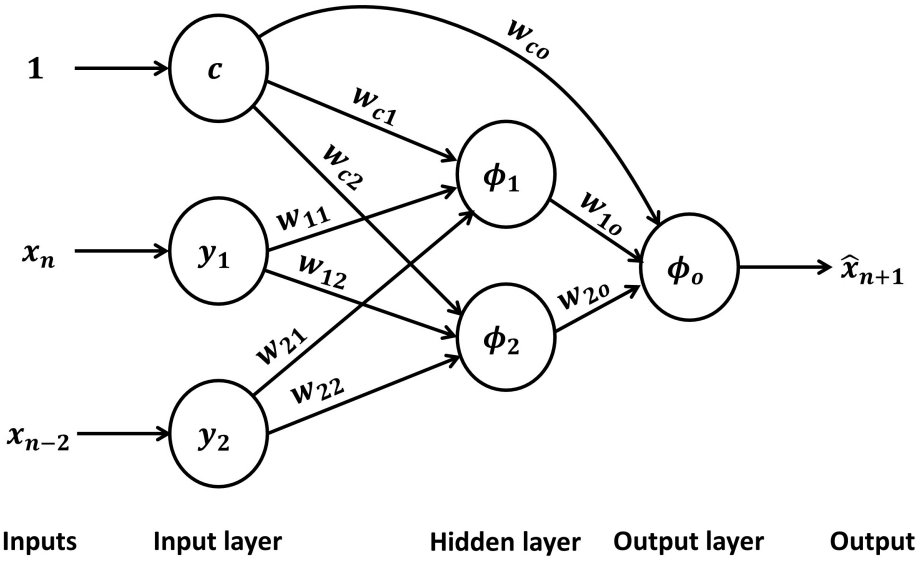

Figure 3.10: Illustrative example of a neural network (NN) with three inputs and one hidden layer of two neurons that is used to predict the next sample of a DT signal using the current and previous samples.

Here, this NN is used to predict FVs of signal x_n. We predict one step ahead ($\hat{x}_{n+1}$) based on the present value of the signal (x_n) and lagged value (x_{n-2}). In this NN, each input is connected to the two neurons of the hidden layer, and these neurons are connected to the output. There are also direct connections from

the constant input to the two neurons of the hidden layer and the output. The "strength" of each connection is called a weight (denoted by a subscripted w), which is assumed to be constant over time. Each neuron transforms the sum of the weighted inputs using a function called activation function (denoted by $\phi(\cdot)$).

The prediction equation for the illustrated network is

$$\hat{x}_{n+1} = \phi_0 \left(c\, w_{co} + \sum_{h=1}^{2} w_{ho}\, \phi_h \left(c\, w_{ch} + \sum_{i=1}^{2} w_{ih}\, y_i \right) \right) , \tag{3.15}$$

where $c = 1$, $y_1 = x_n$, $y_2 = x_{n-2}$, $\{w_{ch}\}$ denotes the weights for the connections between the constant (c) and hidden neurons, $\{w_{ih}\}$ denotes the weights for the connections between the input layer (y_1 and y_2) and hidden neurons, and $\phi_h(\cdot)$ and $\phi_o(\cdot)$ denote the activation functions used at the hidden layer and output respectively. In the context of this example, $\phi_h(\cdot)$ is the logistic function (i.e., $\phi_h(z) = 1/(1 + e^{-z})$), which gives values in the range $(0, 1)$, and $\phi_o(.)$ is a linear function [19].

We can generalize (3.15)—which corresponds to one hidden layer of 2 neurons and 3 inputs—to one hidden layer of H neurons and k inputs as

$$\hat{x}_{n+1} = \phi_0 \left(c\, w_{co} + \sum_{h=1}^{H} w_{ho}\, \phi_h \left(c\, w_{ch} + \sum_{i=1}^{k} w_{ih}\, y_i \right) \right) . \tag{3.16}$$

The weights of the NN model are estimated from the data by minimizing the sum of squares of the within-sample one-step prediction errors, i.e. $S = \sum_N (\hat{x}_{n+1} - x_{n+1})$, over a large enough portion of data. This non-linear optimization problem is not easy to solve.

Numerous algorithms and packages exist to solve the NN optimization problem. However, even the better algorithms may take several thousand of iterations to converge, and they may converge only to a local minimum. The difficulty is mainly due to (1) the large number of parameters (the weights) to estimate, and (2) the non-linear nature of the objective function [19].

For further details about signal forecasting using NNs, one can refer to [19].

Once a NN network has been built, it can be viewed as being a model. One could thus use the term "NN model" and, more generally, "ML model", which is the present counterpart of "RP model".

3.5.3 Predicting "first hitting time" and "survival probability" using ML techniques

Neural network survival analysis (NNSA) is a branch of NNs that has been used to predict the time to event and survival probability directly from the given explanatory variables [89].

One can apply NNSA to predict the FHT and the SP for a given signal if one considers the lagged values of the signal as explanatory variables.

NNSA is essentialy based on replacing the conventional Cox model (presented in Section 3.3.1.7) with a simple feed-forward NN (i.e., a NN without feedback) [34, 21].

For further details about predicting the first hitting time and survival probability using NNSA or other ML techniques, one can refer to [89].

3.6 Random process models as an appropriate framework for prediction

In Sections 3.4 and 3.5, we presented two possible prediction frameworks, i.e., "prediction using RP models" and "prediction using ML techniques" (which we can also refer to as "prediction using ML models"). At this point, it seems quite natural to ask which of these two frameworks to choose for our needs in the domain of drowsiness prediction.

In any domain, to choose among these two prediction frameworks, one should consider at least the following factors [19]:

1. goal of prediction,
2. available amount of data (aka cost),
3. accuracy of prediction (aka performance),
4. complexity,
5. expertise of analyst,
6. other relevant contextual factors.

Most of the time, researchers focus on the third factor (accuracy of prediction), while totally ignoring the other factors. However, accuracy of prediction is not always the overriding factor. A simple procedure that is only marginally less

accurate than a much more complicated one will generally be preferred in practice [19]. However, it is often challenging to convince researchers to use a simple prediction method when a complicated prediction method can also be used [4, p. 150].

Below, we describe the first four elements of the above-mentioned list.

3.6.1 Goal of prediction

In any prediction problem, the analyst must clarify the objective in producing predictions, and find out exactly how the predictions will be used. Very often, the predictions are an integral part of a planning system. This is called a system approach [19].

It is of the utmost importance for the analyst to determine whether providing predictions is sufficient or whether one also needs to be able to explain/interpret them [19].

In the context of this research, we are not only interested in producing different types LoD-related predictions, but we also wish to ultimately shed some light on the evolution of drowsiness with time by obtaining an interpretable model for the LoD. Indeed, obtaining such a model for the LoD would be a major contribution to basic science.

With regard to this factor "goal of prediction", it is clear that the framework of "prediction using RP models" is preferred over the framework of "prediction using ML techniques".

3.6.2 Available amount of data (aka cost)

The available amount of data varies greatly from one problem to another. The framework of "prediction using ML techniques" always requires a large amount of data [19].

In our work on LoD-related predictions, we have only a very limited amount of data, i.e., 90 LoD signals with a total number of 7248 samples.

Therefore, in our work, we cannot consider using the framework of "prediction using ML techniques". Consequently, the only possible framework for us is "prediction using RP models".

3.6.3 Accuracy of prediction (aka performance)

Statisticians often measure the prediction accuracy by the "prediction mean square error (PMSE)" defined by

$$PMSE = \frac{\sum_{n=1}^{m} e_n^2}{m}, \tag{3.17}$$

where m is the number of predicted samples, and e_n is the prediction error at time index n, i.e., $e_n = x_n - \hat{x}_n$.

One can find many other accuracy measures in the literature. However, most of them are based on the "mean square error (MSE)" [19].

While accuracy is an important factor to choose between the two considered frameworks, it is not the only factor. One should note that as Chatfield says, in [19], "it is not always clear how accuracy should be measured and different measures of accuracy may yield different recommendations."

Chatfield also makes an interesting remark about the prediction accuracy in his book "Time-Series Forecasting" [19, p. 163]:

> "Whichever measure of forecast accuracy is selected, the analyst will often find that the results for different forecasting methods appear to be quite similar, so that there is no clear "winner". Rather, the "best" method may be only a little better than alternatives as judged by the measure of forecast accuracy."

In the same context, he adds [19, p. 174]:

> "Whenever I see claims that one method is much better than all alternatives, I get suspicious. Close examination of the results may show that the "winner" has some unfair advantage. Alternative methods may have been implemented poorly or silly alternatives have been chosen."

Consequently, only based on the prediction accuracy, one cannot select an appropriate prediction framework.

3.6.4 Complexity

ML techniques typically require a large number of parameters to be estimated using sophisticated optimization algorithms (as described in Section 3.5.1). Therefore, the framework of "prediction using RP models" will have edge over the framework

of "prediction using ML techniques" if one finds an appropriate RP model with a small number of parameters.

3.6.5 Final choice of framework

Based on the above examination of the first four factors among the six considered in Section 3.6, we reach the following conclusions:

1. Goal of prediction: we highly favor being able to explain the predictions, so that "prediction using RP models" is preferred.
2. Available data: given the small amount on data we have in our work on drowsiness, the only solution is "prediction using RP models".
3. Accuracy of prediction: this is generally not a relevant factor.
4. Complexity: RP models with small number of parameters are best.

The above list indicates in a clear way that we should highly favor "prediction using RP models" over "prediction using ML techniques".

As a heads-up, it is appropriate to mention here the fact that the RP model that is at the core of this thesis, i.e., the geometric Brownian motion (GBM) RP model has a low number of parameters.

Therefore, at this time, the path of "prediction using RP models" seems particularly appropriate for making predictions in the domain of drowsiness monitoring.

3.7 Conclusion

All significant drowsiness monitoring systems that reasonably claim to estimate and produce the LoD of an operator in real-time do, in fact, produce an LoD that is representative of the recent past and not of the present time. In fact, even if this LoD did somehow correspond to the present time, it might be too late to take proper action to avoid an accident.

Accordingly, it is absolutely necessary to estimate how the LoD will evolve in time and to make LoD-related predictions.

In this chapter, we presented three types of predictions, i.e., predicting future values of the signal, the first hitting time, and the survival probability. We also presented two main frameworks to produce these predictions, i.e., based either on "RP models" or on "ML techniques".

We determined that, given our current knowledge and data available, among other things, the use of RP models to perform predictions in operational conditions in the field of drowsiness monitoring seems particularly appropriate.

Chapter 4

Random processes and related models

This chapter presents the conventional random process (RP) models and the geometric Brownian motion (GBM) RP model. Section 4.1 explains why the level of drowsiness (LoD) signals must be treated as realizations of an underlying RP. Section 4.2 provides precise definitions of continuous-time (CT) and discrete-time (DT) RPs. Section 4.3 provides an overview of the conventional RP models. Section 4.4 provides an overview of the GBM RP model, which is the cornerstone of this thesis. Section 4.5 concludes the chapter.

4.1 Introduction

In Section 3.6, we concluded that prediction using random process (RP) models appears to be the most appropriate framework to produce different types of LoD-related predictions. In Section 3.4.1, we indicated that the main step to produce the predictions in this framework is to identify an appropriate RP model for a given signal.

Consequently, to produce the LoD-related predictions, it is unavoidable to treat the real-life LoD signals as the realizations of an underlying RP. One of main goals of our research is to identify an appropriate RP model for LoD signals.

In this chapter, first, we provide a precise definition of a RP. Second, we introduce the conventional RP models. Third, we introduce the geometric Brownian motion (GBM) RP model, which is the cornerstone of this thesis.

4.2 Random processes (RPs)

A random process (RP) X is an indexed collection of random variables (RVs) X_i,

$$\{X_i,\, i \in I\} = \{X_i(\omega),\, i \in I,\, \omega \in \Omega\}\ , \tag{4.1}$$

over the same sample space Ω [75, p. 23].

As indicated in Section 3.4.1, a sample space is the set of all possible outcomes of a random experiment.

For further details about the concepts of sample space, RVs, and RPs, one can refer to [80].

In the context of this thesis, the index parameter i in (4.1) refers to time, but it could also refer to other quantities such as a spatial dimension in other applications.

Depending upon whether the time is considered to be discrete or continuous, a RP fall into one of two broad categories of discrete-time (DT) RPs or continuous-time (CT) RPs.

4.2.1 Discrete-time random processes (DT RPs)

A discrete-time random process (DT RP) is defined as,

$$\{X_n,\, n \in J\} = \{X_n(\omega),\, n \in J,\, \omega \in \Omega\}\ , \tag{4.2}$$

where $J = \{0, 1, 2, \cdots, N-1\}$, and $N \in \mathbb{N}$ [19, 75].

A DT RP X is a function of the two variables n and ω. For a fixed time n_0, it is a RV,

$$X_{n_0} = X_{n_0}(\omega), \quad \omega \in \Omega.$$

For a fixed outcome $\omega_0 \in \Omega$, it is a deterministic DT signal,

$$X_n = X_n(\omega_0), \quad n \in J\,.$$

This DT signal is called a realization of RP X or, equivalently, a trajectory of RP X.

In this thesis, for simplicity, the DT RP is generally denoted by X_n, i.e., $X_n \triangleq \{X_n,\, n \in J\}$.

4.2.2 Continuous-time random processes (CT RPs)

A continuous-time random process (CT RP) is defined as,

$$\{X_t,\, t \in K\} = \{X_t(\omega),\, t \in K,\, \omega \in \Omega\}\ , \tag{4.3}$$

where $K = [0, T)$ or $[0, T]$ and $T \in \mathbb{R}$ [19, 75].

A CT RP X is a function of the two variables t and ω. For a fixed time t_0, it is a RV,

$$X_{t_0} = X_{t_0}(\omega), \quad \omega \in \Omega.$$

For a fixed outcome $\omega_0 \in \Omega$, it is a deterministic CT signal,

$$X_t = X_t(\omega_0), \quad t \in K\ .$$

This CT signal is called a realization of RP X or, equivalently, a trajectory of RP X.

In this thesis, for simplicity, the CT RP is generally denoted by X_t, i.e., $X_t \triangleq \{X_t,\, t \in K\}$.

4.2.3 Remarks

In this thesis, we often need to show one or more realizations of some CT RP $X_t(\omega)$. Figure 4.1 shows how we go about showing such CT realizations.

This figure is important because, strictly speaking, it does not make any sense to show the RP X_t as a function of time.

The same remark can be made for the DT case.

In this thesis, the signals of interest, i.e., the LoD signals, are "discrete-time" (DT) and "real-valued". Therefore, we restrict our attention to real-valued DT RPs and we often—without loss of generality—develop the results for such RPs.

4.2.4 Key concepts

In this subsection, we present key concepts for RPs. Without any loss of generality, we develop the concepts only for the DT case.

4.2.4.1 Statistical moments for a single RP

Consider a DT RP X_n. We distinguish between the (statistical) moments at a single instant n and the ones at two instants n_1 and n_2.

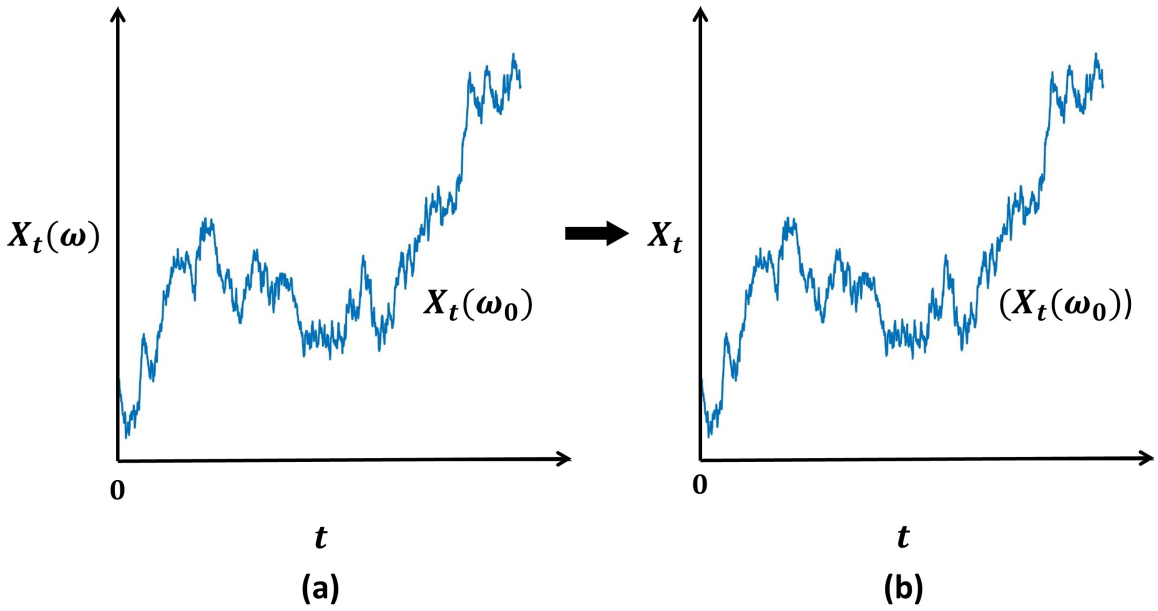

Figure 4.1: Subfigure (a) shows the correct way to represent a particular CT realization $X_t(\omega_0)$, i.e., for a specific $\omega = \omega_0 \in \Omega$, of a CT RP $X_t(\omega)$. Subfigure (b) shows a slightly simplified representation of the graph in (a), where we replace $X_t(\omega)$ on the ordinate axis by X_t, and where we may drop $X_t(\omega_0)$.

The moments at a single instant n are the mean, mean-square, and variance (of the RP X_n) [48]

$$\mu_X(n) \triangleq E[X_n]\,, \tag{4.4}$$

$$r_X^2(n) \triangleq E[|X_n|^2]\,, \tag{4.5}$$

$$\sigma_X^2(n) \triangleq E[|X_n - \mu_X(n)|^2]\,. \tag{4.6}$$

These three quantities are deterministic (1-D) sequences (or signals, or functions) of n.

One can easily show that the three quantities above obey the relation [48]

$$\sigma_X^2(n) = r_X^{(2)}(n) - |\mu_X(n)|^2\,. \tag{4.7}$$

The moments at two time instants n_1 and n_2 are the (auto)correlation (function) (of the RP X_n) [48]

$$r_X(n_1, n_2) = E[X_{n_1} X_{n_2}^*]\,, \tag{4.8}$$

the (auto)covariance (function) [48]

$$\gamma_X(n_1, n_2) = E[(X_{n_1} - \mu_X(n_1))(X_{n_2} - \mu_X(n_2))^*] \,, \tag{4.9}$$

and the (auto)correlation coefficient [48]

$$\rho_X(n_1, n_2) = \frac{\gamma_X(n_1, n_2)}{\sigma_X(n_1)\sigma_X(n_2)} \,. \tag{4.10}$$

These three quantities are deterministic (2-D) sequences (or signals, or functions) of n_1 and n_2.

One can show that the following relation holds [48],

$$\gamma_X(n_1, n_2) = r_X(n_1, n_2) - \mu_X(n_1)\mu_X^*(n_2) \,. \tag{4.11}$$

All of the above quantities can be extended to the case of two RPs X_n and Y_n, but this is not needed in the present context.

4.2.4.2 Stationarity and impact on statistical moments

Consider a DT RP X_n and corresponding RVs at the "given" instants n_1 and n_2, i.e., X_{n_1} and X_{n_2}.

The RV X_{n_1} is characterized by a (1-D) PDF which we denote by $f_X(\alpha_1; n_1)$.

The pair of RVs X_{n_1} and X_{n_2} is characterized by a (2-D) joint PDF which we denote by $f_X(\alpha_1, \alpha_2; n_1, n_2)$.

If the (1-D) function $f_X(\alpha_1; n_1)$ is the same for all n_1s, the RP X_n is said to be the first-order stationary (FoS). In this case it is obvious that the quantities in (4.4), (4.5) and (4.6) are constant, i.e., [48]

$$\mu_X(n) \stackrel{\Delta}{=} E[X_n] = \mu_X \,, \tag{4.12}$$

$$r_X^2(n) \stackrel{\Delta}{=} E[|X_n|^2] = r_X^{(2)} \,, \tag{4.13}$$

$$\sigma_X^2(n) \stackrel{\Delta}{=} E[|X_n - \mu_X|^2] = \sigma_X^2 \,. \tag{4.14}$$

where μ_X, $r_X^{(2)}$, and σ_X^2 are constants. Relation (4.7) becomes

$$\sigma_X^2 = r_X^{(2)} - \mu_X^2 \,. \tag{4.15}$$

If the (2-D) function $f_X(\alpha_1, \alpha_2; n_1, n_2)$ depends on n_1 and n_2 only through their difference $l \stackrel{\Delta}{=} n_1 - n_2$, the RP X_n is said to be second-order stationary (SoS).

One can easily show that a SoS RP is also FoS [48], so that results (4.12)-(4.14) holds. Which says that the mean, mean-square, and variance (functions) of a SoS RP are constant. Of course, (4.15) holds as well. We emphasize that these sequence have constant values/samples.

One can also show that the correlation function $r_X(n_1, n_2)$ of an SoS RP depends on $n_1 - n_2$ only through difference $l \stackrel{\Delta}{=} n_1 - n_2$.

Since $r_X(n_1, n_2)$ only depends on, $n_1 - n_2$ one can introduce the 1-D function $r_X(.)$ that relates to $r_x(.,.)$ via $r_X(n_1, n_2) = r_X(n_1 - n_2)$. One can show that [48]

$$r_X(l) = r_X(n, n-l) = r_X(n+l, n)\,, \tag{4.16}$$

and, hold, which says

$$r_X(l) = E[X_n X^*_{n-l}] = E[X_{n+l} X^*_n]\,. \tag{4.17}$$

In the case of an SoS RP, (4.12) allows us to rewrite (4.11) as

$$\gamma_X(n_1, n_2) = r_X(n_1, n_2) - |\mu_X|^2\,. \tag{4.18}$$

Since the RHS depends on n_1 and n_2 only through their difference l, we conclude that the LHS, i.e., $\gamma_X(n_1, n_2)$ also depends on n_1 and n_2 only thorough l. One can thus introduce the 1-D function $\gamma(.)$ that relates to $\gamma_X(.,.)$ via $\gamma_X(n_1, n_2) = \gamma_X(n_1 - n_2)$.

We can thus express (4.18) as

$$\gamma_X(l) = r_X(l) - |\mu_X|^2\,. \tag{4.19}$$

For $\gamma_X(l)$, one can write expression similar to (4.16) and (4.17). Focussing on the pair $(n, n-l)$, we get

$$\gamma_X(l) = \gamma_X(n, n-l)\,, \tag{4.20}$$

$$\gamma_X(l) = E[(X_n - \mu_X)(X_{n-l} - \mu_X)^*]\,. \tag{4.21}$$

One can easily check that (4.21) is equal to (4.19).

For an SoS RP, the expression (4.10) for $\rho_X(n_1, n_2)$ becomes

$$\rho_X(n_1, n_2) = \frac{\gamma_X(n_1, n_2)}{\sigma_X \sigma_X} = \frac{\gamma_X(n_1, n_2)}{\sigma_X^2}\,. \tag{4.22}$$

Since $\gamma_X(n_1, n_2)$ depends on n_1 and n_2 only through $l = n_1 - n_2$, one can introduce a 1-D function $\rho_X(.)$ that relates $\rho_X(.,.)$ via $\rho_X(n_1, n_2) = \rho_X(n_1 - n_2)$. We can thus express (4.22) as

$$\rho_X(l) = \frac{\gamma_X(l)}{\sigma_X^2}\,. \tag{4.23}$$

For $l = 0$, (4.19) becomes $\gamma_X(0) = r_X(0) - |\mu_X|^2$. Using (4.17), we get $r_X(0) = r_X^{(2)}$. Hence, we get

$$\gamma_X(0) = r_X^{(2)} - |\mu_X|^2 .$$

Using (4.15), we get

$$\gamma_X(0) = \sigma_X^2 . \tag{4.24}$$

We can thus also write (4.23) as

$$\rho_X(l) = \frac{\gamma_X(l)}{\gamma_X(0)} . \tag{4.25}$$

This gives an interpretation of $\rho_X(l)$ as a normalized version of $\gamma_X(l)$.

4.2.4.3 Summary of key quantities

In the present context, the key quantities are the first- and second-order moments introduced above. Here, we focus on the second order moments.

For an arbitrary RP X_n, the second-order moments are

- (auto)correlation function (ACorF), $r_X(n_1, n_2)$
- (auto)covariance function (ACovF), $\gamma_X(n_1, n_2)$
- (auto)covariance coefficient function (ACovCF), $\rho_X(n_1, n_2)$.

For an SoS RP, the same quantities are of interest, but they can be expressed in term of $l \triangleq n_1 - n_2$. The functions of interest are the $r_X(l)$, $\gamma_X(l)$, and $\rho_X(l)$.

We have shown that $\rho_X(l)$ can be interpreted as scaled version of $\gamma_X(l)$,

$$\rho_X(l) = \frac{\gamma_X(l)}{\gamma_X(0)} . \tag{4.26}$$

The quantity $\rho_X(l)$ can be called by either of the following names.

- (auto)covariance coefficient function (ACovCF)
- normalized (auto)covariance function (NACovF).

4.2.4.4 Case of zero mean

When a RP X_n has zero mean, i.e., when $\mu(n) \stackrel{\Delta}{=} E[X_n] = 0$, the correlation function $r_X(n_1, n_2)$ is the same as the covariance function $\gamma_X(n_1, n_2)$.

This may lead to confusion. Indeed, in the literature, some developments may talk about a correlation when they should in fact talk about a covariance. In many cases, there is an underlying assumption of zero mean that is not explicitly mentioned.

4.2.4.5 Computation of moments

Consider the (auto)correlation function $r_X(l)$ in (4.17), say

$$r_X(l) = E[X_n X_{n-l}^*] \,. \tag{4.27}$$

In practice, one can easily approximate this "theoretical" function by using the samples available. One could thus compute [48]

$$r'_X(l) = \sum_{n=-\infty}^{\infty} x_n x_{n-l}^* \,, \tag{4.28}$$

where the x_n represents the available samples.

To distinguish between $r_X(l)$ and $r'_X(l)$, one would call $r_X(l)$ the "statistical ACorF" and $r'_X(l)$ the "sample ACorF".

In the experiments described later, we compute the sample ACorF based on samples available.

4.2.4.6 Notation

The literature on time-series has practices and conventions that often differ from the ones of (statistical) signal processing.

Below, we use "autocorrelation function (ACF)" to mean the normalized ACovF (NACovF) introduced above.

In the same spirit, we define and use the term "partial ACF (PACF)".

4.2.4.7 Partial autocorrelation function (PACF)

For a SoS RP X_n, the partial autocorrelation at lag k is the autocorrelation between the RVs X_n and X_{n-k} after removing any linear dependence on $X_1, \cdots, X_{n-k-1}$ [11, p. 64].

There are algorithms, not discussed in this thesis, for computing the PACF based on the sample ACF [13].

For further details about the algorithms to compute the PACF, one can refer to [74, 11, 13].

4.3 Conventional RP models

In subsequent subsections, we introduce and define the conventional RP models of interest for us.

4.3.1 White noise (WN) RP

The white noise (WN) RP model is used as a "building block" in many other RP models.

A WN RP, here is denoted by Z_n, is a sequence of uncorrelated, identically distributed RVs with zero mean and constant variance [19]. One can show the ACF of Z_n is

$$\rho_Z(l) = \begin{cases} 1 & l = 0 \\ 0 & \text{otherwise}\,. \end{cases} \tag{4.29}$$

One should note that there is some disagreement among authors on how to define the WN RP. Some authors use the term WN to refer to a sequence of independent, rather than uncorrelated, RVs [12, p. 142]. However, there is no difference with regard to second-order properties and one can prove that the independency implies uncorrelation [48]. In addition, the converse is true when the RP is a Gaussian RP (as it will often be assumed to be) [19].

Here, we often use a particular type of WN RP called "standard white Gaussian noise (SWGN)" RP. A SWGN RP, here denoted by ϵ_n, is a sequence of uncorrelated "standard" Gaussian RVs, i.e., with $E[\epsilon_n] = 0$, and $\mathrm{Var}[\epsilon_n] = 1$ [12, 64, 18].

4.3.2 Autoregressive (AR) RP

A RP X_n is said to be an autoregressive (AR) RP of order p, denoted by AR(p), if

$$X_n = \phi_1 X_{n-1} + \phi_2 X_{n-2} + \cdots + \phi_p X_{n-p} + Z_n\,, \tag{4.30}$$

where Z_n is a WN RP, and the ϕs are constant weights/coefficients.

If we define a backward shift operation B such that

$$B\,X_n = X_{n-1}\,, \tag{4.31}$$

the AR(p) RP model can be written as

$$\phi(B)\,X_n = Z_n\,, \tag{4.32}$$

where $\phi(B) = 1 - \phi_1\,B - \phi_2\,B^2 - \cdots - \phi_p\,B^p$ is a polynomial operator in B of order p [19].

The ACF of X_n can be found by solving a set of difference equations called the Yule-Walker equations, given by [19]

$$\rho_X(l) = \phi_1\,\rho_X(l-1) + \phi_2\,\rho_X(l-2) + \cdots + \phi_p\,\rho_X(l-p), \quad l = 1, 2, \cdots\,, \tag{4.33}$$

with the initial condition $\rho_X(0) = 1$.

From the classical signal processing point of view, the equivalent of (4.30) is the WN RP Z_n filtered with the infinite impluse response (IIR) digital filter [48] with system function

$$H_{\mathrm{AR}}(z) = \frac{1}{1 - \sum_{k=1}^{p} \phi_k z^{-k}}\,. \tag{4.34}$$

One can easily prove that both of definitions of the AR RP are equivalent, this by taking the z-transform of both sides of (4.30) [11].

4.3.3 Moving average (MA) RP

A RP X_n is said to be a moving average (MA) RP of order q, denoted by MA(q), if

$$X_n = Z_n + \theta_1\,Z_{n-1} + \cdots + \theta_q\,Z_{n-q}\,, \tag{4.35}$$

where Z_n is a WN RP, and the θs are constant weights/coefficients.

Using (4.31), the MA(q) RP model can be written as

$$X_n = \theta(B)\,Z_n\,, \tag{4.36}$$

where $\theta(B) = 1 + \theta_1\,B + \cdots + \theta_q\,B^q$ is a polynomial operator in B of order q.

The ACF of X_n is given by [19]

$$\rho_X(l) = \begin{cases} 1 & l = 0 \\ \dfrac{\sum_{i=0}^{q-l} \theta_i\,\theta_{i+l}}{\sum_{i=0}^{q} \theta_i^2} & l = 1, 2, \cdots, q \\ 0 & l > q\,, \end{cases} \tag{4.37}$$

where $\theta_0 = 1$. From (4.37), we conclude that the ACF of a MA(q) RP "cuts off" at lag q. This is an important property, which can be used to assess the order of a MA(q) RP model.

From the classical signal processing point of view, the equivalent of (4.35) is the WN RP Z_n filtered with the finite impluse response (FIR) digital filter [48] with system function

$$H_{\mathrm{MA}}(z) = 1 + \sum_{k=1}^{q} \theta_k \, z^{-k} \, . \tag{4.38}$$

One can easily prove that both of definitions of the MA RP are equivalent, this by taking the z-transform from the both sides of (4.35) [11].

4.3.4 Autoregressive moving average (ARMA) RP

An autoregressive moving average (ARMA) RP with p autoregressive terms and q moving average terms, denoted by ARMA(p, q), and is defined as follows:

$$\phi(B) \, X_n = \theta(B) \, Z_n \, , \tag{4.39}$$

where Z_n is a WN RP, B is the backward shift operation (defined by (4.31)), $\phi(B) = 1 - \phi_1 \, B - \phi_2 \, B^2 - \cdots - \phi_p \, B^p$, and $\theta(B) = 1 + \theta_1 \, B + \cdots + \theta_q \, B^q$.

From the classical signal processing point of view, the equivalent of (4.39) is the WN RP Z_n filtered with the IIR digital filter [48] with system function

$$H_{\mathrm{ARMA}}(z) = \frac{1 + \sum_{k=1}^{q} \theta_k \, z^{-k}}{1 - \sum_{k=1}^{p} \phi_k z^{-k}} \, . \tag{4.40}$$

One can easily prove that the both definitions of the ARMA RP are equivalent, this by taking the z-transform from the both sides of (4.39) [11].

4.3.5 Autoregressive integrated moving average (ARIMA) RP

In practice, many signals are non-stationary and, thus, one cannot use stationary AR, MA or ARMA RP models directly. One possible method to deal with non-stationary signals is to apply "differencing" to make them stationary [19]. Using (4.31), the first difference can be written as follows:

$$X_n - X_{n-1} = (1 - B) X_n . \tag{4.41}$$

Similarly, the dth difference could be written as $(1-B)^d$.

If the original signal is differenced d times before fitting an ARMA(p,q) RP model, then the model for the original undifferenced signal is said to be an ARIMA(p,d,q), which is mathematically defined as follows [19]:

$$\phi(B)(1-B)^d X_n = \theta(B)\, Z_n\,, \tag{4.42}$$

where Z_n is a WN RP, B is the backward shift operator (defined by (4.31)), $\phi(B) = 1-\phi_1 B-\phi_2 B^2-\cdots-\phi_p B^p$, $\theta(B) = 1+\theta_1 B+\cdots+\theta_q B^q$, and $(1-B)^d$ is the dth difference operator.

From the classical signal processing point of view, the equivalent of (4.41) is WN Z_n filtered with the digital filter with system function

$$H_{\text{ARIMA}}(z) = H_{\text{ARMA}}(z)\, H_{\text{Integ}}(z)\,, \tag{4.43}$$

where

$$H_{\text{ARMA}}(z) = \frac{1+\sum_{k=1}^{q}\theta_k\, z^{-k}}{1-\sum_{k=1}^{p}\phi_k z^{-k}},$$

$$H_{\text{Integ}} = \frac{1}{(1-z^{-1})^d}\,.$$

One can easily prove that both of definitions of the ARIMA RP are equivalent, this by taking the z-transform from the both sides of (4.41) [11].

4.4 Geometric Brownian motion (GBM) RP model

In this section, we first progressively introduce the Geometric Brownian motion (GBM) RP model, which is the cornerstone of this thesis, and we then present its remarkable history and some of its applications.

4.4.1 Wiener process

The Wiener process (WP), aka the Brownian motion (BM) RP, is used as a building block in the GBM RP (as well as in many other RPs). Below, we progressively introduce the WP and its interesting properties.

4.4.1.1 Discrete-time Wiener process

A DT Wiener process, or DT WP, is denoted by W_n and is defined as

$$\begin{cases} W_n = 0 & n = 0 \\ W_{n+1} = W_n + \epsilon_n \sqrt{\Delta t} & n > 0\,, \end{cases} \tag{4.44}$$

where ϵ_n is a SWGN (defined in Section 4.3.1), and Δt is the sampling period [12]. Using (4.44), we can write, for $k > j$,

$$W_k - W_j = \sum_{i=j}^{k-1} \epsilon_i \sqrt{\Delta t}\,, \tag{4.45}$$

which implies that

$$E[W_k - W_j] = 0 \tag{4.46}$$

$$\mathrm{Var}[W_k - W_j] = (k - j)\,\Delta t. \tag{4.47}$$

Figure 4.2 shows ten different realizations of W_n for $\Delta t = 1/300$, and $n \in [0, 299]$.

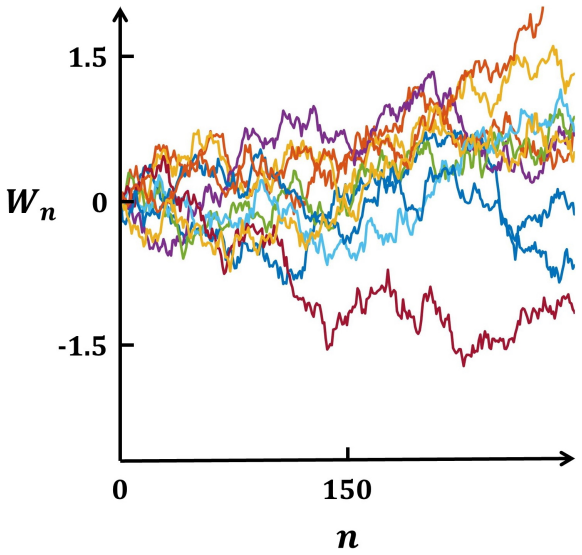

Figure 4.2: Ten different realizations of a DT Wiener process (WP) W_n, for $\Delta t = 1/300$ and $n \in [0, 299]$.

4.4.1.2 Continuous-time Wiener process

A CT Wiener process, or CT WP, is denoted by W_t, and is defined as the RP characterized by the following properties:

1. $W_0 = 0$, which is a convention.
2. For any given time interval $[s, t]$, the increment RV $W_t - W_s$ is normally distributed such that
$$W_t - W_s \sim \mathcal{N}(0, t - s) \,.$$
These increments $W_t - W_s$ are said to be stationary, in the sense that the PDF of the RV $W_t - W_s$ depends only on the width of the time interval (i.e., $t - s$), but not on its location.
3. Increments are independent, i.e., if we take time instants $t_1 < t_2 \leqslant t_3 < t_4$, defining two nonoverlapping time intervals, then $W_{t_2} - W_{t_1}$ and $W_{t_4} - W_{t_3}$ are independent RVs [12].

4.4.1.3 A word about notation "dW_t"

On Figure 4.2, we observe that the realizations of the WP look continuous, but not differentiable. In fact, precisely verifying the continuity and differentiability calls for specifying a rigorous concept of stochastic convergence, as we should say that "the Wiener process is nowhere differentiable with probability 1" [12, p. 165]. To get some intuition for this fact, consider the following increment ratio,

$$\frac{dW_t}{dt} = \frac{W_{t+dt} - W_t}{dt} \,. \tag{4.48}$$

From definition of the WP, we can easily show that

$$\mathrm{Var}\left[\frac{dW_t}{dt}\right] = \frac{\mathrm{Var}[W_{t+dt} - W_t]}{dt^2} = \frac{1}{dt} \,. \tag{4.49}$$

If we take the limit for $dt \to 0$, this variance goes to infinity. While this is not a proof of nondifferentiability of W_t, this suggests that there is some problem in using dW_t/dt.

In this thesis (and also in the literature), one almost never sees a notation like dW_t/dt, but one will often see dW_t. We can think of dW_t as being a normal RV with distribution $\mathcal{N}(0, dt)$. Another way of thinking of dW_t is as an increment, which may be integrated as follows,

$$\int_s^t dW_\tau = W_t - W_s \,. \tag{4.50}$$

In the next subsection, we often use dW_t in mathematical developments.

4.4.2 Itô process

A RP X_t is said to be an Itô process if it obeys the stochastic differential equation (SDE)

$$dX_t = a(t, X_t)\, dt + b(t, X_t)\, dW_t\,, \tag{4.51}$$

where $a(x, y)$ and $b(x, y)$ are deterministic functions.

This equation can be written as the following stochastic integral equation,

$$X_t = X_0 + \int_0^t a(s, X_s)\, ds + \int_0^t b(\tau, X_\tau)\, dW_\tau\,, \tag{4.52}$$

where the first integral on the RHS is a traditional Riemann integral, and the second one is an Itô stochastic integral.

For further details about the Itô integral, one can refer to [12, 75].

4.4.2.1 Drifted Brownian motion

A RP X_t is said to be a drifted Brownian motion if it is an Itô process with

$$\begin{aligned} a(t, X_t) &= a \\ b(t, X_t) &= b\,, \end{aligned}$$

where a and b are constants. Therefore, the drifted Brownian motion is defined by the SDE

$$dX_t = a\, dt + b\, dW_t\,, \tag{4.53}$$

where W_t is a WP. By using this relation and the Itô lemma (which is not covered in this thesis), we can write [12]

$$X_t = X_0 + a\, t + b\, W_t\,. \tag{4.54}$$

Hence, for any given time t_0, we find

$$X_{t_0} \sim \mathcal{N}(X_0 + a\, t_0, b^2\, t_0).$$

Figure 4.3 shows an illustrative example of one realization of the drifted Brownian motion RP $X_t = 1 + 2\, t + W_t$, and the corresponding, deterministic drift line $y(t) = 1 + 2\, t$.

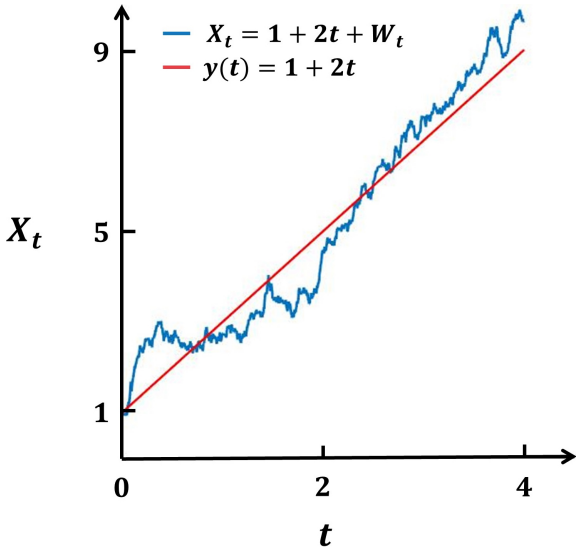

Figure 4.3: The graph shows (1) one realization of the drifted Brownian motion RP $X_t = 1 + 2\,t + W_t$ and (2) the corresponding, deterministic drift line $y(t) = 1 + 2\,t$.

4.4.2.2 Geometric Brownian motion (GBM)

A RP X_t is said to be a geometric Brownian motion (GBM) if it is an Itô process with

$$a(t, X_t) = \mu\, X_t$$
$$b(t, X_t) = \sigma\, X_t\,,$$

where μ and σ are constant parameters referred to as drift and volatility, respectively [12]. Therefore, GBM is defined by the SDE

$$dX_t = \mu\, X_t\, dt + \sigma\, X_t\, dW_t\,, \tag{4.55}$$

where W_t is the WP.

Intuition would suggest to write (4.55) as

$$\frac{dX_t}{X_t} = \mu\, dt + \sigma\, dW_t\,. \tag{4.56}$$

By using this relation and the Itô lemma (which is not covered in this thesis), we can write [12]

$$X_t = X_0\, \exp\left(\left(\mu - \frac{\sigma^2}{2}\right) t + \sigma\, W_t\right)\,. \tag{4.57}$$

Now, by taking the natural logarithm, i.e., "$\ln(\cdot)$", of both sides of (4.57), we find

$$\ln(X_t) = \ln(X_0) + (\mu - \sigma^2/2)t + \sigma W_t \,. \tag{4.58}$$

Hence, for any given time t_0, we get

$$\ln(X_{t_0}) \sim \mathcal{N}\left(\ln(X_0) + (\mu - \sigma^2/2)t_0, \sigma^2 t_0\right) \,. \tag{4.59}$$

So, at any given time instant t_0, X_{t_0} is lognormally distributed, and one can thus show that [12, 75]:

$$E[\ln(X_t/X_0)] = \nu\, t \,, \tag{4.60}$$
$$\mathrm{Var}[\ln(X_t/X_0)] = \sigma^2\, t \,, \tag{4.61}$$
$$E[X_t/X_0] = e^{\mu\, t} \,, \tag{4.62}$$
$$\mathrm{Var}[X_t/X_0] = e^{2\mu\, t}(e^{\sigma^2\, t} - 1) \,, \tag{4.63}$$

where $\nu = \mu - \sigma^2/2$.

Figure 4.4 shows an illustrative example of 20 realizations of the GBM RP $X_t = 50\, \exp((0.5 - (0.2)^2/2)t + 0.2\, W_t)$.

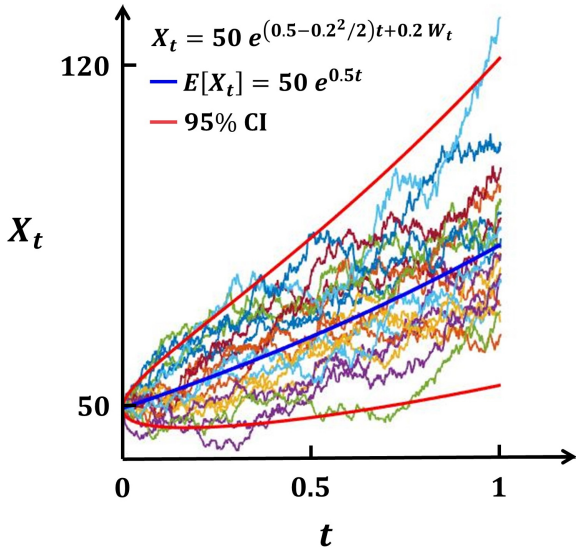

Figure 4.4: The graph shows 20 realizations of the GBM RP $X_t = 50\, \exp((0.5 - (0.2)^2/2)t + 0.2\, W_t)$ and the corresponding 95% confidence interval (CI).

4.4.3 History and interpretation

The GBM RP plays a key role in financial mathematics. It is mainly used to model the evolution of a risky stock. In finance, a stock represents a share in the ownership of an incorporated company. Through the years, mathematicians and financial engineers have developed many models for the evolution of stock price in order to predict its future values (FVs) and, ultimately, to minimize the risks of investments.

The stock price is usually described as a stochastic process S_t for $t \geqslant 0$.

Louis Bachelier (1900) was the first person to use Brownian motion as a model for stock price fluctuations on the Paris stock market [37].

In 1964, Professor Paul Samuelson (MIT) suggested to replace Brownian motion (BM) by geometric Brownian motion (GBM), i.e., by

$$\frac{dS_t}{S_t} = \mu\, dt + \sigma\, dW_t\,,$$

or, equivalently, by

$$\frac{S_{t+dt} - S_t}{S_t} = \mu\, dt + \sigma\, dW_t\,.$$

The quantity on the LHS of the last relation is the relative return from the stock in the time period $[t, t+dt]$. The RHS tells us that there is a linear trend $\mu\, dt$ plus a stochastic noise term σdW_t. The constant μ is called the mean rate of return, and σ is called the volatility. The effects of the parameters μ and σ are shown in Figures 4.5 and 4.6 respectively.

In Figure 4.5 (a), one observes an exponential growth of S_t, which is insightful, because economists also believe in exponential growth (or decay) of stock price, which explains why they like the GBM model [75]. (Figure 4.5 (b) shows a corresponding exponential decay.)

Figure 4.6 shows that, the larger σ is, the larger the fluctuations of S_t are. Thus, σ is a measure of the riskiness of the asset [75].

One should always remember that, despite the apparent simplicity and true elegance of the GBM model, this model is rooted in the very complex field of stochastic differential equations (SDEs).

It is quite significant and remarkable that the use of GBM in finance led to two Nobel Prizes, i.e., to Professor Paul Samuelson (MIT) in 1970 [71], and to Professor Robert Merton and Professor Myron Scholes (Stanford and MIT, respectively) in 1997 [8, 16, 85].

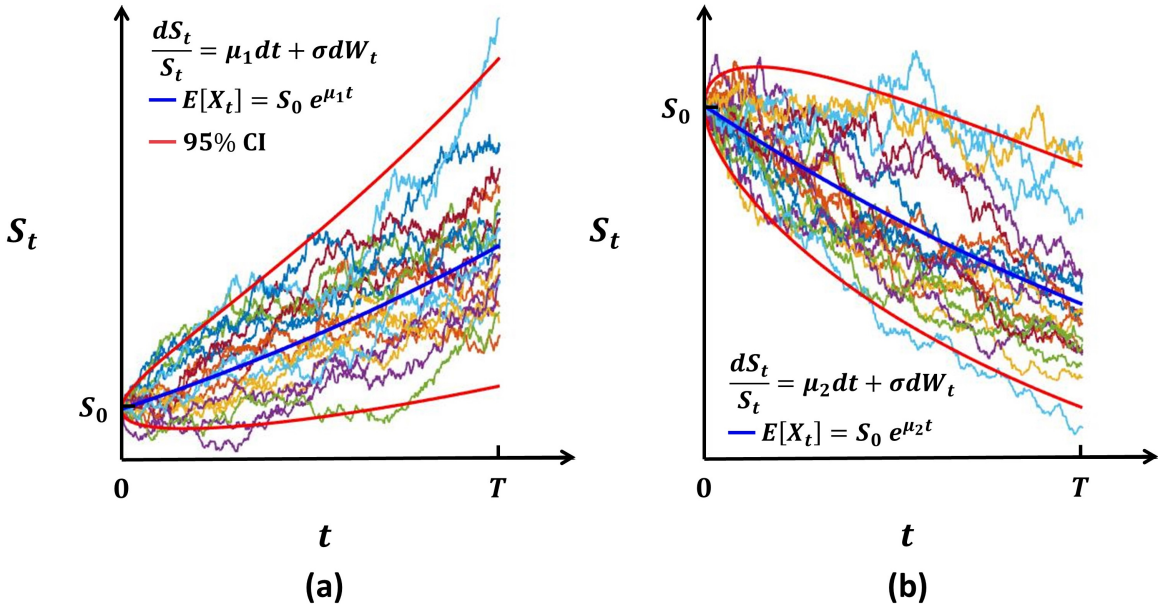

Figure 4.5: The figure shows the effect of the parameter μ on the shape of the realizations of a GBM RP. (a) shows that, for $\mu > 0$, the realizations are generally increasing, and (b) shows that, for $\mu < 0$, the realizations are generally decreasing.

4.5 Conclusion

In order to produce the LoD-related predictions, one must treat the real-life LoD signals as the realizations of an underlying RP. One of our main goals in this research is to identify this underlying RP model.

We provided the precise definitions of a CT RP and a DT RP, and we introduced the related concepts of stationarity, ACF, and PACF.

We also provided an overview of the conventional RP models, i.e., the WN, SWGN, AR, MA, ARMA, and ARIMA RP models. Finally, we presented the geometric Brownian motion (GBM) RP model, which is the main focus of this thesis.

Although the GBM RP model is elegant and relatively simple to use, one should always keep in mind that it is rooted in the very complex field of stochastic differential equations and that it led to two Nobel Prizes in Economic Sciences.

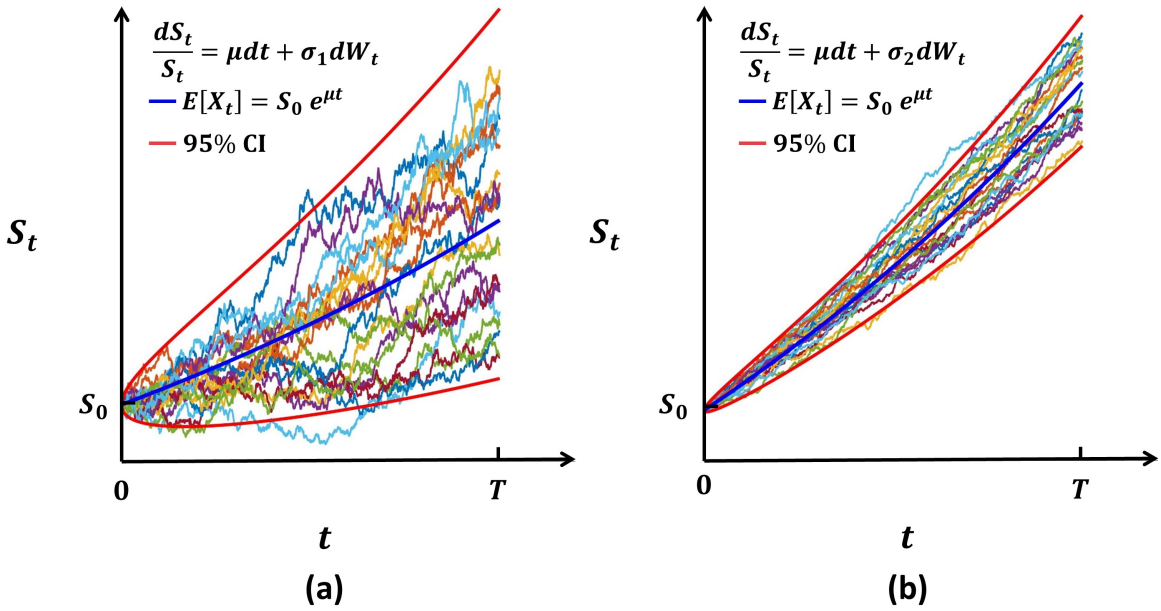

Figure 4.6: The figure shows the effect of the parameter σ on the shape of the realizations of a GBM RP. (a) shows 20 realizations for σ_1, and (b) shows 20 realizations for σ_2 ten times smaller than σ_1, i.e., $\sigma_2 = \sigma_1/10$. The two graphs show that the larger σ is, the larger the fluctuations of the realizations of a GBM RP are.

Chapter 5

Prediction using conventional random process models

This chapter describes how to use conventional random process (RP) models to produce the different types of predictions of interest. Section 5.1 describes the importance of prediction using conventional RP models. Section 5.2 describes the Box-Jenkins method, which is useful to identify an appropriate conventional RP model for a given signal. Section 5.3 explains in detail how to produce the three types of predictions (i.e., predicting future values of a signal, the first hitting time, and the survival probability) using conventional RP models. Section 5.4 presents the main weaknesses of the Box-Jenkins method. Section 5.5 concludes the chapter.

5.1 Introduction

In Section 4.3, we presented the conventional RP models of interest. Indeed, prediction using conventional RP models can be found in many diffrent areas, such as sales forecasting, budgeting, production and capacity planning, financial risk managment, and many other areas [19].

Prediction using conventional RP models is a topic that one can find in many standard time-series (i.e. signals) forecasting books [28].

In this chapter, first, we describe how to select an appropriate conventional RP model for a given signal using the Box-Jenkins method. Second, we describe how to use the selected RP model to produce the different types of predictions. Third, we address the main weaknesses of the Box-Jenkins method.

5.2 Box-Jenkins method

The forecasting method based on the ARIMA RP models is often called the Box-Jenkins (BJ) method. The method is named after the two statisticians George Box and Gwilym Jenkins.

The BJ method involves two procedures: (1) selection of model and of its order, and (2) estimation of parameters of model.

In this section, we explain the above-mentioned procedures.

5.2.1 Selection of RP model and of its order

Below, we call upon the autocorrelation function (ACF) and partial ACF (PACF) introduced in Section 4.2.4. The functions that are used are in fact the sample ACF and the sample PACF, which are estimates of the underlying, theoretical statistical ACF and statistical PACF.

For DT signals, the BJ model selection procedure involves two steps [11]:

1. Determining whether the signal is a realization of a stationary RP, and if is not, successively differencing it to attain the stationarity.

   The autocorrelation function (ACF) and partial autocorrelation function (PACF) of a realization of a stationary RP decay exponentially (or cut off completely after a few lags).

2. Identifying the model and its order based on the sample ACF and sample PACF.

   For an AR RP, the ACF decays gradually, but the PACF cuts off after a few lags, and the cut-off lag indicates the order of the model. Conversely, for an MA RP, the ACF cuts off after a few lags, and the cut-off lag indicates the order of the model, but the PACF decays gradually. If both the ACF and PACF decay gradually, then an ARMA model should be considered.

Figures 5.1 and 5.2 show illustrative examples of the ACF and PACF of the realizations of an arbitrary AR(1) RP and an aribitary MA(5) RP, respectively.

5.2.2 Estimation of parameters of RP model

Consider the block diagram shown in Figure 5.3, where (1) ϵ_n is a realization of an SWGN, (2) $\hat{x}_n$ and x_n are the output of the ARIMA model and the signal to be modeled, respectively, and (3) $e_n = \hat{x}_n - x_n$.

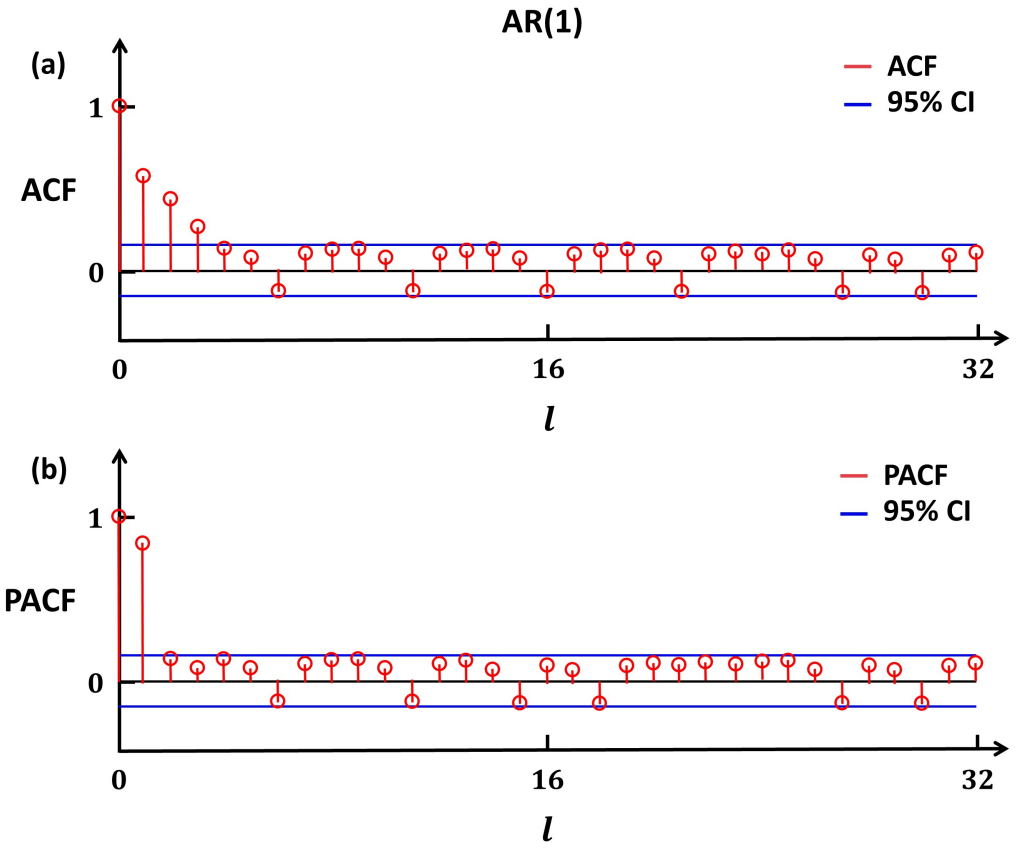

Figure 5.1: Subfigures (a) and (b) respectively show the ACF and PACF computed using a single realization of an AR(1) RP. Both subfigures also show the 95% confidence interval (CI).

Then, estimating the parameters of the ARIMA(p, d, q) model usually involves numerically approximating the solutions of the nonlinear equations

$$\frac{\partial \xi_{\mathrm{LS}}}{\partial \phi_k} = 0\,; \quad k = 1, \cdots, p \tag{5.1}$$

$$\frac{\partial \xi_{\mathrm{LS}}}{\partial \theta_k} = 0\,; \quad k = 1, \cdots, q\,, \tag{5.2}$$

where $\xi_{\mathbf{LS}}$ is the so-called least squares error, i.e.

$$\xi_{\mathrm{LS}} = \sum_{n=0}^{N-1} (\hat{x}_n - x_n)^2\,,$$

and N is the length of the signal.

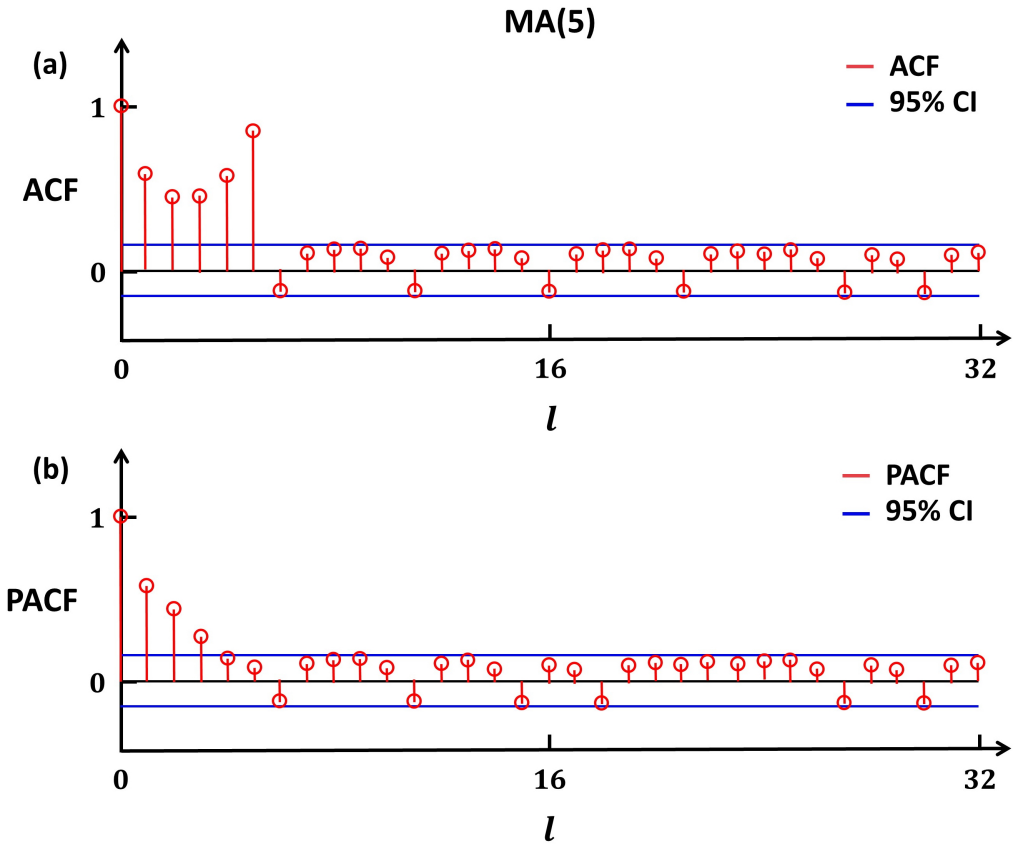

Figure 5.2: Subfigures (a) and (b) respectively show the ACF and PACF computed using a single realization of a MA(5) RP. Both subfigures also show the 95% confidence interval (CI).

There are several methods and many different packages to solve the above-mentioned equations, but they are not discussed in this thesis.

One should note that, for long signals (of several hundred samples or more), the choice of the estimation method usually makes little difference, but, for short signals, the choice of the estimation method becomes more important [19].

For further details about different estimation approaches, one can refer to [48, 19].

5.3 Prediction using conventional RP models

Below, we describe how to produce the three types of predictions of interest, i.e., predicting the future values of a signal, the first hitting time, and the survival

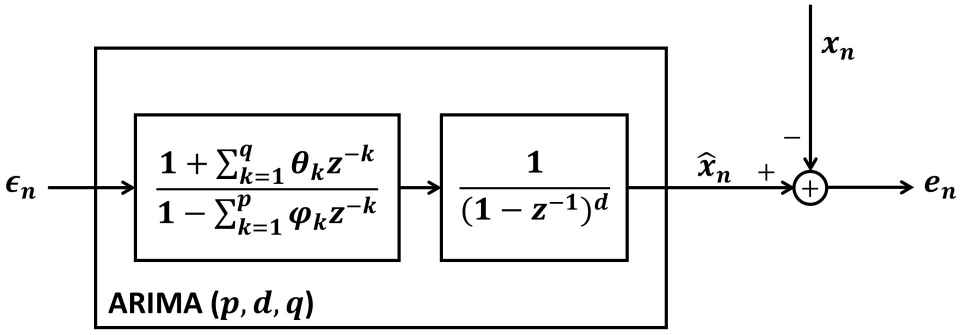

Figure 5.3: Modeling the signal x_n of interest as the response of an LTI filter of type ARIMA(p, d, q) to one realization ϵ_n of an SWGN RP. The goal is to find the parameters θ_k, ϕ_k, and d of ARIMA(p, d, q) filter that minimize e_n.

probability, using conventional RP models.

5.3.1 Predicting future values of a signal using conventional RP models

As indicated in Section 3.4.2, once one has identified an appropriate RP model for the underlying RP X_n corresponding to a given signal x_n, one can predict FVs of x_n from the present time index p, and for the forecasting horizon h, using the following formula

$$\hat{x}_{p+h} = E(X_{p+h}|I)\,, \tag{5.3}$$

where $I = \{x_n : n \in [0, p]\}$ [19].

One should note that (5.3) is valid for any RP.

We now provide an illustrative example of applying (5.3) to a conventional RP model, namely of type MA(2), to predict FVs of a given signal.

5.3.1.1 Example: MA(2)

Consider the following MA(2) RP,

$$X_n = Z_n + \theta_1 Z_{n-1} + \theta_2 Z_{n-2}\,, \tag{5.4}$$

where Z_n is a WN RP, and θs are constants.

Let us assume (1) that the above MA(2) RP corresponds to a given signal/realization x_n, and (2) that we know the values of this signal up to the present time, i.e., for the times $0, \cdots, p$, which means that we know $I = \{x_0, x_1, \cdots, x_p\}$.

Now, using (5.4) and $I = \{x_n : n \in [0, p]\}$ one can find the values of the realization z_n (of the underlying WN RP Z_n) up to the present time, i.e., $\{z_n : n \in [0, p]\}$ is also known [19].

By using (5.3) and (5.4), one can show that is the predicted value for the forecasting horizon h is given by [19]

$$\hat{x}_{p+h} = E(X_{p+h}|I) = \begin{cases} \theta_1 z_p + \theta_2 z_{p-1} & h = 1 \\ \theta_2 z_p & h = 2 \\ 0 & h \geqslant 0\,. \end{cases} \tag{5.5}$$

5.3.2 Predicting "first hitting time" and "survival probability" using conventional RP models

As indicated in Section 3.4.3, once one has identified an appropriate RP model for the underlying RP X_n corresponding to a given signal x_n, one can estimate the FHT for a threshold level α by

$$\hat{t}_\alpha \triangleq E(T_\alpha)\,,$$

where

$$T_\alpha \triangleq (\inf\{n \geqslant 0 : X_n \geqslant \alpha\})\,\Delta t\,,$$

where Δt is the sampling period.

The above relation looks very simple. However one should note that finding an analytic, closed-form formula for the FHT for an ARIMA(p, d, q) RP is an advanced and complicated mathematical problem, and beyond the scope of this thesis. To date, we did not find such a formula in the literature. This remark is also valid for its corresponding survival probability.

One can find the analytic formulas for the FHT of simpler RP models such as AR(1), ARMA(1,1) and AR(p) [7]. However, the formulas are still very complicated.

5.4 Weaknesses of Box-Jenkins method

The main weakness of the BJ method is that it requires human intervention in its model building process [28]. As indicated in Section 5.2.1, to identify the model and its order using the BJ method, one must visually investigate the ACF and PACF graphs. Consequently, the BJ is not an automatic method, and it always requires human intervention in its modeling process.

Furthermore, as indicated in Section 5.2.2, in order to estimate the parameters of the RP model—that are often numerous—the BJ method requires to solve sophisticated optimization problems, which are computationally heavy to deal with.

Consequently, the BJ method is not suitable for real-time applications [28].

5.5 Conclusion

Conventional RP models are used in many different areas to produce different types of predictions.

We explained how to use the BJ method to identify an appropriate conventional RP model and estimate its parameters to produce the three types of predictions of interest, i.e., predicting FVs, the FHT, and the SP.

We saw that finding an analytic, closed-form formula in order to predict the FHT and the SP using conventional RP models is a significant mathematical challenge.

We also saw that the BJ method requires human intervention, and is thus not suitable for real-time applications.

Chapter 6

Prediction using GBM random process model

This chapter describes how to use the geometric Brownian motion (GBM) RP model to produce different types of predictions. Section 6.1 motivates the use of the GBM RP model to produce different types of predictions. Section 6.2 describes the methodology that is typically used to determine whether the GBM RP model is a valid model for a given signal. Section 6.3 describes how to estimate the parameters of the GBM RP model. Section 6.4 describes in detail how to produce different types of predictiosn using the GBM RP model. Section 6.5 provides a list of the advantages of the GBM RP model over conventional RP models. Section 6.7 concludes the chapter.

6.1 Introduction

The GBM RP model is frequently used in finance to produce different types of predictions. However, this powerful and elegant RP model is generally unknown in other important domains, such as in engineering.

The GBM RP model is a model that has been largely overlooked in books on time-series (i.e., signals) forecasting [28].

Below, we progressively describe how to use the GBM RP model to produce the three types of predictions of interest, i.e., to predict future values (FVs) of a signal, the first hitting time (FHT), and the survival probability (SP).

6.2 Validation of GBM assumption: checking normality and independency conditions

We describe the methodology that is typically used to determine whether the GBM RP model is a valid RP model for a given DT signal.

Before describing this methodology, we introduce some key concepts. As described in Section 4.2.1, one can treat a RP as a sequence of random variables (RVs), thus ordered in time. However, rather than considering these RVs, one works here with the related log-ratio (LR) RVs. The LR RV at some time index n is defined as the natural logarithm of the ratio of the RV at n and the RV at $n-1$. The collection of LR RVs constitutes a new RP, called here the LR RP. (Note that the number of RVs in the LR RP is necessarily one unit less that in the original RP.)

Of course, in practice, we (only) have one realization of the original RP, and thus one realization of the LR RP, and, consequently, one realization of each original RV or LR RV. We often refer to this single realization as a "signal" or as an "observed signal". While all theoretical developments must be done in terms of RPs and RVs, the methodology only uses the single available realization of the original RP and that of the corresponding LR RP, as well as of their corresponding RVs.

At the theoretical level, if the original RP is a GBM RP, then one can show that the LR RP is characterized by the following pair of properties [75, 12]:

1. All LR RVs are individually characterized by a normal (i.e., Gaussian) PDF, and the PDFs of all these RVs are identical (thus with the same mean and the same standard deviation).

2. Any two distinct LR RVs are independent in the usual statistical sense, meaning that their joint (2D) PDF factorizes.

At the methodology level, one must determine whether both of the above properties (or conditions) are verified. The difficulty—which is typical in the type of approach used here—is that the theory deals with all possible realizations, while the methodology has only access to a single one, i.e., the observed signal. The methodology must thus do its best with a single signal/realization to establish one or more properties that pertain to all possible realizations. In short, the methodology must replace considerations across a statistical ensemble by considerations across time. Below, we simply describe the methodology, and we do not attempt to justify it in terms of the theory.

In light of the above discussion, there are thus two conditions to be verified on the signal/realization available to establish whether this realization can be modelled by a GBM RP. We refer to these two conditions as the "normality condition" and the "independency condition".

Below, we explain how the methodology checks each of these two conditions in practice. The explanations are cast in terms of the available realizations of the LR RVs; we refer to them as the LR samples, or LR sample values. Remember that LR stands for "log-ratio". Useful references are [28, 71, 12].

Note that, if the conditions are satisfied, one can conclude, in accordance with standard procedures, that GBM is a valid choice of RP model for the realization at hand.

6.2.1 Techniques for checking normality condition

The underlying idea of this check is to determine whether the ensemble of LR samples "comes", or not, from some normal (i.e., Gaussian) PDF. The following three techniques can be used to deal with the normality condition. They differ in their sophistication and effectiveness. Ideally, one should apply all three.

6.2.1.1 Histogram

This is a graphical technique that consists in plotting a histogram of the LR samples and comparing it to the "normal distribution fit", which is the normal (i.e., Gaussian) PDF—i.e., the one with the mean and standard deviation of the LRs—multiplied by the total number of LR samples.

While this graphical technique is intuitive and simple, it is not the most precise. It is thus recommended to also apply the following two other techniques.

6.2.1.2 Quantile-quantile (Q-Q) plot

This is a graphical technique that consists in producing a quantile-quantile (Q-Q) plot to determine whether a set of n sample values can be considered to be n realizations of a RV with a specified PDF.

To produce the Q-Q plot, one ranks/orders the n samples by increasing numerical values, and one plots the n points that have the following (x, y) coordinates: ith ordered sample, $i/(n+1)$th quantile of the PDF of interest.

The n quantiles are the n successive abscissas of the PDF curve that produce $n+1$ equal areas under it.

If the n plotted points lie close to a straight line, then one can conclude that the n samples can be considered to be n realizations of a RV with the specified PDF. The PDF of interest is often the normal (i.e., Gaussian) PDF. In this case, the conclusion of the test is independent of the parameters of the normal PDF, so that one typically chooses the standard normal PDF, i.e., with a mean of 0 and a standard deviation/variance of 1, denoted by $\mathcal{N}(0,1)$ [30].

6.2.1.3 Shapiro-Wilk (S-W) test

The Shapiro-Wilk (S-W) test uses the (non-graphical) technique of testing the null hypothesis, called H_0.

Here, the hypothesis H_0 is "the log-ratio samples come from a normal PDF (with unspecified mean and standard deviation)".

The test gives the value of the statistic W and the corresponding p-value.

The p-value is compared to the selected/specified level of significance α. If the obtained p-value is greater than α, then one can conclude that the H_0 hypothesis cannot be rejected. But this does not allow one to conclude that the samples come from a normal PDF. If the p-value is smaller than, or equal to, α, then one can conclude that the H_0 hypothesis must be rejected. This means that the samples do not come from a normal PDF.

One should note that this test never provides an "accept H_0" answer, i.e., a positive answer.

The limitations of the S-W test are described in the experimental results of Chapter 9.

6.2.2 Techniques for checking independency condition

The technique used for this test may appear, at first sight, quite remote from that of checking the independence of pairs of RVs, but it can, of course, be justified on theoretical grounds [71].

6.2.2.1 Linear regression

This is a graphical technique that consists in (1) plotting all successive LR sample values as a function of time (thus producing a plot of the LR realizations available), (2) computing the regression straight line (via least-square fit), and (3) determining whether this straight line is nearly horizontal.

This line can intercept the vertical axis of the plot (at time index 1) at any

height (i.e., not necessarily zero). Ideally, the regression line should be horizontal, thereby indicating that there is no correlation between the underlying LR RVs [71, 28, 67].

6.3 Estimation of parameters of GBM RP model

In the previous section, we presented a methodology to determine whether the GBM RP model is a valid RP model for a given signal by checking the "normality condition" and the "independency condition" for the so-called LR samples. In this section, we describe how to use the LR samples to estimate the parameters of the underlying GBM RP model, i.e., the drift μ and the volatility σ.

Let x_n be an N-sample realization of the GBM RP X_n. Then, one can compute the estimates $\hat{\mu}$ and $\hat{\sigma}$ of the parameters μ and σ of the corresponding GBM RP model using the following relations [68, 71, 28],

$$\hat{\sigma} = \sqrt{\frac{\mathrm{Var}(r)}{\Delta t}}\,, \tag{6.1}$$

$$\hat{\mu} = \frac{E(r)}{\Delta t} + \frac{\hat{\sigma}^2}{2}\,, \tag{6.2}$$

$$r = \left\{ \ln\left(\frac{x_{n+1}}{x_n}\right) : n \in \{0, \cdots, N-1\} \right\}\,, \tag{6.3}$$

where Δt is the sampling period.

These relations show that the parameters $\hat{\mu}$ and $\hat{\sigma}$ of the GBM RP model are given by closed-form formulas. This should be contrasted with the case of the conventional RP models, where sophisticated optimization methods are generally required.

6.4 Prediction using GBM RP model

Below, we describe how to produce the three types of predictions of interest—as defined in Section 3.3—using the GBM RP model.

6.4.1 Predicting future values of a signal using GBM RP model

Consider a realization x_n of an underlying GBM RP X_n.

Let us denote, as usual, the estimate, at the present time $n = p$, of the (future) value of x_n at time $n = p + h$ by $\hat{x}_{p+h}$.

Using (4.62) and (5.3) one can show that this estimate is given by

$$\hat{x}_{p+h} = x_p \, e^{\mu(h\Delta t)} \,, \tag{6.4}$$

where x_p is the known value of x_n at the present time, Δt is the sampling period, μ is the drift parameter (as defined in Section 4.4.2.2), h is the forecasting horizon, and $\mu(h\Delta t)$ is the product of μ, h, and Δt.

We do not provide here the mathematical developments that lead to (6.4). One can find the corresponding mathematical developments in [12, 75].

6.4.2 Predicting "first hitting time" and "survival probability" using GBM RP model

Consider a realization x_n of an underlying GBM RP X_n.

Let us denote, as usual, at the present time $n = p$, the estimate of the first hitting time (FHT) of x_n for a specified threshold level α by $\hat{t}_\alpha$.

Using (3.10) and (4.57), one can show that this estimate is given by [20, p. 448]

$$\hat{t}_\alpha = \frac{1}{(\mu - \sigma^2/2)} \ln\left(\frac{\alpha}{x_p}\right) \,, \tag{6.5}$$

where x_p is the known value of x_n at the present time, and μ and σ are, respectively, the drift and volatility parameters of the GBM RP model.

One should note that (6.5) is valid only for "$\mu > \sigma^2/2$" and "$\alpha \geqslant x_p$" [20].

We do not provide here the mathematical developments that lead to (6.5). One can find them in [20, 51].

Furthermore, for the same signal x_n and threshold level α, one can predict the survival probability (SP), from the present moment $n = p$, using the survival function

$$S(t) = 1 - \left[\mathcal{N}\left(\frac{-a + bt}{\sqrt{t}}\right) + e^{2ab}\mathcal{N}\left(\frac{-bt - a}{\sqrt{t}}\right)\right] \,, \tag{6.6}$$

where

$$a = \frac{1}{\alpha} \ln\left(\frac{\alpha}{x_p}\right) \,,$$
$$b = \frac{(\mu - \sigma^2/2)}{\sigma} \,,$$
$$\mathcal{N}(x) = \frac{1}{\sqrt{2\pi}} \int_{-\infty}^{x} e^{-u^2/2} du \,.$$

One should note that (6.6) is valid only for "$\sigma > 0$" and "$x_p < \alpha$".

We do not provide here the mathematical developments that lead to (6.6). One can find them in [51, 22].

6.5 Advantages of the GBM RP model over the conventional RP models

Below, we provide a list of the advantages of the GBM RP model over the conventional RP models.

1. Conventional RP models require human intervention to build their models (i.e., to select the type of model and its order), whereas the GBM RP model does not require such intervention [28, 67].
2. Conventional RP models require the use of sophisticated optimization methods to estimate the parameters of the models, whereas the GBM RP model provides straightforward formulas to estimate these parameters [28, 67].
3. Conventional RP models do not offer analytic, closed-form formulas to predict the corresponding FHT and SP, whereas the GBM RP offers such formulas.
4. Conventional RP models cannot produce values that are exclusively positive, whereas the GBM RP model can, which makes the GBM RP model an excellent choice when dealing with positive datasets, as is the case for LoD signals [28, 67].
5. Conventional RP models require, for their construction, sophistication in statistics, whereas the GBM RP model does not [28].

Despite the fact—mentioned in the last point above—that it is easier to build a GBM RP model than conventional a RP model, one should note that the GBM RP model is rooted in the very complex field of stochastic differential equations (SDEs).

6.6 Powerful strategy for finding the best possible RP model

Figure 6.1 shows a flowchart suggesting a powerful strategy for modeling a real valued-signal with a RP model [28, 67].

The flowchart comprises two possible (choices of) models, i.e., GBM or ARIMA.

The flowchart shows clearly that, if the signal/data is strictly positive (> 0), then one should start by examining the GBM RP model. It also shows clearly that, if GBM is a good fit, then one should not even consider ARIMA (in major part because of the considerable added complexity of this RP model). In other words, one should consider ARIMA only if the signal/data is not positive and/or GBM is not a good fit.

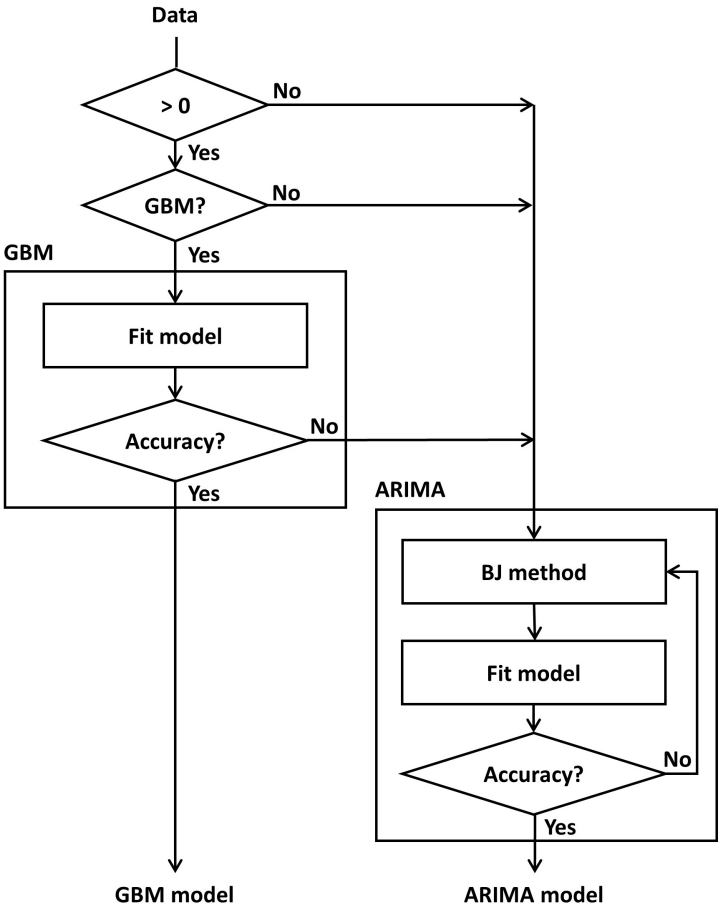

Figure 6.1: The flowchart describes the overall procedure for building a RP model from data, with a choice between the GBM and ARIMA RP models, with the GBM RP model being always favored [28].

6.7 Conclusion

The GBM RP model is frequently used in finance. However, it is generally unknown in other important domains, such as in engineering.

We described how to determine whether the GBM RP model is a valid RP model for a given signal, and we then explained how to use the GBM RP model to produce the three types of predictions of interests, i.e., predicting future values of signal, the first hitting time, and the survival probability.

We also explained why, for positive-valued signals, one should always consider the GBM RP model first.

Chapter 7

Collection of experimental data

This chapter describes the procedure use to collect data and the resulting sleep-deprivation dataset used in this thesis. Section 7.1 provides an introduction to the laboratory-based studies that we performed. Section 7.2 describes the general characteristics of the participants. Section 7.3 describes the protocol applied in the laboratory-based studies. Section 7.4 describes the drowsiness monitoring system used in the laboratory-based studies. Section 7.5 describes the measurements setup. Section 7.6 mentions another, confidential data collection. Section 7.7 concludes this chapter.

7.1 Introduction

In this thesis, we use data from two laboratory-based studies, referred to here as Study A and Study B.

As a part of our research, we also used data from a third study, referred to here as Study C, but the nature of the data (and the results obtained) is confidential.

Studies A and Study B used the same overall (experimental) protocol, and they differed only by (1) the groups of participants/subjects who took part in each study, and (2) the nature of the tests/tasks that each participant was asked to submit to in each study.

7.2 Participants

We recorded experimental data from N = 30 healthy participants aged 19-33. Study A contributed 17 subjects (mean age: 22.7; 8 men, 9 women), and Study B

13 subjects (mean age: 23.7; 7 men, 6 women).

7.3 Protocol

In each of the Study A and Study B, the corresponding participants were each asked to submit to three successive, time-separated test sessions in different sleep-deprivation conditions over two days. During each test session, the level of drowsiness (LoD) signal of each participant was produced using a drowsiness monitoring system designed, built, and validated by our team [38]. This system is described in the next section.

In Study A, each test session consisted in performing a Psychomotor Vigilance Test (PVT); the three successive sessions all had durations of 10 minutes.

In Study B, each test session consisted in driving in a high-fidelity driving simulator; the three successive sessions had durations of 45, 45, and 60 minutes.

For ease of explanation, the overall two-day experiment for each participant (for either type of test) can be viewed as the succession of Night 1, Day 1, Night 2, and Day 2, and as consisting of three successive test sessions. Figure 7.1 provides an illustration of the overall data-acquisition protocol used for both studies.

On Night 1, the participant slept at home and was asked to report the number of hours of sleep using a sleep diary (mean $\pm$ standard deviation for all participants is 7.57 ± 0.8 h of sleep, range 6.5–9.0 h). Then, the participant was not allowed to sleep from the time he woke up on Day 1 until the end of the study (12:00 noon on Day 2). (All times are in 24 h notation.) At 8:00 on Day 1, the participant arrived at our laboratory and submitted to the first test session between 8:00 and 10:00. The participant was then free to leave the laboratory to carry out his normal activities but was equipped with an actigraph (either Actiwatch 2 or Philips Respironics) in order to check that he/she had not slept while away. The participant came back to our laboratory at 20:30 on Day 1.

On Night 2, the participant submitted to the second test session between 2:00 and 4:00 and, after breakfast on Day 2, he submitted to the third test session between 11:00 and 13:00 (and after at least 28 hours of sleep deprivation). At the end of the study, the participant was sent back home. From noon on Day 1 until end of third test session, the participant was asked not to consume any stimulant (coffee, tea, etc.).

This protocol was approved by the Ethics Committee of the University of Liège [40, 38].

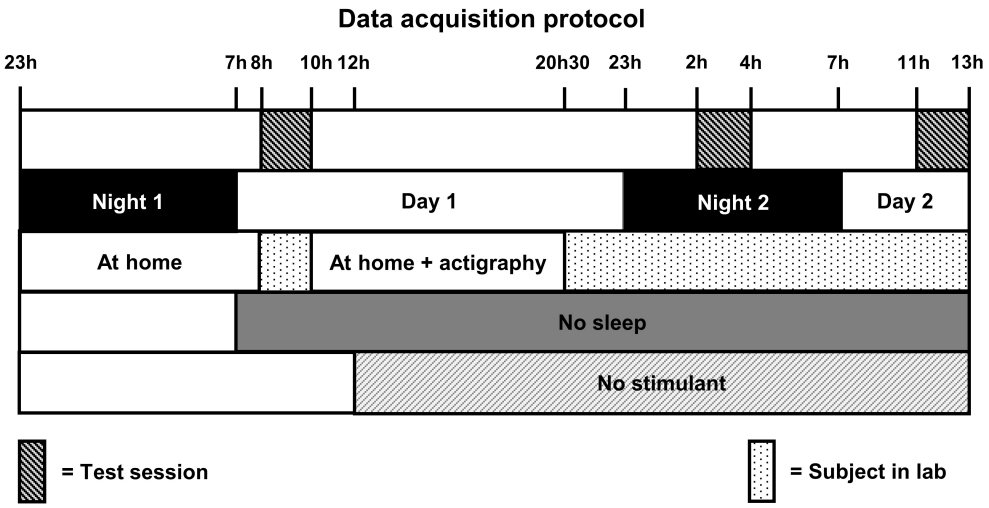

Figure 7.1: Graphical overview of overall protocol common to both studies, i.e., to Study A (PVT) and to Study B (driving in a simulator). The successive five rows below the timeline show: (1) when each participant had to submit to a test; (2) the succession of nights and days; (3) the presence at home or in our lab; (4) the period of sleep deprivation; (5) the period of stimulant deprivation [30, 40, 38].

7.4 Instruments

Our team designed, built, and validated [38, 41, 39] a fully automatic drowsiness monitoring system based on the physiological state of a person.

The system consists in a pair of specially-made eyeglasses linked to a computer via a cable. The eyeglasses contain a controlled source of illumination in the infrared (IR) and a high-speed (120 images/second) camera sensitive in the IR.

The algorithms running on the computer use ocular parameters extracted from images of one of the eyes—i.e. POG (described in Section 2.4.2.1.2)—to determine, periodically in time, an LoD on a numerical scale from 0 to 10, with 0 corresponding to "very awake" (or "very vigilant") and 10 to "very drowsy" [38].

Figure 7.2 shows our data collection system.

For further details about the drowsiness monitoring system, one can refer to [38].

Figure 7.2: The figure shows, our data collection system, consisting of a pair of eye-glasses (conceived by our team) linked to a computer used to acquire the images of one eye and to automatically produce a validated LoD signal.

7.5 Measurements

We setup our drowsiness monitoring system to produce one sample of the LoD (and PERCLOS) every 5 sec in Study A and every 20 sec in Study B. One reason for considering two distinct sampling intervals was to examine whether the conclusion concerning the nature of the underlying random process (RP) for LoD signals would dependent on the value of the sampling interval. One other reason for decreasing the sampling interval to 5 sec—thereby producing LoD signals with 4 times as many samples—was to provide more data for the statistical analysis.

7.6 About Study C

As part of a contract with a Belgian company and a car manufacturer, another data collection was performed, referred to as Study C.

However, since the work was done under a non-disclosure confidentiality agreement, we cannot report here in the experimental setup, the nature of the data collected, and the results obtained.

7.7 Conclusion

For the work reported in this thesis, we used data from two studies—called Study A and Study B—with a total number of 30 (17+13) participants.

Both studies used the same overall experimental protocol, and they differed only by (1) the groups of participants who took part in each study, and (2) the nature of the tests that each participant was asked to submit to in each study.

In both studies, we used the same drowsiness monitoring system designed, built, and validated by our team to determine the LoD of each participant periodically during test sessions.

We setup our drowsiness monitoring system to produce one sample of the LoD (and PERCLOS) every 5 sec in Study A and every 20 sec in Study B.

We also participated actively in (processing data from) Study C, under a non-disclosure confidentiality agreement.

Chapter 8

Adaptation in time of GBM RP model: need, challenges, and solutions

This chapter describes the need, challenges, and possible solutions for adaptation in time of the geometric Brownian motion (GBM) random process (RP) model. Section 8.1 motivates the use of the adaptive approach and describes its challenges. Section 8.2 presents possible solutions for adaptation. Section 8.3 briefly describes the adaptive approach for level of drowsiness (LoD) signals. Section 8.4 describes a pragmatic solution for an adaptive approach. Section 8.5 provides a novel interpretation of the proposed solution for adaptation. Section 8.6 describes the issue of real-time checking of the validity of the GBM hypothesis in a sliding time window. Section 8.7 describes the limitations due to the shortness of signals available to us. Section 8.8 describes a supporting experiment on synthetic data. Section 8.9 describes the relation between a GBM signal and portions thereof, and specifically, in terms of the conditions of normality and independence. Section 8.10 explores further the issue of normality. Section 8.11 describes the application of results to the problem of interest, i.e., drowsiness monitoring. Section 8.12 briefly alludes to the need for adaptation in finance. Section 8.13 concludes the chapter.

8.1 Introduction

We explain (1) why using a single, fixed GBM RP model (when relevant)—i.e., with parameters that are fixed once and for all—is not an acceptable approach in most applications, and, consequently, (2) why it is important to periodically adapt

the GBM RP model as a function of time.

In the subsequent sections, we address these issues in as much detail as possible, based on our current state of knowledge.

We suggest a potential, pragmatic strategy that should be workable in practical applications, such as in drowsiness monitoring, which is the central motivation for this thesis.

The GBM (RP) model is characterized by two parameters, namely the drift μ and the volatility σ. It is important to keep in mind that—by definition of the GBM model—these two parameters are necessarily fixed. This is clear from the stochastic differential equation (SDE) describing a GBM RP, where these parameters appear as fixed values (i.e., as constants), i.e., without any time dependence.

Since μ is fixed, the realizations of a given GBM RP will show only one of three possible behaviors/trends: growing, steady-state (i.e., constant), or decaying. Furthermore, the growth and decay are exponential in nature. We emphasize that, with fixed parameters, a realization can only show one of these trends and, furthermore, with a fixed "level of strength", both for the drift/trend and the volatility.

While it is often true that, during a long drive, the level of drowsiness (LoD) of a person generally increases, it would be extremely limiting to have a model that can only handle a single behavior, furthermore fixed at the beginning of a trip. For all practical purposes, such a model would be useless.

We should already mention that the idea of adapting the parameters of a GBM model with time leads to a philosophical question/dilemma. Indeed, strictly speaking, a GBM RP is characterized by fixed parameters μ and σ. We will see that some pragmatism will be needed to achieve potentially-useful results.

The above discussion shows, beyond a doubt, that there is an absolute need to adapt the GBM model as time progresses. This question is examined in some detail below.

8.2 Possible solutions for adaptation

One solution to address the issue mentioned above concerning the limitation of a unique, fixed model would be to define a model where the parameters μ and σ (and especially μ) are functions of time. Perhaps surprisingly, some of the mechanics for this exists, but apparently not all of it. The basis for this lies in the Îto process introduced in Section 4.4.2.

We start with a reminder of some fundamentals of the Îto process, and of the

special cases thereof, i.e., drifted Brownian motion (DBM) and geometric Brownian motion (GBM).

The SDE defining the Îto process is given in (4.51), which is repeated here for convenience, i.e.,

$$dX_t = a(t, X_t)dt + b(t, X_t)dW_t \,, \tag{8.1}$$

where $a(.,.)$ and $b(.,.)$ are deterministic functions.

The two special cases of interest are characterized by special forms for $a(t, X_t)$ and $b(t, X_t)$, i.e.,

- DBM: $a(t, X_t) = a$; $b(t, X_t) = b$,
- GBM: $a(t, X_t) = \mu X_t$; $b(t, X_t) = \sigma X_t$,

where a, b, μ, and σ are constants. In the important case of GBM, on gets the SDE of (4.55), i.e.,

$$dX_t = \mu X_t dt + \sigma X_t dW_t \,. \tag{8.2}$$

One should note that, in the case of GBM, $a(t, X_t)$ and $b(t, X_t)$ are necessarily RPs with independent parameter t, say A_t and B_t, this as a result of the presence of the RP X_t (and thus of a RV X_t at each t).

One should note that the Îto process is defined in a more general way in some references, such as in [31], namely by the SDE

$$dX_t = A(t)dt + B(t)dW_t \,, \tag{8.3}$$

where $A(t)$ and $B(t)$ are (general) RPs. One should note that the RP X_t defined by (8.3) is more general than RP X_t defined by (8.1) and thus (8.2). Indeed, the RP $A(t)$ in (8.3) is fully general, whereas the RP $a(t, X_t)$ is restricted to a special form. Among other things, the random nature of $a(t, X_t)$ is fully linked to the specific RP X_t, which is also the RP that is being defined by (8.1). This thus constitute a circular situation since $a(t, X_t)$ is defined in terms of the solution of the SDE. We emphasize that, in $a(t, X_t)$, the randomness is exclusively linked to the quantity X_t that we are trying to solve for, whereas $A(t)$ is a fully general RP. The same can be said for $b(t, X_t)$ and $B(t)$.

If we wish to make $\mu(t)$ and $\sigma(t)$ functions of time, we would need to consider the following forms for $a(.,.)$ and $b(.,.)$,

- "Adaptive" GBM: $a(t, X_t) = \mu(t)X_t$; $b(t, X_t) = \sigma(t)X_t$,

which yields the SDE

$$dX_t = \mu(t)X_t dt + \sigma(t)X_t dW_t \,. \tag{8.4}$$

Since the randomness in $a(t, X_t)$ and $b(t, X_t)$ comes exclusively from X_t, the above functions $\mu(.)$ and $\sigma(.)$ are necessarily deterministic functions.

Equation (8.4) is a special form of the general linear SDE [61, p. 110]

$$dX_t = (a(t)X_t + b(t))dt + (g(t)X_t + h(t))dW_t\,, \tag{8.5}$$

where $a(.)$, $b(.)$, $g(.)$, and $h(.)$ are deterministic functions.

Indeed, while there appears to be ways to solve this SDE [61], this would not really help us.

Indeed, as indicated above, the functions $\mu(t)$ and $\sigma(t)$ would necessarily need to be deterministic functions, as implied by both (8.1) and (8.5). This means that one would need to know them exactly before one can produce a solution, i.e., before one can use the corresponding model. This is clearly unrealistic.

We thus need to be able to deal with parameters μ and σ that evolve with time, but in ways that are not predictable in advance. One way to think about this is that the evolution of each of these parameters is itself a realization of some underlying RP.

It is critical to note, once again, that, in the general linear SDE in (8.5) (which can be solved), the four functions $a(.)$, $b(.)$, $g(.)$, and $h(.)$ are deterministic functions. Whereas this SDE can be solved, we are not aware of any method of solution for the general form of the Îto-process SDE, i.e., (8.3).

The above remark is linked to a comment made earlier (in Section 3.3.1) regarding the explanatory variables in survival analysis (SA). Indeed, in typical applications of SA, such as for medical trials, these variables are (fixed) constants. In a sense, the challenge in our type of application is that we are not dealing with constant values of the relevant parameters, but with parameters that are effectively RPs themselves.

In the case of the GBM RP model, on should thus conceptually view the parameters μ and σ as being RPs. Indeed, from one drive/trip to the next, the realizations of these RPs will be quite different.

Going from parameters μ and σ that are constants to parameters μ and σ that are RPs would represent a formidable challenge, not so much conceptually, but certainly from an implementation and calculation point of view.

As indicated above, one needs to deal with a RP that is governed by an SDE that is (1) a special form of the general Îto-process SDE (8.3), and/but (2) more complex than the general linear SDE (8.5). To the best of our knowledge, the particular type of SDE that we would need does not appear to be covered in the literature. Furthermore, it is very likely that developing the necessary theory and tools for such a RP would be a formidable challenge.

Given that dealing with the GBM RP, and making it useful in some applications, such as drowsiness monitoring, is already quite a challenge, we need to find pragmatic solutions for making a GBM model adapts with time.

8.3 Looking ahead

The previous chapter (Chapter 7) briefly describes the studies that have provided LoD signals for our research work, namely, Studies A, B, and C. In this section, we make some comments about the results described in the next chapter (Chapter 9). Indeed, these results are connected to the need for adaptation discussed in the present chapter.

In the next chapter, we will see that all signals from Studies A and B are well described by a GBM model with fixed parameters. The likely reason for this is that each of these signals is short, and that the trend in this short signal is mostly increasing, or mostly steady-state, or mostly decreasing. We will see that this is also confirmed by experiments where we estimate the two parameters (μ and σ) using a sliding window, that is moved in successive one-time-step increments. Indeed, the parameters generally evolve relatively slowly with time.

We should point out that, since we are dealing with LoD signals that are relatively short, at least for Studies A and B, these signals do not exhibit a behavior that is visually exponential, either growing or decaying. A fortiori, in these two studies, we have not encountered LoD signals that show significant (exponential) growth or decay. The fact that a signal does not exhibit a visually-obvious exponential trend (whether growing or decaying) is not a reason for saying that a signal is not GBM. We illustrate this in a later section.

In fact, in a safe drive/trip, one should not expect to see such extreme behaviors during most of the time, except under exceptional circumstances (susceptible to lead to an accident). However, one should be ready to handle them at any point in time. This is one more reason for adapting the underlying model, for example to almost instantly change, e.g., from a steady-state trend to an exponential-growing trend. The solution that we ultimately suggest is perfectly capable of such a feat.

One should note that the exponential growth and decay that are exhibited in Figure 4.5 (a) and (b), respectively, do not have an opportunity to develop fully in the cases of Studies A and B.

8.4 Pragmatic solution for adaptation

The net result of the strategy just described is that we have a GBM model that evolves with time, with its two parameters being estimated as often as deemed necessary, on the fly and in real-time.

The above strategy means that we consider that the realization at hand behaves "locally" (in time) and, more precisely, in the recent past (up to the present) according to a GBM model. In other words, we do not assume that that there is a single GBM model underlying the whole processing, but a multitude of such models, with parameters adapted both periodically and locally.

In the next chapter, we show examples of adaptation on signals from Study A and Study B. Because the signals in these studies are relatively short, we use windows with a duration of 5 minutes. This means that we assume that the realization at hand (and, thus, the underlying RP) evolves according to a fixed GBM model over the last five minutes. In an actual, operational system, one might envision using longer windows, such as of 30 minutes. The idea is to be able to continuously capture the developing trends, i.e., growing, steady-state, or decaying. In Study C, where the LoD signals are longer, we had the possibility of experimenting with windows longer than 5 minutes. However, the results obtained cannot be reported in this thesis.

8.5 Novel interpretation of proposed solution for adaptation

Earlier, we pointed out that what we would ideally need is an Îto-process model where its defining deterministic functions $a(t, X_t)$ and $b(t, X_t)$ would first be reduced to $a(t)$ and $b(t)$, and where these two deterministic functions would then be treated as two distinct RPs. These RPs would correspond to the drift and volatility, and would thus logically be denoted by $M(t)$ and $\Sigma(t)$.

The idea and solution of using a sliding window to estimate the parameters μ and σ (of a GBM RP model) on the fly can thus be viewed as a very pragmatic/practical way of effectively implementing an Îto-process model where $a(t, X_t)$ and $b(t, X_t)$ would be the RPs $A(t) \equiv M(t)X_t$ and $B(t) \equiv \Sigma(t)X_t$.

Another way of describing this solution is to say that we effectively replace an Îto-process model with defining functions that are the RPs $M(t)$ and $\Sigma(t)$ (which is fully unconventional) by a multitude of successive GBM RPs where the fixed parameters μ and σ are estimated on the fly using past data, typically by using a

sliding window.

Still another way of describing/interpreting this solution is to say that using a GBM RP model with parameters μ and σ that are adapted on the fly is effectively very close to using an Îto-process model where the deterministic functions $a(t, X_t)$ and $b(t, X_t)$ are "replaced" by the RPs $A(t) \equiv M(t)X_t$ and $B(t) \equiv \Sigma(t)X_t$.

To the best of our knowledge, this way of looking at the problem at hand is novel.

This view could thus be applied to any domain where the GBM parameters μ and σ need to be estimated on the fly such as in the present application of drowsiness monitoring and in finance.

8.6 Real-time checking of validity of GBM hypothesis in a window

In the above proposal of adapting–continuously and in real-time–the GBM model using a sliding time window butting against the present time, one should, strictly speaking, have the assurance that the data in the window is GBM, or have the means (i.e., algorithms) to determine whether this is the case or not.

Let us immediately say that, even if the data is not GBM in a given window, we can still compute the parameter μ and σ, and use them to make predictions. The real question is what the consequences are of using a GBM RP model for prediction when the data in the window is not GBM. This specific question is not addressed here.

One should remember that, to check whether a given signal is GBM or not, the standard procedure is to check that the samples of this signal verify the two conditions of normality and independence. Strictly speaking, for each new window, one should check that the samples in the window verify these two conditions. Since the most reliable tests for these conditions are graphical, it seems that it would be difficult, if not impossible, to apply them in real-time to each new window.

If there was a possibility of checking whether the samples in a window are GBM or not, one might imagine having a flag that tells the drowsiness monitoring system whether the GBM assumption is valid or not. If the samples are not GBM, one can simply skip modeling and predicting at that particular moment in time.

This is similar to a GPS system that issues a warning (either to an automated system or to an operator) when not enough satellites are in view, and that the navigation may not be reliable.

One should note that there could be separate flags for the results of the tests

of normality and independency. Some later developments suggest that this may in fact be a good idea, as the implementation of the test(s) for each of these two conditions (if at all possible) may have different degrees of complexity.

In the present state of research, and in the present thesis, we always make the hypothesis that the data in a window is GBM.

Future research might lead to developing new ways of verifying the validity of the GBM assumption in each successive, present window, in real-time. Developing new automatic algorithms to deal with such checking would constitute a great contribution to the field.

8.7 Limitations due to shortness of signals available to us

In the next chapter, we show that all the signals in Study A and Study B are GBM when taken in their entirety.

For these particular signals, we have, in principle, the possibility of checking whether the samples within each window of interest are GBM or not. However, since the signals are short (at most 110 samples), each window is necessarily quite small and thus has few samples; one should thus expect that there would be insufficient data to apply the tests of normality and independency in a meaningful way.

We have applied the pairs of graphical tests to a few windows applied to one of signals in Study A, called Signal A, and we have effectively noticed that the plots are not convincing. These results are thus not shown here. However, this does not indicate that the principles used, and the assumptions made, are incorrect. It is simply a reflection of the fact that the signals available are too short. Therefore, all experiments described later, in Chapters 9 and 10, using sliding windows should be viewed as proofs of concepts. This being said, we emphasize that we used window of more meaningful lengths in the experiments performed in the context of Study C.

Because of the lack of appropriate real-life data to demonstrate the validity of the use of a sliding window to adapt the parameters of the GBM RP model (and to perform predictions), we performed a related experiment using synthetic data. This experiment is described in the next section.

8.8 Supporting experiment on synthetic data

We wish to answer the following question: if a signal is known (in some way) to be GBM as a whole, can one assume that the "subsignal" within any window (whether sliding of not) is also GBM?

As an illustration, consider the case of Study A and Study B. As already indicated, we show in the next chapter that each LoD signals in these studies can reasonably be assumed to be GBM. We wish to know whether one can expect/assume the subsignals defined by each window of interest to be also GBM (perhaps with different parameters). As already pointed out, these signals are too short to apply the graphical tests of normality and independency in a meaningful way.

Therefore, we decided to have recourse to synthetic data to examine this question. In short, we generate a long synthetic signal that is guaranteed to be GBM, we extract various portions of it, and we check whether these portions are also GBM. For the whole signal and for each subsignal, we apply all tests of Section 6.2, both graphical and numerical.

Figure 8.1 (a) shows the original, long, synthetic DT signal, referred to below as the base signal. This signal is, by construction, guaranteed to be GBM. Figure 8.1 (b) shows the first half of the base signal, Figure 8.1 (c) the first quarter of the base signal, and Figure 8.1 (d) the first eighth of the base signal. The four signals have respective lengths of 2048, 1024, 512, and 256 (samples). (All four signals are denoted by the generic notation x_n.)

To verify that the base signal is GBM and to determine whether the 3 subsignals extracted from it are GBM, we applied to each of these four signals the full battery of tests of Section 6.2 to the log-ratio (LR) samples, i.e.,

1. for normality condition: histogram, Q-Q plot, S-W test
2. for independency condition: linear regression.

Figure 8.2 shows, for each of the four signals of Figure 8.1, (1) the corresponding histogram of LR samples for the signal, and (2) the corresponding "normal distribution fit". The subfigures of both figures are "registered", which means, e.g., that the upper-left plot of Figure 8.2 is the histogram of signal in the upper-left plot of Figure 8.1.

Figure 8.3 shows, in a similar way, the Q-Q plots of the four signals of interest.

We also applied the S-W test to all four signals. In all four cases, the test succeeded, in the sense that it could not reject the hypothesis of normality. Recall that this test can only accept or reject the hypothesis of normality. An acceptation

is, however, not a guarantee that the data is normally distributed. However, this is the best that the S-W test can do.

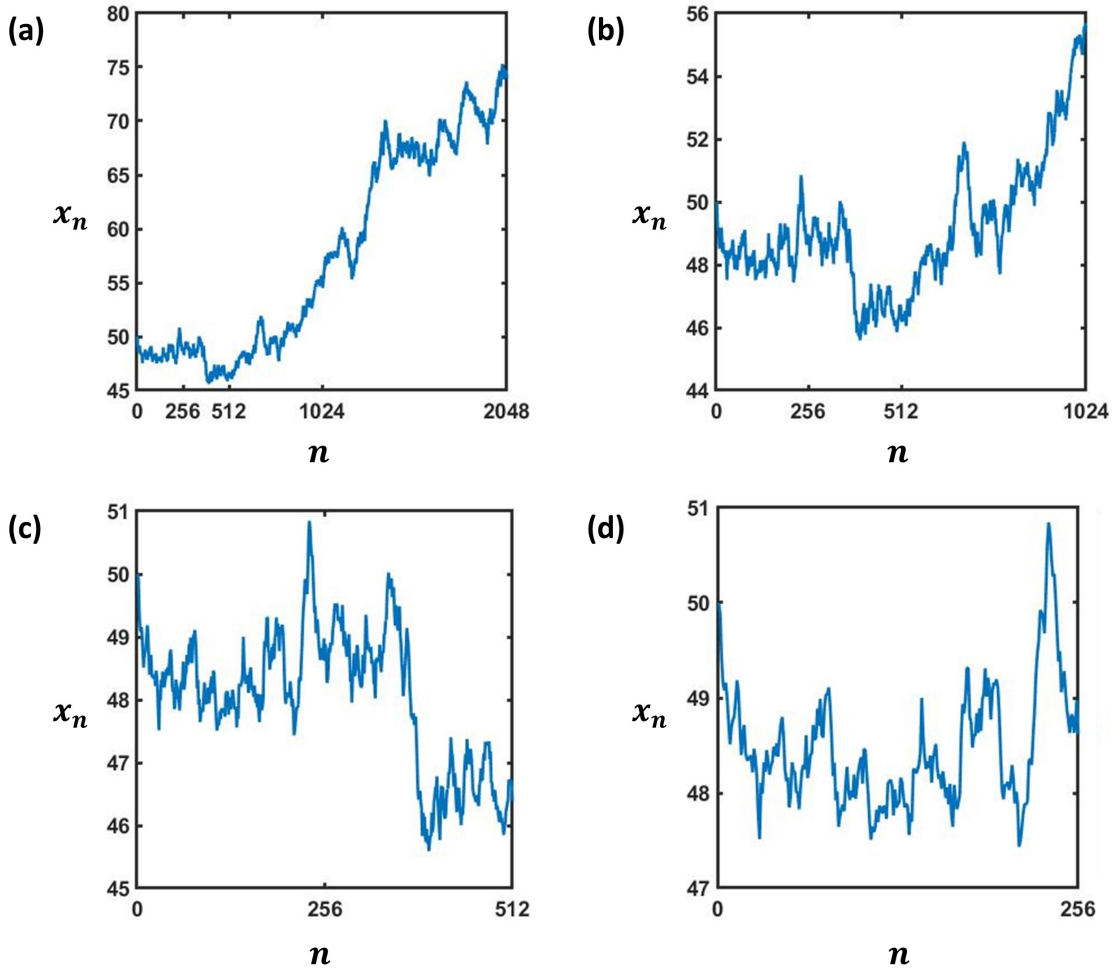

Figure 8.1: Example, synthetic, GBM signal and 3 shorter signals extracted from it. (a) Synthetic GBM signal produced by an algorithm, referred to as the "base signal". (b)-(d) Portions of the base signal corresponding respectively to its first half, first quarter, and first eighth, with each referred to as a "subsignal". The 4 successive DT signals have the following numbers of samples: 2048, 1024, 512, and 256.

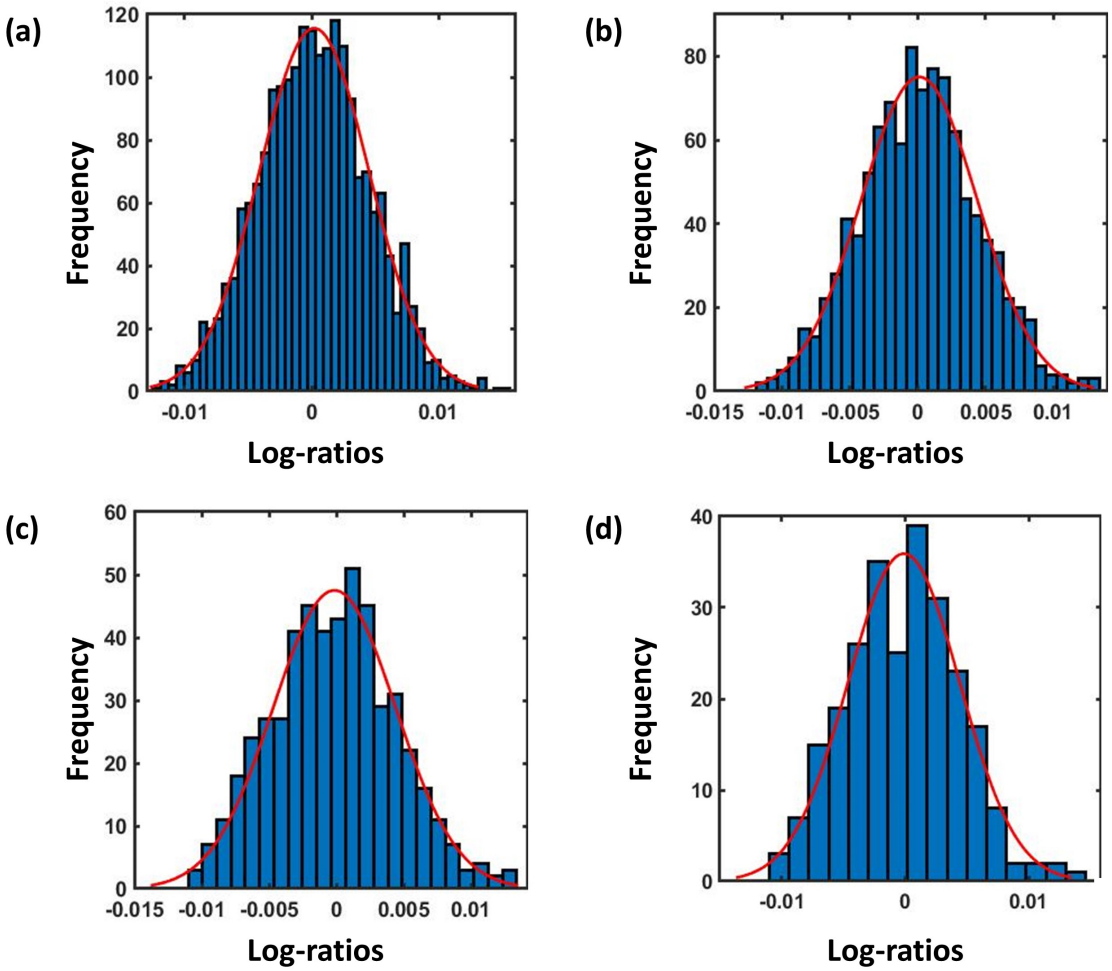

Figure 8.2: Assessment of the normality condition (for GBM realizations) for each of the 4 signals of Figure 8.1, using histograms of log-ratios (LR) samples. Each plot shows the histogram and the corresponding "normal distribution fit".

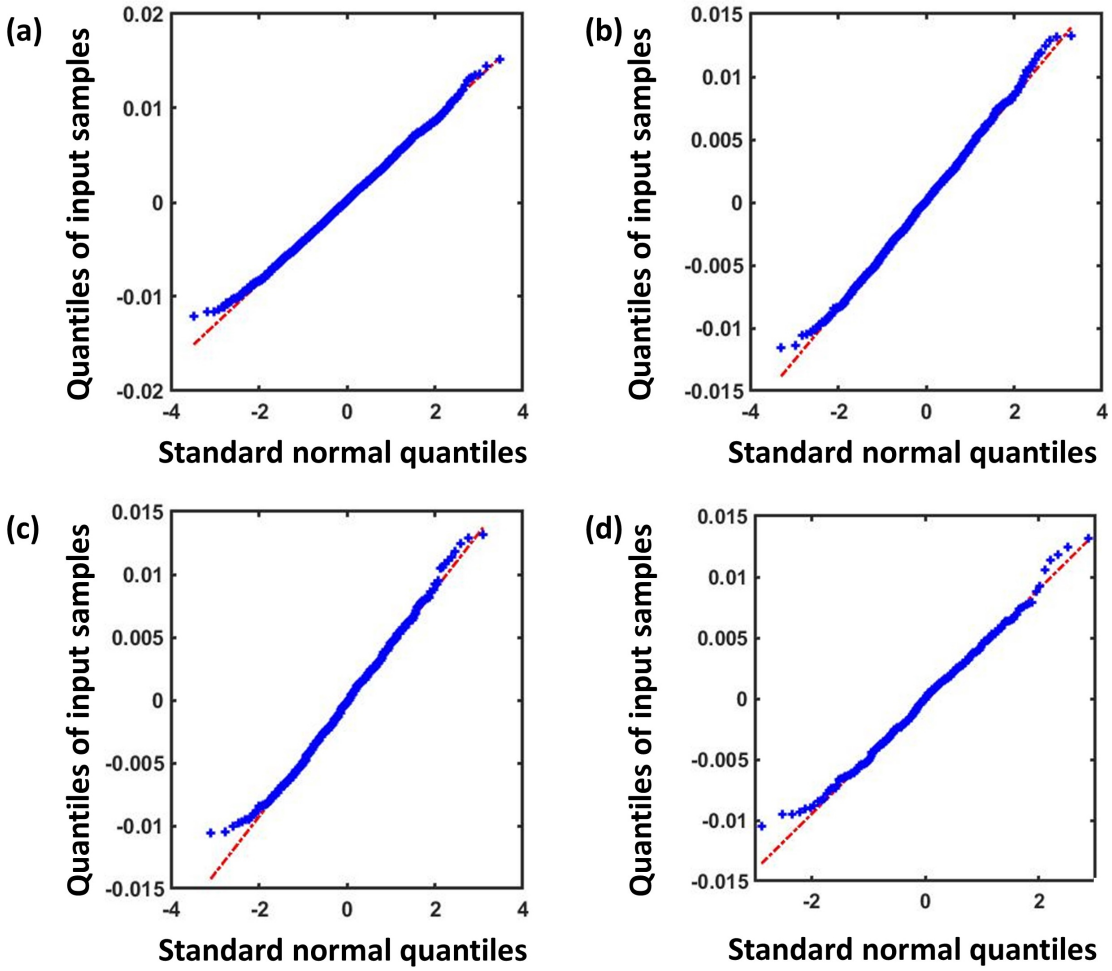

Figure 8.3: Assessment of the normality condition (for GBM realizations) for each of the 4 signals of Figure 8.1, using Q-Q plots of log-ratios (LR) samples. Each plot shows the scatter plot and the corresponding regression line.

Based upon the 3 tests above (2 graphical and 1 numerical), we can conclude that the LR samples are normally distributed, and thus satisfy the normality condition.

Figure 8.4 shows, similarly to the two previous figures, the regression plots of the LR ratios. The examination of the four plots allows us to conclude that all four signals of interest satisfy the independency condition.

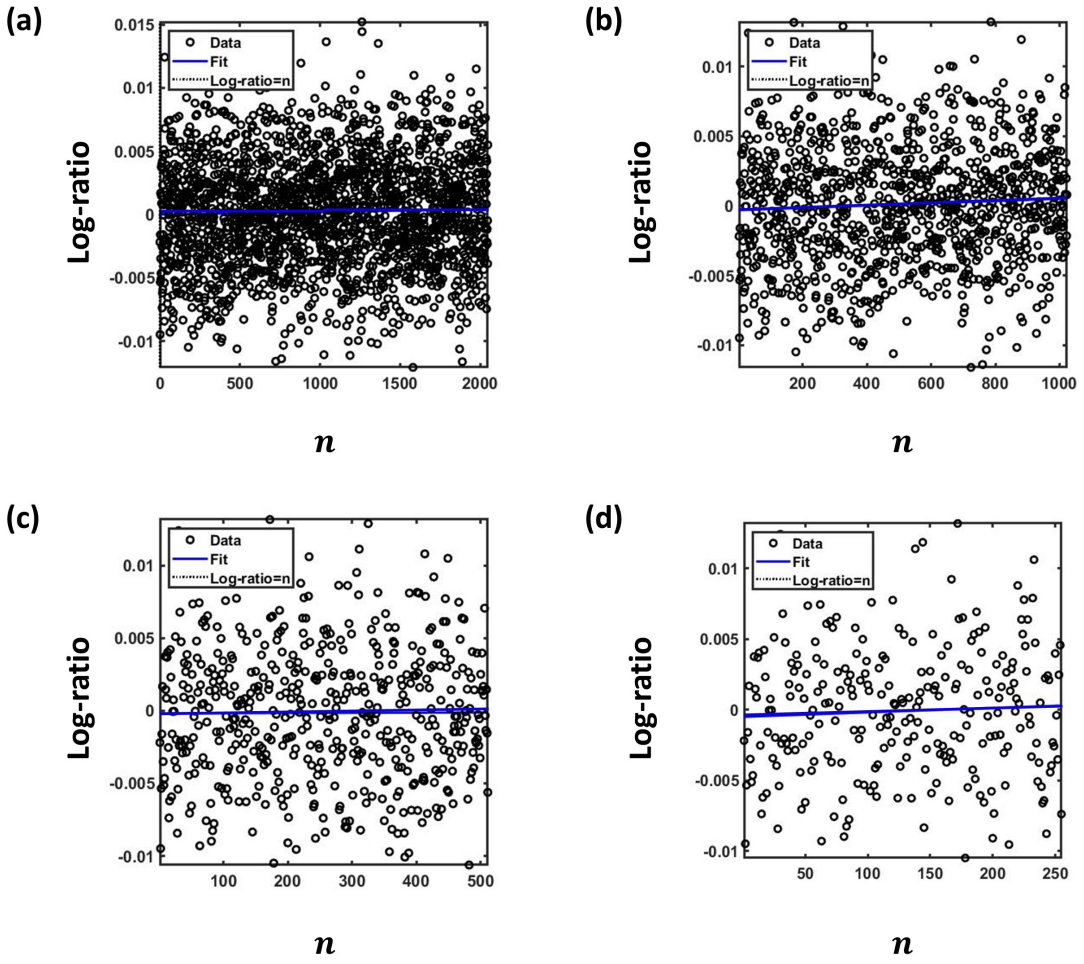

Figure 8.4: Assessment of the dependency condition (for GBM realizations) for each of the 4 signals of Figure 8.1, using regression plots of log-ratios (LR) samples.

Based upon the results of the above tests, we conclude that the four signals of interest, i.e., shown in Figure 8.1, are GBM and, more precisely, are (valid) realizations of an underlying GBM model.

Of course, since the base signal was mathematically constructed to be GBM, it is reassuring that all tests of normality and independency are satisfied for this specific signal. The interesting outcome of the experiment is that the first half, first quarter, and first eighth of the base signals also successfully pass all tests of normality and independency, allowing us to conclude that they are also GBM.

We emphasize that the numerical test of normality, i.e., the S-W test is successfully passed by all four signals. In the next chapter, one will appreciate the

significance of this remark.

It is worth examining again the four plots of Figure 8.1. The base signal clearly exhibits a growth, which is exponential in nature. This exponential growth is also visible in the first half of the base signal. By contrast, the first quarter and the first eighth of the base signal do not exhibit an exponential growth, and not even a growth. In the case of the first quarter of the base signal, one might even argue that there is a decay.

One should take notice of the fact that all four signals of Figure 8.1 are realizations of the very same underlying GBM RP with a pair of fixed parameters μ and σ. Despite this common underlying model, the appearances of the four signals in Figure 8.1 are widely different.

We take this opportunity for pointing out that, by just looking at a signal, it is generally difficult to determine visually whether this signal is GBM, especially if there are no clues of significant exponential growth or decay.

The subsignals of Figure 8.1 (c)-(d) are akin to what we might encounter in a short window. We have computed the values of the parameters μ and σ for each of the four signals of Figure 8.1. It turns out that these values of μ and σ are different in all four cases. At first sight, one might be surprised that, for the subsignals, one does not find the values of the parameters used to produce the base signal. However, it is clear that the "drift" behavior is different in the four cases. As pointed earlier, whereas the first two signals exhibit a growth (of exponential nature), the 3^{rd} shows a mix of steady state and decay, and the 4^{th} a steady state.

We also take this opportunity to point out that looking at a long GBM signal only through a time window is akin to looking at the world through a real house window. If one looks at a landscape through a house window and sees a flat garden, one cannot exclude the possibly that there is a steep hill just outside the field of view. In other words, one should not expect to understand the full state of the world or signal by looking at it through a window.

While the present experiment with synthetic data does not prove in a formal way the validity of adapting the parameters of the GBM model, it goes a long way toward showing that it is reasonable and meaningful to do so.

We also point out that the numerical S-W test works well on the four synthetic signals. This may indicate that it might work better on longer signals. However, we will see that the test also becomes very sensitive as the number of samples increases. The real reason for the success of this very sensitive test is thus almost certainly due to the fact that the signal is mathematically constructed to have the desired Gaussian property. In this regard, one should note that "things" in the real world may be Gaussian-like, but never perfectly.

In the next subsection, we examine in a more formal way the relationship

between the GBM property of a long signal and the potential GBM property of subsignals extracted from it, e.g., using a window (typically a sliding window).

8.9 About the relation between a GBM signal and portions thereof

We revisit here the question examined above using a long synthetic signal. In short, if we have a long signal that is GBM, what can we say about contiguous portions of this signal, obtained, say, using a window (whether sliding or not)? More specifically, can we say that these portions, or subsignals, are automatically GBM?

8.9.1 First argument

Consider a long signal, referred to (as before) as the base signal. Assume that we know that this signal is GBM, either by construction, or as a result of the satisfaction of both the normality condition and the independency condition. One should remember that these two conditions apply to the log-ratio (LR) samples, not to the signal samples themselves. We now successively examined the two conditions.

For the normality condition, the question at hand can be phrased as follows. Knowing that the base signal necessarily satisfies the normality condition, does a subsignal thereof automatically verifies this condition? We examine this question in detail in the next subsection. As a heads-up, we can already say that the answer is "no", at least in general.

For the independency condition, the question at hand can be phrased as follows. Knowing that the base signal necessarily satisfies the independency condition, does a subsignal thereof automatically verifies this condition? The answer is essentially "yes". We now justify this positive answer.

In highly simplified terms, the independency condition essentially looks at all pairs of LR samples of the base signal and determines whether they are independent. (For this sentence to be meaningful, one must treat the LR samples as realization of RVs, as discussed elsewhere.) Consider two (LR) samples of the subsignal. These two samples are also two samples of the (longer) base signal. If these two samples are known to be independent for the base signal, then they are automatically independent for the subsignal.

The above discussion suggests that, in the present context, the issue of normality is more problematic than the issue of independency.

8.9.2 Second argument

We have indicated in Section 4.4.2.2 that, when a RP X_n is GBM, the RP consisting of the log-ratios (LRs) RVs of X_n is a white Gaussian noise (WGN) RP, i.e., a white noise (WN) where each sample comes from a common Gaussian PDF.

Therefore, a realization of the LR RP is a realization of a WGN, and a plot of any such realization "looks like WGN", something that we have some visual intuition for.

It seems clear that, if we extract any contiguous portion of a WGN, we will get a WGN. In making this statement, we appeal, in part, to one's intuition.

This second argument offers a strong support to the hypothesis that, if a base signal is GBM, then any contiguous portion of it (e.g., obtained by windowing) is also GBM.

Therefore, this constitutes a reinforcement of the conclusion reached with the synthetic signal considered above.

8.10 Further exploration of issue of normality

Above, we indicated that two conditions must be met for a RP to be GBM, namely the normality condition and the independency condition.

The question raised above can be phrased as follows. If a signal is known to be GBM, can one say the same about any contiguous portion thereof, e.g., extracted using a window (sliding or not)? As before, we refer to the full signal as the base signal, and to the portions extracted from it as subsignals.

The earlier discussion indicates that, if the independency condition is satisfied for the base signal, the condition is also necessarily satisfied for a subsignal thereof. By contrast, the same discussion indicates that this is generally not true for the normality condition.

Below, we explore in more detail this question concerning the normality condition. We explore the question from a more theoretical point of view, to examine what we can affirm and what we cannot affirm.

8.10.1 Setting up of problem

We consider that there exist some underlying population (in the usual sense of statistics and clinical studies). The exact nature of the population is irrelevant for the present discussion. Ultimately, we will use the conclusion of the present

development in the case where the population consists of all the samples of a DT signal of interest, and, specifically, of an LoD signal recorded for a long period of time, say, for 1 hour to be concrete.

We assume that the population is characterized by a RV X. This RV X is, of course, characterized by a PDF/distribution, which we denote by the generic notation $f_X(x)$. Recall that the "independent"/running variable x corresponds to realizations of the RV X. At this stage, $f_X(x)$ is fully general. Specifically, there is no requirement that it be Gaussian, i.e., normal.

For future reference, we denote its mean by μ and its standard deviation by σ; σ^2 is, of course, the corresponding variance. We refer to μ and σ^2 as the population mean and population variance, respectively.

In statistical problems and applications, one often considers drawing several values, or samples, from the population of interest, and these values are assumed to be drawn independently of each other.

For later developments, the right way to proceed is to represent the "values" that are drawn by RVs. If one draws n values, then one uses n RVs, denoted by X_1, X_2,$\cdots$, X_n. It is crucial to realize that all these RVs correspond to the same underlying sample space (or universal set) Ω. A specific drawing thus corresponds to considering/picking a specific elementary (experimental) outcome $\omega_0 \in \Omega$. As soon as ω_0 is fixed, one gets deterministic values $x_1 \stackrel{\Delta}{=} X_1(\omega_0)$, $x_2 \stackrel{\Delta}{=} X_2(\omega_0)$,$\cdots$, $x_n \stackrel{\Delta}{=} X_n(\omega_0)$. One thus deals with both the RVs X_i and their realizations x_i, for $i = 1, \cdots, n$. One could give a precise meaning the phrase "independent drawing". However, this boils down to saying that the X_is are independent RVs, i.e., with a joint PDF that factorizes.

Since all the X_is correspond to (i.e., come from) the same underlying population described by the PDF $f_X(x)$, one can immediately state that the PDF of each X_i is identical to the PDF $f_X(x)$ (of RV X), which means that $f_{X_i}(x) \equiv f_X(x)$ for $i = 1, \ldots, n$. The X_is are thus identically distributed (i.d.).

Given that the X_is are independent (RVs), we conclude that the X_is are independent, identically distributed (i.i.d.) (RVs). Since we assume that the population has mean μ and variance σ^2, each X_i also has mean μ and variance σ^2.

8.10.2 Sample mean and sample variance of drawn samples

Given n samples/realizations x_n, one can compute their mean and variance. We refer to these parameters as the sample mean and the sample variance. Importantly, these should be treated as RVs. Indeed, as ω_0 changes, these parameters

change. The pair of relevant RVs is now introduced.

The sample mean (for n realization) is denoted by $\bar{X}_n$, and is defined as [80, 63]

$$\bar{X}_n = 1/n \sum_{i=1}^{n} X_i \,, \tag{8.6}$$

and the sample variance (for the n realization) is denoted by $\bar{S}_n$, and is defined as [80, 63]

$$\bar{S}_n = \frac{1}{n-1} \sum_{i=1}^{n} (X_i - \bar{X}_n)^2 \,. \tag{8.7}$$

As a check, note that the RHSs are RVs, so that the LHS are also RVs, as they should be.

As alluded to above, as ω_0 changes, the realizations of $\bar{X}_n$ and $\bar{S}_n$ generally change.

We emphasize that the sample mean (whether RV or realization thereof) is generally not equal to the population mean μ. One additional clue of this is that μ is fixed whereas $\bar{X}_n$ generally change at each draw, i.e., for each ω_0. One can make a similar statement for the variance.

We repeat that, above, we did not make any assumption about the shape/form of the PDF $f_X(x)$. Specifically, we did not assume that it is a Gaussian/normal PDF.

8.10.3 Hypothetical distribution of drawn samples

Above, we described a draw via n RVs X_i and their realizations x_i. We know that the X_is all have the same PDF. However, despite this fact, the X_is are distinct RVs. Since the X_is are distinct RVs, we cannot talk about a PDF for the X_is. Of course, we could place the X_is in a vector and treat this vector as a random vector (with a multidimensional PDF) but this would not help here. Even though we cannot talk about a PDF of the X_is, we can produce a histogram of the realizations x_i. Then, one can talk about the shape/form of this histogram, and it is meaningful to compare the histogram with properly-scaled PDFs, in particular with the PDF of the population, i.e., $f_X(x)$.

One thing is absolutely certain. It is a complete utopia to think that the histogram of the x_is could have a shape identical, or similar, to the shape of $f_X(x)$.

As an example, assume that $f_X(x)$ is bell-shaped, such as would be the case for a Gaussian. It could very well be that the histogram of the x_is is U-shaped (with

cutoff or rolloff at the extremities). Indeed, no one has any control on what values show up for the x_is in any particular draw. As another example, the histogram could be completely flat/constant.

If $f_X(x)$ is actually Gaussian, there does not exist any principle that allows us to say that the histogram of the x_is is Gaussian-like. On the contrary, we will definitely encounter many instances of histograms that are not at all Gaussian-like.

Therefore, in light of what we know at this point, one should not expect the histogram of n samples drawn from a population with PDF $f_X(x)$ to have a histogram of the same shape as $f_X(x)$. For completeness, let us repeat that it is meaningless to talk about a PDF of the x_is. Among other things, the x_is are realizations (i.e., deterministic quantities) and not RVs.

Since the case of a Gaussian $f_X(x)$ is important in our context, let us specifically say that, if the population has a Gaussian PDF, one should not expect the histogram of the x_is to have a Gaussian shape.

Even though we cannot say anything about the shape of the histogram of the n values/samples drawn from a given population, we can make useful statements about the sample mean and variance (introduced above) in comparison with the population mean and variance. Admittedly, these statements do not shed further light on the question of the normality/Gaussianity of a subsignal.

8.10.4 Important property of sample-mean RV of drawn samples

The central limit theorem (CLT) provides a key limiting property of the sample-mean RV $\bar{X}_n$ (introduced above) of n independent sample RVs X_1, X_2,$\cdots$, X_n. (Recall that these n independent RVs are the way to represent the independent draw of n samples from the underlying population.) The CLT requires that μ and σ be finite, but this can just be viewed here as being a mere "technical" condition.

The CLT says that, as the number of samples becomes large, i.e., as $n \to \infty$, the RV $\bar{X}_n$ tends to a Gaussian(/normal) PDF with mean μ and variance σ^2/n, i.e.,

$$\bar{X}_n \sim \mathcal{N}(\mu, \sigma/\sqrt{n}) \text{ as } n \to \infty \,.$$

This limiting behavior can also be expressed in terms of the normalized RV [63]

$$\bar{Z}_n = \frac{\bar{X}_n - \mu}{\sigma/\sqrt{n}} \,.$$

Indeed, one gets

$$\bar{Z}_n \sim \mathcal{N}(0,1) \,,$$

which means that the PDF of $\bar{Z}_n$ is the standard normal/Gaussian PDF.

It is useful to note that that the CLT is valid for any (population) PDF $f_X(x)$ with (finite) mean μ and variance σ^2. Specifically, there is no need here for $f_X(x)$ to be a Gaussian PDF.

In the case where the X_is correspond to an underlying population, the X_is are automatically identically distributed (i.d.). However, the CLT also applies if the PDFs $f_{X_i}(x)$ of the X_is are different, provided that they all have the same/common (finite) mean μ and variance σ^2.

8.10.5 Important property of the sample-variance RV of drawn samples

The development in the previous section (on the sample-mean RV) is based entirely on the CLT. Since the CLT only requires the PDFs of the individual $f_{X_i}(x)$ to have the same (finite) mean and variance, there was no need to require (above) that all $f_{X_i}(x)$ be identical and that they be Gaussian. One should also keep in mind that the CLT applies only in the limit as n becomes large, i.e., as $n \to \infty$.

By contrast, in the present section, we need to assume that the population PDF $f_X(x)$ is Gaussian. (This is not really a problem in our current application since the LR RVs are, in principle, Gaussian. In fact, the analysis that we are in the midst of is fully motivated by this issue of whether the samples of a subsignal are Gaussian.)

It follows that all X_is have the Gaussian $f_X(x)$ as their common PDF. We thus assume that

$$X_i \sim \mathcal{N}(\mu, \sigma)\,.$$

This means that, for the normalized RV

$$Z_i \triangleq \frac{X_i - \mu}{\sigma}\,,$$

we have

$$Z_i \sim \mathcal{N}(0, 1)\,.$$

Below, we do not derive in detail the PDF of the sample-variance RV, which we have denoted by $\bar{S}_n$. We just outline the main steps. The details can be found in [80, 63].

Since we wish to deal with the sample-variance RV, one should expect to have to deal with the squares of the RVs X_i, or of their normalized versions Z_i. Below, we consider the square of Z_i, i.e., Z_i^2.

It is well known that the RV Z_i—i.e., the square of the standard normal RV—is chi-square with one (1) degree of freedom (DOF) [63]. We can thus write

$$Z_i^2 = (\frac{X_i - \mu}{\sigma})^2 \sim \chi^2(1)\,, \tag{8.8}$$

where the number in parenthesis is the number of DOFs, here 1.

It is also well-known that the RV that is the sum of the squares of n independent RV Z_is is chi-square with n DOFs [63]. We can thus write

$$S \triangleq \sum_{i=1}^{n} Z_i^2 = \sum_{i=1}^{n} (\frac{X_i - \mu}{\sigma})^2 \sim \chi^2(n)\,. \tag{8.9}$$

Relation (8.8) is obviously (8.9) with n set to 1.

Note that, so far, by contrast with what we did in the previous section, we are considering some arbitrary, finite value of n. Specifically, we have not, so far, looked at what happens as $n \to \infty$.

When carrying out the full development, it is crucial to notice that (8.8) and (8.9) involve the population mean μ and variance σ^2, and not the sample mean and/or variance.

Furthermore, the quantity that is of interest here is the sample-variance RV $\bar{S}_n$ introduced via (8.7), and repeated here for convenience, i.e.,

$$\bar{S}_n = \frac{1}{n-1} \sum_{i=1}^{n} (X_i - \bar{X}_n)^2\,. \tag{8.10}$$

One should note that this relation does not involve the population mean μ and variance σ^2.

One can show [63] that

$$\bar{S}_n \sim \chi^2(n-1)\,. \tag{8.11}$$

The fact that (8.9) and (8.11) respectively feature n and $n-1$ DOFs can be interpreted as follows. Using the sample mean instead of the population mean leads to a loss of one DOF.

We denote the PDF for a $\chi^2(k)$ RV by $f_{X,k}(x)$, where k is, of course, the number of DOFs. On can show that this PDF is given by [32]

$$f_{X,k}(x) = \begin{cases} \dfrac{x^{\frac{k}{2}-1} e^{-\frac{x}{2}}}{2^{\frac{k}{2}} \Gamma(\frac{k}{2})} & x > 0 \\ 0 & \text{otherwise}\,. \end{cases} \tag{8.12}$$

One should note that this PDF is fully characterized by k, which is the number of DOFs.

Figure 8.5 shows the PDF $f_{X,k}(x)$ for several values of k.

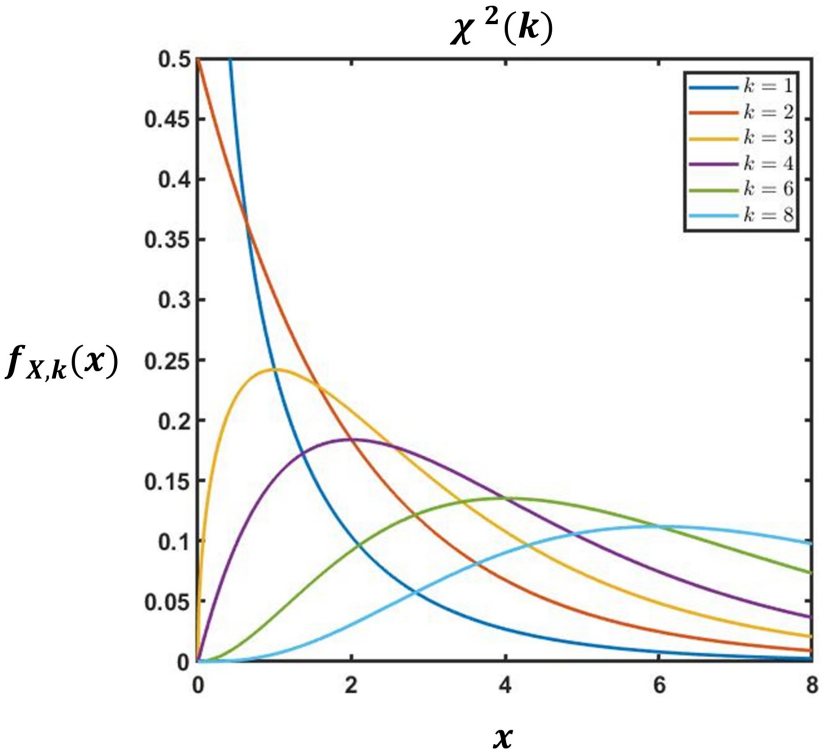

Figure 8.5: Probability density function (PDF) $f_{X,k}(x)$ of the $\chi^2(k)$ RV for several values of its parameter k, which is the number of degrees of freedom (DOFs) [63].

The key parameter of the $\chi^2(k)$ PDF are as follows:

- mean $= k$
- median $\approx k(1-\frac{2}{9k})^3$
- mode $= \max(k-2, 0)$
- variance $= 2k$.

We can use some of these formulas to obtain useful results for some developments below.

From (8.8), we know that the (normalized) RV $Z_i^2 = (X_i - \mu/\sigma)^2$ is $\chi^2(1)$. Using the above formulas for the mean and variance, we find that Z_i is characterized by

$$\begin{aligned} &\text{mean}(Z_i) = k = 1\,, \\ &\text{variance}(Z_i) = 2k = 2\,. \end{aligned} \tag{8.13}$$

From (8.9), we know that the RV $S \stackrel{\Delta}{=} \sum_{i=1}^n Z_i^2 = \sum_{i=1}^n (X_i - \mu/\sigma)^2$ is $\chi^2(n)$. Using the above formulas for the mean and variance, we find that S is characterized by

$$\begin{aligned} &\text{mean}(S) = k = n\,, \\ &\text{variance}(S) = 2k = 2n\,. \end{aligned} \tag{8.14}$$

Rather than considering the straight sum S, we can consider the average RV $A = S/n$. From the results just above, we find that A is characterized by

$$\begin{aligned} &\text{mean}(A) = n/n = 1\,, \\ &\text{variance}(A) = 2n/n^2 = 2/n\,. \end{aligned} \tag{8.15}$$

If we compare these values to those for (a single) Z_i, we see that the mean remains equal to 1, while the variance is divided by n. For future comparison, note that we have the following relation: $\text{standard-deviation}(A) = \sqrt{2/n}$.

As in the previous section, we now examine what happens for large values of n, i.e., as $n \to \infty$.

We consider two distinct approaches.

The first approach for examining the behavior for large n is as follows.

One should recall that the quantity of interest is the sample mean $\bar{S}_n$, rather than A just above. Relation (8.10) reads $\bar{S}_n \sim \chi^2(n-1)$. One can show that the PDF of a $\chi^2(k)$ RV becomes more and more Gaussian as k increases [32]. One can also see this trend in Figure 8.5.

The second approach for examining the behavior for large n is as follows.

From (8.8), we know that the (normalized) RV $Z_i^2 = (X_i - \mu/\sigma)^2$ is $\chi^2(1)$. Using the above formulas for the mean and variance, we find that this RV is characterized by

$$\begin{aligned} &\text{mean}(Z_i) = 1\,, \\ &\text{variance}(Z_i) = 2\,. \end{aligned} \tag{8.16}$$

This result is already given above.

The LHS of (8.9) contains a sum of RVs that are each $\chi^2(1)$. The key point here is that these RVs all have the same mean (1) and variance (2). (They are also identically distributed, but this is not important here.) We are thus in a position to invoke the CLT.

The CLT say that, as the number of samples becomes large, i.e., as $n \to \infty$, the sample-mean RV of interest here, i.e., the RV A introduced above, tends to a Gaussian(/normal) PDF with mean μ and variance σ^2/n, i.e.,

$$A \sim \mathcal{N}(\mu, \sigma/\sqrt{n}) \text{ as } n \to \infty \,.$$

The value to be used here for the mean and variance are 1 and 2, respectively (see above), which yields

$$A \sim \mathcal{N}(1, \sqrt{2/n}) \text{ as } n \to \infty \,.$$

It is useful to note that the mean and variance of the RV A are identical to the ones found via the first approach above.

The CLT approach also confirms the observation made above that a $\chi^2(k)$ becomes more and more Gaussian as k increases, which implies that the RV $\bar{S}_n \sim \chi^2(n-1)$ also becomes more and more Gaussian as n increases.

8.11 Application of results to problem of interest

We can now apply the general principles given above to the case of particular interest to us.

First, the equivalent of the population is the long signal, which we have called the base signal.

Second, the equivalent of drawing n samples from the population is the extraction of a subsignal using a window. Therefore, the relation between a population and a drawing of n samples from it translates into the relation between the base signal and a subsignal of n samples. All conclusions obtained above for the case of a (general) population can thus be applied to the case of the base signal.

In a nutshell, the mean and variance of the samples in the subsignal approach those of the base signal as n increases.

Of course, these results are far from answering the initial question of verification of the normality condition by a subsignal if the base signal verifies this condition. However, these results probably go as far as one can go analytically to address this question.

In light of this, it is important to keep in mind the experiment described above using synthetic data. Indeed, this experiment shows that one can reasonably expect that a sufficiently long subsignal extracted from a GBM base signal is also GBM.

8.12 View and practice in finance

The GBM model is often used in finance to model the evolution of stock price. It seems clear that a single GBM model, i.e., with fixed parameters, is not very useful for this application. Indeed, a fixed GBM model cannot possibly follow the successive behaviors of a stock, such as increasing (in price), steady state, and decreasing.

One can find examples of adaptation of the GBM model in finance in [3, 49].

8.13 Conclusions

We indicated that, in the next chapter, we show that all the LoD signals of Study A and Study B are appropriately modeled by a single/fixed GBM RP model. We pointed out that, since these signals are relatively short, they exhibit a single behavior, i.e., growing, steady state, or decaying, so that a GBM (RP) model with fixed parameters is appropriate and meaningful.

However, for longer LoD signals (such as in confidential Study C), one should expect the LoD to exhibit different behaviors at different times. As a consequence, it would be meaningless to try to use a single GBM model for long signals. Such long signals correspond to long drives, such as of a few hours. Therefore, one needs to find a solution to deal with such long signals.

Since the GBM model appear to work well on short signals (which can be viewed as being portions of longer signals), it makes a lot of sense to use the GBM model, but to adapt its parameters as time passes. In other words, one should make the GBM model adaptive (in/with time). Since a GBM model is fully characterized by two parameters (the drift μ and the volatility σ), adapting a GBM model means adapting these two parameters (in/with time).

The present chapter is mostly dedicated to this question of adaptation of a GBM model with time.

We pointed out the potential role of the Îto process, of which the GBM RP is a special case. The GBM RP is characterized by quantities aX_t and bX_t, where a is the drift μ and b is the volatility σ. The parameters in each pair are constant. The

quantities aX_t and bX_t are special form of the more general quantities $a(t, X_t)$ and $b(t, X_t)$ that appear in one form of the general Îto SDE. Because of the presence of the RP X_t, these two quantities are necessarily RPs. However, the literature also suggest a more general form of Îto-process SDE, i.e., where the RPs $a(t, X_t)$ and $b(t, X_t)$ are replaced by more general RPs A_t and B_t.

If we replace μX_t by $\mu(t)X_t$, where $\mu(.)$ is a deterministic function, and similarly for σ, we fall under the case of the general linear SDE, which can be solved in some particular cases. As discussed above, having deterministic $\mu(t)$ and $\sigma(t)$ would not help us. Indeed, if we envisioned using an Îto-process model to model the evolution of drowsiness during a long trip, would have to specify these functions ahead of time. This is totally impractical. For example, if the driver was to make an unscheduled stop to eat or take a rest, the functions originally entered into the system would become irrelevant. They could be reinitialized, but then how?

If we let $\mu(t)$ and $\sigma(t)$ become RPs, we fall into a particular form of the general Îto-process model. However, to the best of our knowledge, the corresponding SDE could not be solved (given the general nature of the RPs $\mu(t)$ and $\sigma(t)$).

The above discussion shows that there exists some underlying theoretical framework, linked to the general form of the Îto process. However, it seems that this framework would not help in practice. One thus needs a pragmatic solution for approaching as best as possible what would be theoretically ideal.

The pragmatic solution of adapting the parameters of a GBM model on the fly using recent, past data (typically in a sliding window) is thus a practical way of implementing a utopic, general Îto-process model with quantities "$a(t)$" and "$b(t)$" that are RPs.

The use of a sliding window brings up the following question.

In principle, before computing the parameters μ and σ based on the data in a (sliding) window butting against the present time, one would need to ensure that the data/subsignal in the window is GBM. Checking that a signal/realization is GBM implies checking the conditions of normality and independency. Since these checks (except one) are graphical (i.e., done visually), it would be nearly impossible to implement them on the fly, in real time. The "only" solution to this is that one should develop enough confidence into the hypothesis that LoD signals are locally GBM.

In the next two chapters, we use a sliding window to adapt the parameters μ and σ on the fly. The situation is special in the sense that we know that the full signal that is available is GBM, this as a result of our application of the tests of normality and independency. The question here is thus whether the portion of a signal extracted using a window is also GBM. In the present chapter, we explored this question/implication both theoretically and using synthetic data. The theory

does not seem permit us to guarantee that the above implication is true, but the experiment with synthetic data brings significant support for it.

The bottom line is that one should ultimately reach a point where the related research community has developed enough confidence into the hypothesis that virtually all LoD signals are locally GBM. As pointed earlier, the fact that the subsignal within a window is occasionally not GBM (unbeknown to us, i.e., the user) does not prevent us from modeling it as being GBM, i.e., from estimating/computing the parameters μ and σ, and making predictions based upon these parameters, and thus the corresponding GBM model. Of course, one should then expect occasional degradations in prediction performance.

As an analogy, one can mention the assumption of Gaussian data that is often made in many domains and applications. Most of the time, one does not check whether the data at hand is Gaussian or not before applying techniques that theoretically depend on the data being Gaussian.

The present chapter justifies, in as much detail as possible (given our current state knowledge), the use of a GBM RP model that adapts locally, typically using data in a sliding window, in any application where the realizations can potentially show, at any point in time, a behavior that is growing, steady state, or decaying, and thus certainly in the application of drowsiness monitoring.

Chapter 9

Experimental results for collected drowsiness-related signals: (1) modeling

This chapter is dedicated to the modeling of the level of drowsiness (LoD) signals using RP models. Section 9.1 provides an overview of the collected data. Section 9.2 illustrates the application of the methodology (described in Section 6.2) to signals from Study A. Section 9.3 illustrates the application of the methodology to signals from Study B. Section 9.4 provides illustrative examples of computation of parameters of the GBM RP model. Section 9.5 further describes, and illustrates, the principle of adaptation of the GBM RP model using a sliding time window. Section 9.6 investigates the application of conventional RP models to model signals from Study A. Section 9.7 briefly alludes to the application of the methodology to signals from Study C. Section 9.8 concludes the chapter.

9.1 Introduction

As described in the previous chapter, we collected, using a carefully planned and executed protocol, and a validated drowsiness monitoring system, discrete-time (DT) signals that represent the evolution of the level of drowsiness (LoD) at three increasing levels of sleep deprivation over three days, in two studies (Study A and Study B).

First, we illustrate the application of the methodology (described in Section 6.2) to the signals from Study A and Study B. Second, we describe the principle of adaptation the GBM RP model using sliding time window. Third, we check

whether the conventional RP models also have the ability to model the LoD signals.

9.2 Modeling of LoD & PERCLOS signals using GBM RP model for signals from Study A

Each participant in Study A contributed 3 LoD and 3 PERCLOS signals, with each pair of signals (i.e., for LoD and PERCLOS) corresponding to one of the 3 tests at progressively increasing levels of sleep deprivation. Thus, the 17 participants of Study A (performing PVTs) contributed $17 \times 3 = 51$ pairs of LoD and PERCLOS signals.

In Study A, each signal (LoD or PERCLOS) consists of 110 samples spaced by 5 seconds (for a total duration of 550 sec = 9 min 10 sec).

The time interval of 5 sec is the one at which the drowsiness measurement system was asked to produce its output samples. This should be distinguished from the speed at which the images of the eye were collected, i.e., 120 images/sec in the both studies (Study A and Study B).

The total number of signals and samples obtained from Study A is shown in Table 9.1.

	Number of signals	Number of samples
LoD	$17 \times 3 = 51$	$51 \times 110 = 5,610$
PERCLOS	$17 \times 3 = 51$	$51 \times 110 = 5,610$

Table 9.1: Numbers of LoD and PERCLOS signals and corresponding numbers of samples obtained in Study A.

One should note that all of our signals (LoD or PERCLOS) have positive values. As indicated in Section 6.5, if the signal of interest is positive, it is strongly advisable to examine the applicability of a GBM RP model before any other RP model such as ARIMA.

Consequently, in this section, we first verify the GBM conditions for the LoD and PERCLOS signals.

9.2.1 Level-of-drowsiness (LoD) signals

In this subsection, we first illustrate the application of the methodology (described in Section 6.2) to one example of LoD signal from Study A, and we then give the results for all 51 available LoD signals.

This example LoD signal is referred to as "Signal A", and is shown in Figure 9.1.

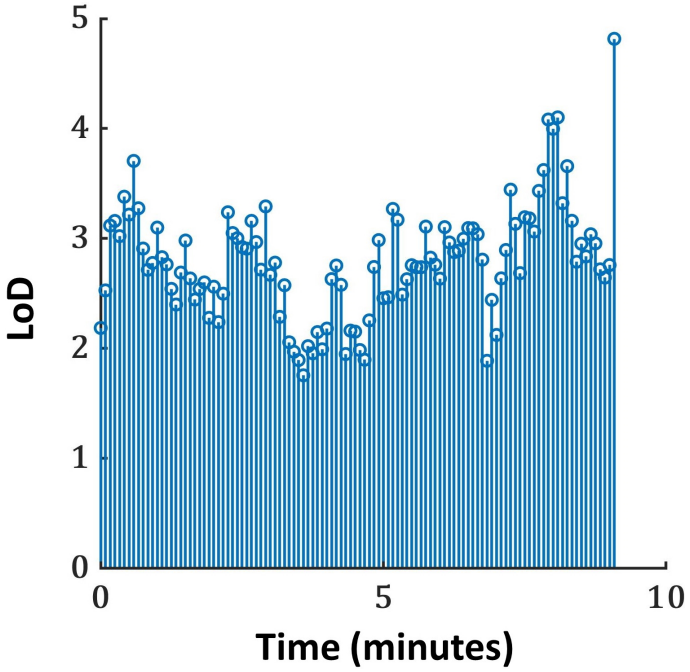

Figure 9.1: The graph shows the example LoD signal from Study A, referred to as Signal A. The signal consists of 110 samples. The horizontal axis shows the time in minutes.

9.2.1.1 Application of methodology to one example signal from Study A ("Signal A")

We present here the results of applying the methodology to Signal A. Specifically, we show the results of applying the three techniques for checking the normality condition (histogram, Q-Q plot, and S-W test) and the one technique for checking the independency condition (linear regression).

9.2.1.1.1 Check of normality condition

Figure 9.2 shows the histogram of log-ratio (LR) sample values—or, simply, log-ratios (LRs)—for Signal A, and the corresponding "normal distribution fit", which is the normal (i.e., Gaussian) PDF—i.e., the one with the mean and standard deviation of the LRs—multiplied by total number of LR samples.

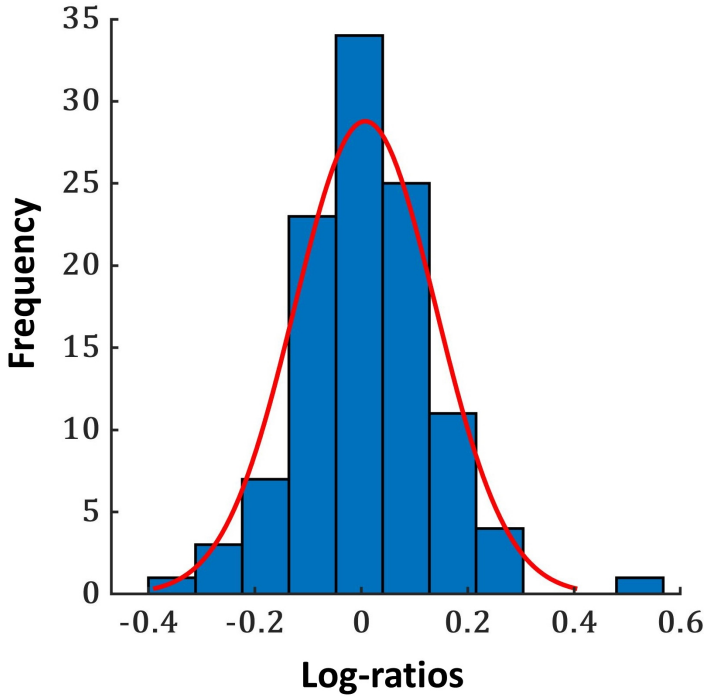

Figure 9.2: The graph shows the histogram of log-ratio sample values (or LRs) for Signal A, and the corresponding "normal distribution fit".

Figure 9.3 shows the Q-Q plot of log-ratios for Signal A, and the corresponding "best-fit" straight line, i.e., the one minimizing the total least-square fit error.

Since the histogram and Q-Q plot techniques are graphical, it is by visual inspection of the plots that one must decide whether the normality condition is verified or not. Through our experience based on looking at tens of such plots in the particular context of LoD signals, as well as at many in the literature for other applications, we conclude with confidence that, according to the histogram and Q-Q plot, Signal A satisfies the normality condition.

For Signal A, the application of the S-W test with significance level $\alpha = 0.05$ leads to the p-value of 0.01. Since this p-value is smaller than 0.05, we must reject the H_0 hypothesis. This allows us to conclude that Signal A does not verify the normality condition according to the present test.

The results of the three techniques (histogram, Q-Q plot, and S-W test) bring us to the conclusion that the pair of graphical tests indicates that Signal A satisfies the normality condition, whereas the S-W test indicates that it does not.

Since the graphical techniques both show in a convincing way that Signal A verifies the normality conditions, we decided to declare that Signal A verifies the

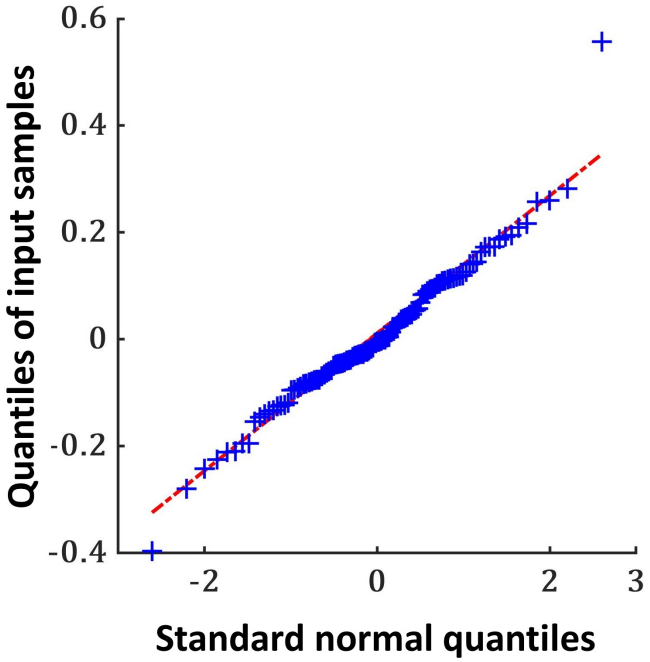

Figure 9.3: The graph shows the Q-Q plot of log-ratio sample values (or LRs) for Signal A, and the corresponding "best-fit" straight line.

normality condition.

9.2.1.1.2 Check of independency condition

Figure 9.4 shows the plot of log-ratio sample values (or log-ratios) for Signal A as a function of time, and the corresponding "best-fit"/regression straight line.

Since the linear regression technique is graphical, it is by visual inspection of the plots that one must decide whether the independency condition is verified or not. As for the histograms and Q-Q plots, through our experience of looking at many such plots, we conclude with confidence—from the regression line—that Signal A verifies the independency condition.

9.2.1.1.3 Conclusion for Signal A

Since Signal A can reasonably be said to verify both the normality condition and the independency condition, we conclude that the GBM RP model is a valid choice of model for Signal A.

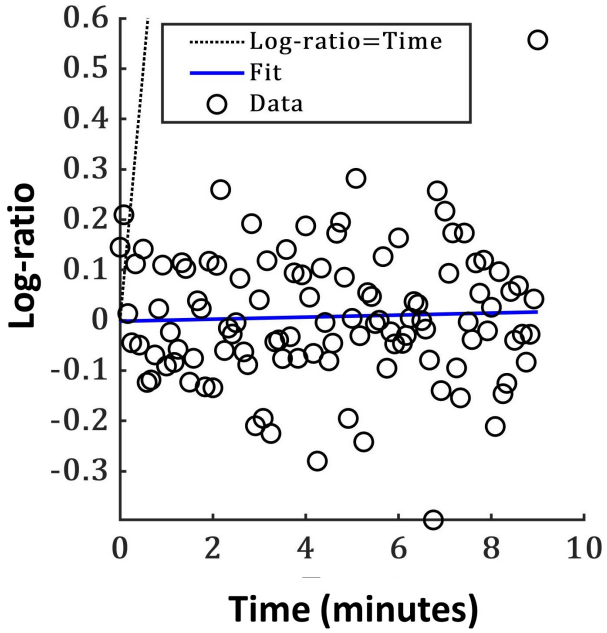

Figure 9.4: The graph shows plot of log-ratio sample values (or LRs) as a function of time, and the corresponding "best-fit" straight line for Signal A. The dotted line corresponds to equal values on both axes, i.e., to the line at "45 degrees."

9.2.1.2 Results for all 51 LoD signals from Study A

We applied to all 51 LoD signals available the exact same detailed analysis as the one above for Signal A.

9.2.1.2.1 Check of normality condition

According to the graphical techniques of histogram and Q-Q plot, we concluded that all 51 LoD signals from Study A verify the normality condition.

According to the S-W test with the significance level $\alpha = 0.05$, we concluded that, for each LoD signal in this study, the H_0 hypothesis must be rejected. This allows us to conclude that each such signal does not verify the normality condition according to the S-W test.

However, just as in the case of Signal A above, the graphical techniques of histogram and Q-Q plot allowed us to conclude that all LoD signals in Study A can reasonably be said to verify the normality condition.

In conclusion, all 51 LoD signals from Study A can reasonably be said to verify the normality condition.

9.2.1.2.2 Check of independency condition

The linear regression technique allowed us to conclude that all LoD signals from Study A verify the independency condition.

9.2.1.2.3 Conclusion for all 51 LoD signals from Study A

Since each LoD signal in Study A can reasonably be said to verify the normality condition and the independency condition, we conclude that the GBM RP model is a valid choice of model for the LoD signals in Study A.

9.2.1.2.4 Discussion of issue with Shapiro-Wilke (S-W test)

In earlier sections, we examined whether the log-ratios (LR) samples for each of the signals from Study A obeyed the normality assumption. For this, we used two graphical tests (namely, the histogram and Q-Q plot) and one numerical test (namely, the Shapiro-Wilk (S-W) test).

Recall that the S-W test is designed to test the null hypothesis (H_0), which is "the data samples come from a normal probability density function (PDF)". H_0 is rejected if the test is significant, i.e., if $p < 0.05$, and it is not rejected otherwise. (Here, the data samples are the LR samples.)

One should note that non-rejection does not imply acceptance [36]. In other words, if the test does not reject the H_0 hypothesis, this does not imply that the hypothesis is true, i.e., that the data samples come from a normal PDF.

In most of the cases from Study A, one can notice that the S-W test leads to the conclusion that H_0 should be rejected, i.e., that the (LR) samples do not come from a normal PDF. In all these cases, this appears to be in contraction with the conclusions of both graphical tests. As a result, we essentially decided to ignore the conclusion of the S-W test.

As we now explain, this decision is quite reasonable and is backed up by the related literature on numerical tests of normality.

There are four main numerical tests of normality, including the Kolmogorov–Smirnov (K-S) test and the Shapiro–Wilk (S-W) test [36]. The literature generally agrees on the fact that, among these four tests, the S-W test is often the most appropriate to use because it can reject the H_0 hypothesis at the smallest sample size, i.e., at the smallest possible number of data samples, assuming, of course, that the PDF of interest is indeed not normal.

A main problem with most numerical tests for normality, including the S-W test, is that, at larger sample size, they reject H_0 (normality) even if the samples

tested deviate only slightly from a true normal PDF [36].

The problem is that the numerical tests reject the H_0 hypothesis even when it would be perfectly legitimate to apply, to the samples, statistical methods that assume a normal PDF [36].

One should remember that "perfect"/exact" normality is something that is theoretical and never found in nature and real life.

In our case, the (LR) samples come from LoD signals that have been produced by sophisticated image and signal processing algorithms that operate, first on images of the eye obtained with active illumination in the infrared, and then on a variety of ocular parameters. Therefore, it would be a complete utopia to expect the LR samples of LoD to obey a perfect normal PDF.

Recall that the purpose of checking/examining whether or not the LR sample of LoD signals come from a normal PDF is to determine whether it is appropriate to use the GBM RP model.

Any criticism related to the decision of ignoring the conclusions of the S-W test becomes moot in light of the excellent predictions obtained, not only as described in Chapter 10 for LoD signals from Study A and Study B, but also for LoD signals from Study C, which cannot be discussed here for reasons of confidentiality.

One should also note that the normality of the LR samples for stock prices is probably the most important and the most used assumption in mathematical finance [76]. The important points are (1) that it is well documented in this field that numerical test of normality—including the S-W test—do generally reject the H_0 hypothesis that this samples come from a normal PDF, and (2) that this does not prevent people in research and the finance industry from using the GBM RP model to predict the future evolution of stock prices [76].

The long experience of using the GBM RP model in finance suggests that this model is robust against deviations of the LR samples from perfect/exact normality [76].

Similarly, in the field of drowsiness monitoring, this question of ignoring the conclusions of numerical tests, and, more specifically, of the S-W test, will likely be settled once and for all as soon as drowsiness monitoring systems (DMSs) using the GBM RP model start saving human lives.

In hindsight, the bottom line is that we are searching for major deviation from (i.e., violations of) normality, and that we are essentially not interested in searching for small deviations from normality. Consequently, the graphical tests are perfectly suited for our purpose and give us full confidence to essentially ignore the conclusions of any numerical test, thus including the ones of the S-W test.

9.2.2 PERCLOS signals

We directly applied to all 51 PERCLOS signals available the same detailed analysis as the one above for LoD signals, with the exception of the fact that we did not apply the S-W test (for the reasons explained in Section 9.2.1.2.4).

9.2.2.1 Check of normality condition

For PERCLOS signals, we only performed the graphical tests. According to the graphical techniques of histogram and Q-Q plot, we conclude that all 51 PERCLOS signals from Study A verify the normality condition.

9.2.2.2 Check of independency condition

The linear regression technique allowed us to conclude that all PERCLOS signals from Study A verify the independency condition.

9.2.2.3 Conclusion for all 51 PERCLOS signals from Study A

Since each PERCLOS signal in Study A can reasonably be said to verify the normality condition and the independency condition, we conclude that the GBM RP model is a valid choice of model for all PERCLOS signals in Study A.

9.2.3 Discussion of results for Study A

We have shown that the Geometric Brownian Motion (GBM) model is a valid choice of RP model for modeling all 51 LoD (or PERCLOS) signals obtained from Study A, thus without a single exception. Of course, the GBM RP model corresponding to each of the 51 LoD (or PERCLOS) signals is characterized by a set of parameters specific to this signal.

9.3 Modeling of LoD & PERCLOS signals using GBM RP model for signals from Study B

Each participant in Study B contributed 3 LoD and 3 PERCLOS signals, with each pair of signals (i.e., for LoD and PERCLOS) corresponding to one of the 3 tests at progressively increasing levels of sleep deprivation. Thus, the 13 participants

of Study B (driving in a simulator) contributed $13 \times 3 = 39$ pairs of LoD and PERCLOS signals.

In Study B, each signal (LoD or PERCLOS) consists of 42 samples spaced by 20 seconds (for a total duration of 840 sec = 14 min).

The total number of signals and samples obtained from Study B is shown in Table 9.2.

	Number of signals	Number of samples
LoD	$13 \times 3 = 39$	$39 \times 42 = 1,638$
PERCLOS	$13 \times 3 = 39$	$39 \times 42 = 1,638$

Table 9.2: Numbers of LoD and PERCLOS signals and corresponding numbers of samples obtained in Study B.

One should note that all of our signals (LoD or PERCLOS) have positive values. So, as indicated in Section 6.5, if the given signals are positive, then the GBM model must be considered as the first choice of model.

Consequently, we need to verify the GBM conditions for the LoD and PERCLOS signals.

9.3.1 Level-of-drowsiness (LoD) signals

We first illustrate the application of the methodology (described in Section 6.2) to one example of LoD signal from Study B, and we then give the results for all 39 available LoD signals.

This example LoD signal, referred to as "Signal B", and is shown in Figure 9.5.

9.3.1.1 Application of methodology to one example signal from Study B ("Signal B")

We present here the results of applying the methodology to Signal B. Specifically, we show the results of applying the three techniques for checking the normality condition (histogram, Q-Q plot, and S-W test) and the one technique for checking the independency condition (linear regression).

9.3.1.1.1 Check of normality condition

Figure 9.6 shows the histogram of log-ratio sample values—or, simply, LRs—for Signal B, and the corresponding "normal distribution fit".

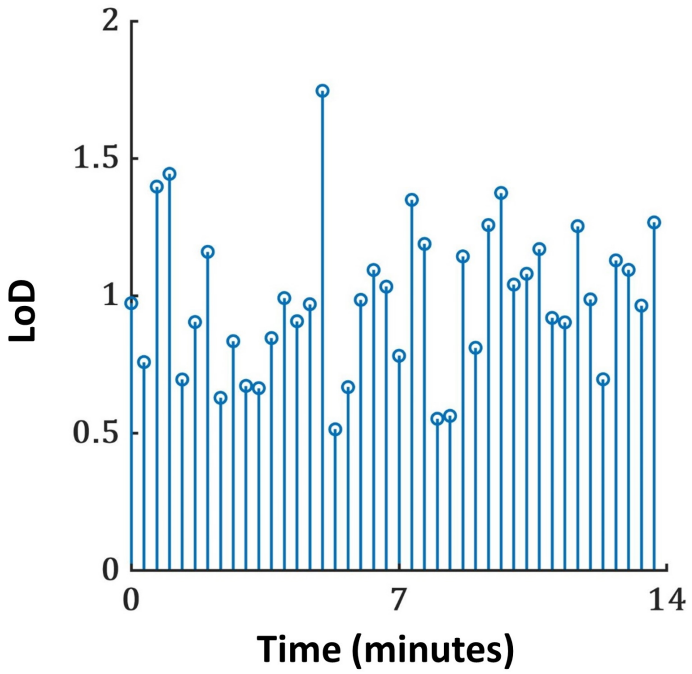

Figure 9.5: The graph shows the example LoD signal from Study B, referred to as Signal B. The signal consists of 42 samples. The horizontal axis shows the time in minutes.

Figure 9.7 shows the Q-Q plot of LRs for Signal B, and the corresponding "best-fit" straight line, i.e., the one minimizing the total least-square fit error.

Since the histogram and Q-Q plot techniques are graphical, it is by visual inspection of the plots that one must decide whether the normality condition is verified or not. Through our experience based on looking at tens of such plots in the particular context of LoD signals, as well as at many in the literature for other applications, we conclude with confidence that, according to the histogram and Q-Q plot, Signal B satisfies the normality condition.

For Signal B, the p-value of the S-W test is 0.10. Since it is greater than 0.05, we cannot reject the H_0 hypothesis that the log-ratio RVs have a normal (i.e. Gaussian) PDF. Recall that this does not allow us to conclude that Signal B then verifies the normality condition.

The results of the three techniques (histogram, Q-Q plot, and S-W test) bring us to the conclusion that the pair of graphical tests indicates that Signal B satisfies the normality conditions, and the S-W test does not allow us to say that it does not satisfy this condition, which is the best one could hope for in light of the two other tests.

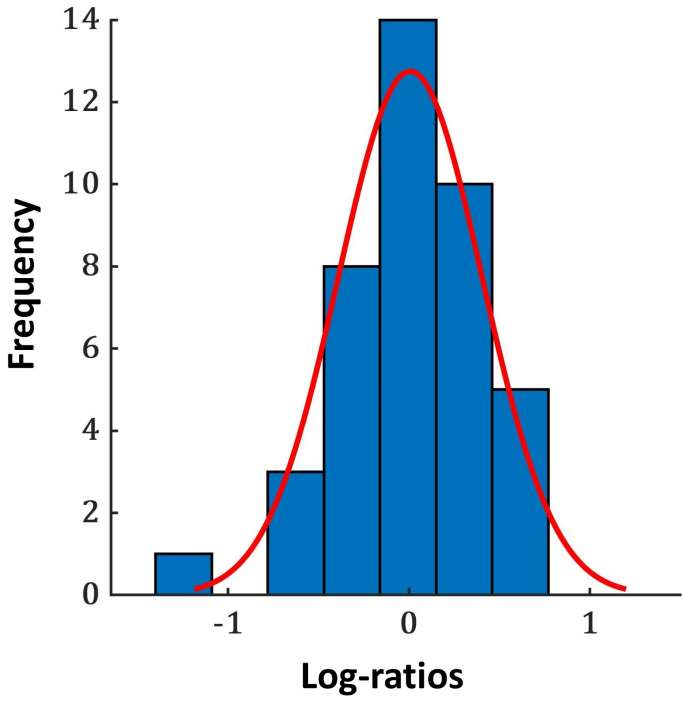

Figure 9.6: The graph shows the histogram of log-ratio sample values (or LRs) for Signal B, and the corresponding "normal distribution fit".

Since all three tests verify the normality conditions, we decided to declare that Signal B verifies the normality condition.

9.3.1.1.2 Check of independency condition

Figure 9.8 shows the plot of log-ratio sample values (or log-ratios) for Signal B as a function of time, and the corresponding "best-fit"/regression straight line.

Since the linear regression technique is graphical, it is by visual inspection of the plots that one must decide whether the independency condition is verified or not. As for the histograms and Q-Q plots, through our experience of looking at many such plots, we conclude with confidence—from the regression line—that Signal B verifies the independency condition.

9.3.1.1.3 Conclusion for Signal B

Since Signal B can reasonably be said to verify both the normality condition and the independency condition, we conclude that the GBM RP model is a valid choice of model for Signal B.

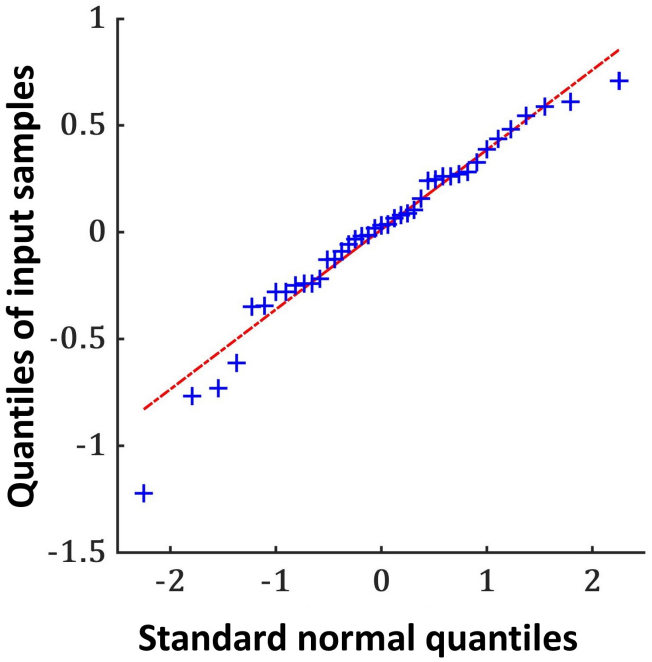

Figure 9.7: The graph shows the Q-Q plot of log-ratio sample values (or LRs) for Signal B, and corresponding "best-fit" straight line.

9.3.1.2 Results for all 39 LoD signals from Study B

We applied to all 39 LoD signals available the exact same detailed analysis as the one above for Signal B.

9.3.1.2.1 Check of normality condition

According to the graphical techniques, and the S-W test, we concluded that all 39 LoD signals from Study B verify the normality condition.

9.3.1.2.2 Check of independency condition

The linear regression technique allowed us to conclude that all LoD signals from Study B verify the independency condition.

9.3.1.2.3 Conclusion for all 39 LoD signals from Study B

Since each LoD signal in Study B can reasonably be said to verify the normality condition and the independency condition, we conclude that the GBM RP model

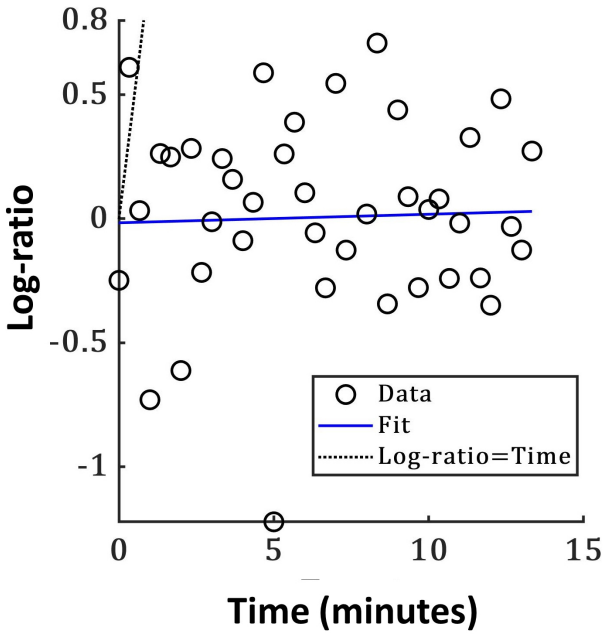

Figure 9.8: The graph shows the plot of log-ratio sample values (or LRs) as a function of time, and the corresponding "best-fit" straight lines for Signal B. The dotted line corresponds to equal values on both axes, i.e., to the line at "45 degrees."

is a valid choice of model for the LoD signals in Study B.

9.3.2 PERCLOS signals

We directly applied to all 39 PERCLOS signals available the same detailed analysis as the one above for LoD signals, with exception of the fact that we did not apply the S-W test (for the reasons explained in Section 9.2.1.2.4).

9.3.2.1 Check of normality condition

For PERCLOS signals, we only performed the graphical tests. According to the graphical techniques of histogram and Q-Q plot, we conclude that all 39 PERCLOS signals from Study B verify the normality condition.

9.3.2.2 Check of independency condition

The linear regression technique allowed us to conclude that all PERCLOS signals from Study B verify the independency condition.

9.3.2.3 Conclusion for all 39 PERCLOS signals from Study B

Since each PERCLOS signal in Study B can reasonably be said to verify the normality condition and the independency condition, we conclude that the GBM RP model is a valid choice of model for all PERCLOS signals in Study B.

9.3.3 Discussion of results for Study B

Applying the same methodology as Section 9.2, we have shown that the GBM RP model is a valid choice of RP model for modeling all 39 LoD (or PERCLOS) signals obtained from Study B, thus without a single exception. Of course, the GBM RP model corresponding to each of the 39 LoD (or PERCLOS) signals is characterized by a set of parameters specific to this signal.

9.4 Illustration of computation of parameters of GBM RP model

Section 9.2 shows that each LoD signal (and PERCLOS signal) from Study A obeys the normality and independency condition, and can thus be modeled by a GBM RP model. Section 9.3 leads to the same conclusion for the signals from Study B.

Once we know that a signal is GBM, we can determine the two parameters of the model, i.e., the drift μ and the volatility σ by using the formulas given in Section 6.3.

As an illustration, we computed these parameters for one LoD signal from Study A and for one LoD signal from Study B. These two signals are shown in the top graphs of Figure 9.9 and Figure 9.10, respectively. To be precise, only the first part of each of these signals is shown.

The values of the parameters are shown in Table 9.3.

Origin of signal	μ	σ
Study A	0.04	0.38
Study B	0.25	0.62

Table 9.3: The parameters μ and σ for one LoD signal from Study A and for one LoD signal from Study B.

For a reason that will soon become clear, we also show the four values of the table as four horizontal line segments in the second and third graphs in each of Figure 9.9 and Figure 9.10. There, the drift parameter is denoted by $\mu_{\text{whole signal}}$ and the volatility parameter by $\sigma_{\text{whole signal}}$. The subscript "whole signal" is used to indicate that the value of the corresponding parameter is computed using the whole signal, i.e., all of its samples. The horizontal line segments cover the full duration of the LoD signal; as indicated above, only the first parts of these signals is shown. As a heads-up, we can say that we later compute values of μ and σ using the samples in a moving window. The use of the horizontal line segment for the full-signal parameters will allow us to visualize how the "local" values of the parameters compare to the "global" ones.

9.5 Adaptation with time of GBM RP model

In Chapter 8, we explained why, in most applications, the GBM RP model must be adapted with time, and we discussed the key issues associated with the adaptation of this model. The chapter concluded that a pragmatic approach is to use a sliding time window and to compute, for each position of the window—with the length of the step from one position to the next to be determined—the values of the parameters of the model, i.e., μ and σ.

In the present section, we successively (1) review the key points discussed in Chapter 8, (2) discuss in more detail the use of a sliding window, and (3) give two illustrative examples of the adaptation of the GBM RP model, the first for one signal from Study A, and the second for one signal from Study B.

9.5.1 Review of key points of Chapter 8

The GBM RP model is characterized by two parameters, i.e., the drift μ and the volatility σ.

A fixed value of μ corresponds to only one of three possible behaviors: (1) growth (for $\mu > 0$), (2) steady state ($\mu = 0$), and (3) decay ($\mu < 0$). In applications

like drowsiness monitoring (which is the application of main interest in this thesis) and stock-price monitoring, it is clear that the level of the quantity of interest (drowsiness and stock price) will evolve over the time durations of interest, i.e., several tens of minutes or several hours for drowsiness, and several days, weeks, months, and years for stock price. It is thus an utopia that a single model—i.e., with fixed/constant μ and σ—would be useful. Over the durations of interest, the quantity of interest (LoD in our case) will show a succession of periods of time with mostly growth, mostly steady-state, and mostly decay, in any meaningful orders and combinations.

A key point is the following. In finance, experts have shown that stock price appears to evolve locally (in time) according to a GBM RP model [75]. In drowsiness, we have shown—in Section 9.2 (for signals from Study A) and Section 9.3 (for signals from Study B)—that drowsiness—and more specifically the LoD and the PERCLOS—also appears to evolve locally according to a GBM RP model.

Of course, if one picks an arbitrary segment of time, it is logically possible that this segment would consist in a growth tendency followed by a decay tendency. One might thus wonder what a GBM RP model with fixed parameters (for this segment) would conclude. It is possible that it would conclude that the net effect is nearly steady-state, and this conclusion could in fact be a reasonable one. We are fully aware that some border effects are inevitable.

If one is fully confident that the signal/process of interest evolves locally (perhaps with some exceptions as just described) according to a GBM RP model, one can go ahead and blindly estimates the parameters μ and σ for each position of the sliding window.

Before estimating the two parameters for a given window (position), one might envision adding a two-pronged check of normality and independency of the samples within the window. If this were done, one could then issue warnings when one or both of these checks fails. This would allow the driver, or the driver monitoring system, to take appropriate action. This was discussed in Chapter 8.

The issue with performing this double check is that the methods for doing so are mostly visual, thus requiring (in principle) human intervention. There is thus an opportunity here for further research to ascertain whether or not the samples in a given window are GBM or not.

Below, we demonstrate—on two real-life example signals—the use of a sliding window to adapt the GBM RP model.

Each signal available to us is of short duration (either 9.2 min or 14 min). We have shown in the two previous sections that all these signals are GBM. The main problem with these short signals is that, when we use a sliding window, the windows are necessarily fairly short.

As indicated in Chapter 8, we have performed the check of normality and independency of several subsignals defined by the corresponding windows. Given the small number of samples in each window, the visual tests generally were not conclusive.

The last remark indicates that we are in a situation where we are computing the values of μ and σ without the assurance that the samples within any given window are GBM. The illustrative examples given and described below should thus viewed as being proofs of concepts.

In a real drowsiness monitoring system, and with a trip of reasonable duration, say, of one or two hours (where it would make sense to use such a system), one could use windows of longer duration. Of course, the issue of checking, or not, whether the samples in a window are GBM, remains.

The signals of Study C are longer that the ones of Study A and B, which allowed us to use windows of more meaningful durations.

With full awareness of the caveats indicated above, we can now (1) give some additional details about the use of a sliding window and (2) present and describe the illustrative examples.

9.5.2 Principle of adaptation

As indicated in Section 3.2 and just above, using a sliding window allows any model to adapt its parameters to the latest data, provided that the complexity of the model allows one to recompute these parameters periodically, in the limit at each time step.

In the case of the GBM RP model, using a sliding time window, and Equations 6.1 and 6.1, the model can adapt its parameters at each time step.

Below, we progressively explain the adaptation procedure using two illustrative example signals from Study A and Study B.

9.5.3 First illustrative example of adaptation for one example signal from Study A

Figure 9.9 illustrates—for one example LoD signal from Study A—the adaptation in time of the GBM RP model. Recall that, for the signals of Study A, the signal samples are spaced by a time interval of 5 sec (which is also the relevant sampling interval). The figure illustrates the case where the adaptation is performed at each time step, i.e., every 5 sec. (One could envision other scenarios where the adaptation is done less frequently.) At each time step, one recomputes/refreshes

the two parameters of the GBM RP model, i.e., the drift μ and the volatility σ, by using the (values of the) LoD samples over the last 5 minutes. The adaptation with time is implemented through the use of a sliding time window, of length 5 min, thus covering 60 samples. At each time step, the window is moved by one time step to the right.

The three successive graphs show—in the form of DT signals—the LoD signal of interest (with a window at a particular position) and the evolution with time of the model parameters μ and σ. For the purpose of explanation, one can assume that the rightmost sample shown in the last two graphs correspond to the present time. (One could also assume that this sample is, e.g., the last one computed, corresponding to the end of a drive and/or of a record.) The window shown thus butts (on its RHS) against the present time, but it does not include the present-time instant. The rightmost sample shown in each of the last two graphs is thus computed using all the samples inside the window shown. The earlier samples in each of these two graphs correspond to earlier "present times" and to corresponding, earlier positions of the sliding window.

The last two graphs show pictorially how the GBM RP model adapts/evolves with time.

One should note that μ can take positive, zero, and negative values, thereby allowing the model to track all possible trends of the LoD, i.e., increasing, constant, and decreasing.

The figure also shows the values of the parameters μ and σ computed for the whole signals. These are the values that one would use if we used a fixed model. However, one should keep in mind that, in an operational setting, the samples of the whole signal would not be available.

One should note that we have shown that the whole signal is GBM. However, as pointed out above, there is no assurance that the subsignal within each window is GBM. Of course, this does not prevent us from computing the local μ and σ. When these parameters are used later to perform predictions, there will likely be a degradation of performance, but the level of degradation is not determined in the present work.

9.5.4 Second illustrative example of adaptation for one example signal from Study B

Figure 9.10 illustrates—for one example LoD signal from Study B—the adaptation in time of the GBM RP model. This figure is the counterpart, for Study B, of Figure 9.9, related to Study A. The main difference between the two figures is the sample separation, which is 5 sec for Study A (and, thus, for Figure 9.9) and 20

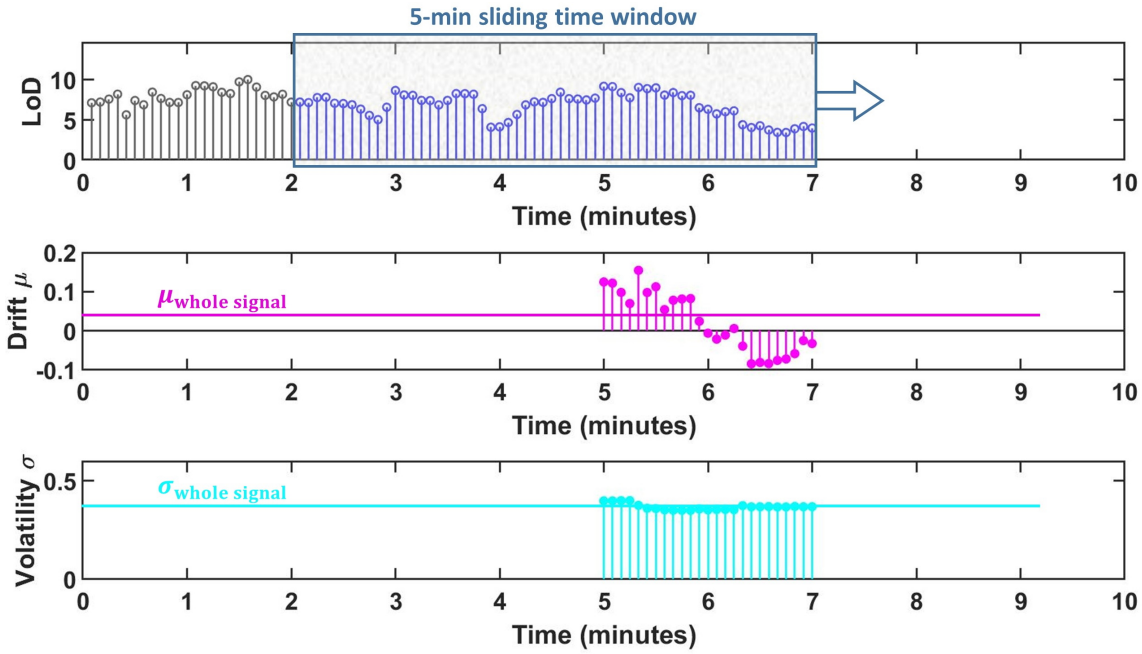

Figure 9.9: The figure illustrates the adaptation in time of the GBM RP model for an example LoD signal from Study A. This signal is shown in the first graph. At each time step, i.e., every 5 sec (for signals from Study A), one adapts the model by computing/refreshing the values of its two key parameters, i.e., the drift μ and the volatility σ. The computation is performed by using all samples of the LoD signal within a window that has a length of 5 min (and, thus, covers 60 samples) and butts against the present time instant, but does not include it. The last two graphs show the evolution with time of the values of μ and σ. These graphs thus show pictorially, at a glance, how the GBM RP model evolves/adapts with time. Observe that, in the present case, μ takes both positive values and negative values, which respectively correspond to increasing and decreasing trends for the LoD. The horizontal lines in the last two graphs are at the heights/ordinates of the values of μ and σ computed over the whole signal.

sec for Study B (and, thus, for Figure 9.10). The length in seconds of the sliding time window is the same for both figures, i.e., 5 minutes. This window covers 60 samples for Study A and 15 samples for Study B. All comments made for Figure 9.9 apply to Figure 9.10, provided that one takes into account the different sample separations.

The last two graphs show pictorially how the GBM RP models adapts/evolves

with time.

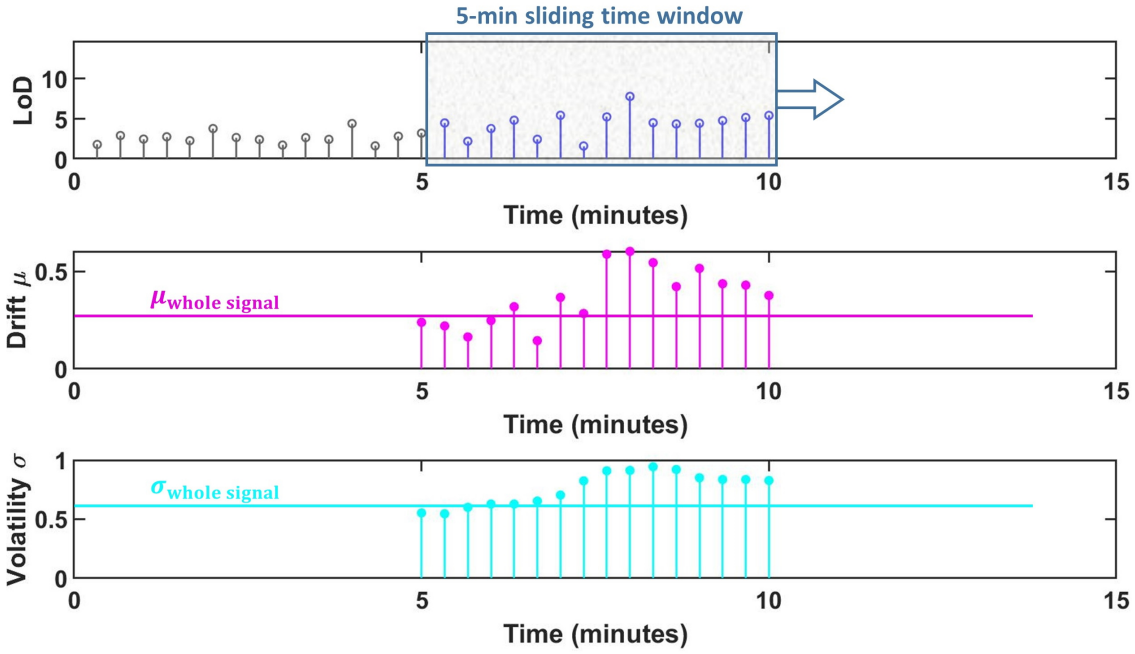

Figure 9.10: This figure is the counterpart, for Study B, of Figure 9.9, related to Study A. It indeed illustrates the adaptation in time of the GBM RP model for an example LoD signal from Study B. This signal is shown in the first graph. At each time step, i.e., every 20 sec (for signals from Study B), one adapts the model by computing/refreshing the values of its two key parameters, i.e., the drift μ and the volatility σ. The computation is performed by using all samples of the LoD signal within a window that has a length of 5 min (and, thus, covers 15 samples) and butts against the present time instant, but does not include it. The last two graphs show the evolution with time of the values of μ and σ. These graphs thus show pictorially, at a glance, how the GBM RP model evolves/adapts with time. Observe that, in the present case, μ takes only positive values, which correspond to increasing trends for the LoD. The horizontal lines in the last two graphs are at the heights/ordinates of the values of μ and σ computed over the whole signal.

9.5.5 Conclusion

We have shown, through two illustrative examples (on one signal from Study A, and on one signal from Study B), that one can adapt the GBM RP at each time step. Indeed, the model is fully adaptable and appears to track well the data.

The adaptation of the GBM RP model is readily and fully characterized by the DT signals of the drift parameter μ and volatility parameter σ. One can thus "visually" observe, at a glance, how the model adapts.

The examples shown demonstrate that the GBM RP model can track increasing trends and decreasing trends in the evolution of the level of drowsiness. Of course, the model then also track a constant (i.e., steady state) trend.

The ability to easily adapt the RP model—as demonstrated in this chapter for GBM—is, of course, key to the design of drowsiness monitoring systems (DMSs).

We emphasize that the two illustrative examples should be viewed as proofs of concept. Indeed, the short durations of the signals in Study A and Study B constrains us to use windows of very short durations, with the consequence that the samples therein may not be GBM.

9.6 Modeling of LoD signals using conventional RP models

Even if one is convinced of the potential power of the GBM RP model, it is a useful and valuable exercise to see whether the conventional RP models also have the ability to model LoD signals.

Of course, even if they are able to do so, there still remain the issues of knowing (1) whether one can use these models to do the predictions of interest and (2) whether one can adapt these models easily, potentially of every time step.

As a heads-up, we can say that we will find that the conventional RP models cannot really meet these constraints, especially if the computational power is limited, as it is in a vehicle.

In this section, we always consider the full signals (from Study A and Study B). Specifically, we do not consider subsignals, e.g., defined by a sliding time window.

9.6.1 Application of Box-Jenkins method to four example LoD signals from Study A

To apply the Box-Jenkins (BJ) method to any signal, one must examine both its sample autocorrelation function (ACF) and its sample partial autocorrelation function (PACF). Below, for conciseness, we generally drop the qualifier "sample" from the last two functions.

We have applied the BJ method to all 51 LoD signals from Study A, and this is a rather time-consuming process.

Its important to note that the BJ method may suggest several possibilities of model. Therefore, there is often some arbitrariness in the final choice of model.

Once this task was completed, we observed that all 51 signals could be modelled by four different conventional RP models, i.e., of types AR(8), MA(5), ARIMA(2,1,2), and ARMA(2,2).

To explain the process we used to arrive at these four models, we chose, for each one of them, a signal from Study A that is modeled by it. In other words, we selected, among the signals from Study A four signals that are respectively AR(8), MA(5), ARIMA(2,1,2), ARMA(2,2). We call these four signals Signal A1, Signal A2, Signal A3, and Signal A4, respectively.

Table 9.4 shows the (sample) ACF and (sample) PACF for each of these four signals.

Below, we explain how we determine, by examining the pair of ACF and PACF, the corresponding type of model.

1. **Signal A1**:
   The ACF and PACF behave as follows. The ACF (on the left) decays quickly to zero (0). The PACF (on the right) cuts off after lag = 8, which means that the PACF essentially remains below the horizontal blue line after lag=8, i.e., the ACF cuts off after 8^{th} lag. The BJ methods indicates that AR(8) is one of the conventional RP models suited for Signal A1.

2. **Signal A2**:
   The ACF and PACF behave as follows. The ACF (on the left) cuts off after 5^{th} lag. The PACF (on the right) cuts off 1^{st} lag. The BJ methods indicates that MA(5) is one of the conventional RP models suited for Signal A2.

3. **Signal A3**:
   The ACF and PACF behave as follows. The ACF (on the left) does not decay to zero, so the signal A3 is not a realization of a stationary RP. Consequently, the signal is of type ARIMA. We observed that Signal A3 attains the

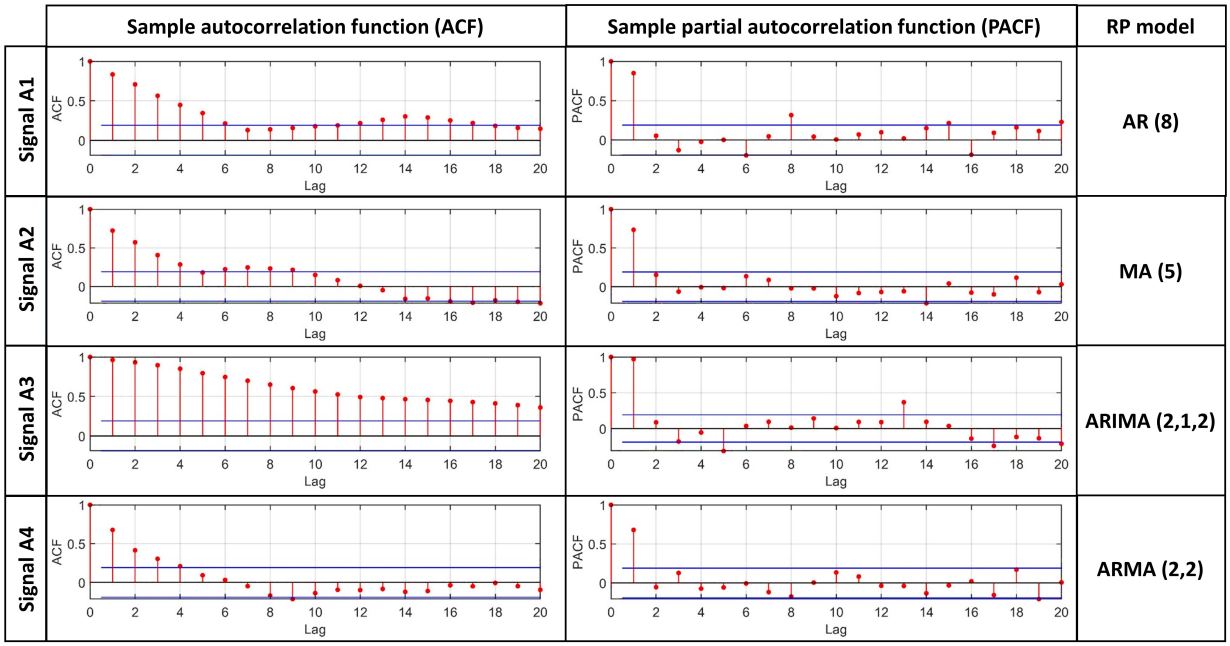

Table 9.4: Each of the four rows in the table correspond to a specific signal from Study A. These four successive signals are called Signal A1, Signal A2, Signal A3, and Signal A4. The first two columns show the sample autocorrelation function (ACF) and the sample partial autocorrelation function (PACF) for each of these four signals. The variable along the horizontal axis is the lag, which is the difference between two time indices. The horizontal blue lines are the 95% confidence intervals for the ACF and PACF of a WGN RP with the same length as the signal. The last column shows the type of the conventional RP model that best fit each of the four signals. This type is deduced by visual analysis of the corresponding ACF and PACF. The four signals were chosen to lead to four distinct models. One or more signals in Study A correspond to each of these models.

stationarity after the first difference, i.e., Signal A3 should be first filtered with,

$$H_{\text{first-diff}} = 1 - z^{-1}\,.$$

By visual analysis of the ACF and the PACF of the differenced/filtered signal and using the BJ method, one can suggest—among several options—the ARIMA(2,1,2) as the corresponding RP model.

4. **Signal A4**:
The ACF and PACF behave as follows. The ACF (on the left) decays quickly

to zero (0). The PACF (on the right) decays quickly to zero (0). The BJ methods indicates that ARMA(2,2) is one of the suited conventional RP models for Signal A4.

9.6.2 Application of Box-Jenkins method to 51 LoD signals from Study A

As already indicated, we applied the procedure illustrated in the previous section to all 51 LoD signals from Study A, and we found that they can all be described at least using one of the four RP models appearing in Table 9.5.

Table 9.5 indicates how many signals from Study A correspond to each of these four RP models.

RP models	Number of signals
AR (8)	16
MA (5)	12
ARIMA (2,1,2)	20
ARMA (2,2)	3

Table 9.5: The first column shows the four conventional RP models that are needed to model all 51 signals from Study A. The second column indicates how many of these signals are modeled by each of the four models.

One should note that the numbers shown are subjective, i.e., using the BJ method, one can associate more than one conventional RP model to a signal.

Given (1) the strategy discussed in Section 6.6, and summarized in Figure 6.1, and (2) the cumbersome nature of determining which conventional RP model is appropriate, we did not examine the question of modeling the signals from Study B using conventional RP models.

9.7 About modeling for signals from Study C

We performed on all signals from Study C the same modeling exercises as the ones described above for Study A and Study B. While we cannot describe the nature of data collected, we can indicate that the GBM RP model also appears to be an excellent RP model for the signals from Study C.

9.8 Conclusion

This chapter is dedicated to the modeling of the level of drowsiness (LoD) signals using RP models.

We considered two types of RP models, i.e., the GBM RP model (which is the cornerstone of this thesis) and the conventional RP models (such as AR, MA, ARMA, and ARIMA).

We examined whether the GBM RP model could model the LoD signals from Study A, Study B, and Study C. We have shown that all 51 signals from Study A and all 39 signals from Study B can be successfully modeled by a GBM RP model. The same conclusion applies to all signals from Study C, the nature of which is protected by a non-disclosure agreement.

We have shown, on illustrative signals, that the GBM RP model can easily be adapted, even at every time step. We have shown that the adaptation of the model can be readily visualized by looking at the time evolution of its two parameters μ and σ.

We have shown that the GBM RP model can track the three possible trends of the evolution of (the level of) drowsiness, i.e., increasing, constant, and decreasing.

Even though we were convinced of the potential power of the GBM RP model to model drowsiness, we also modeled the LoD signals from Study A using conventional RP models. We found, without surprise, that using these models is much more cumbersome and much more demanding in terms of computational power.

We concluded that the GBM RP model proves to be an excellent candidate for modeling LoD signals, as well as related biological signals, such as the PERCLOS signal.

In the next chapter, we show that it is also very well suited for making various types of predictions.

Chapter 10

Experimental results for collected drowsiness-related signals: (2) prediction

This chapter is dedicated to produce the three types of predictions of interest, i.e., future values (FVs) of a signal, the first hitting time (FHT), and the survival probability (SP) for LoD signals using RP models. Section 10.1 provides a brief introduction to the chapter. Section 10.2 illustrates the potential of the GBM RP model to predict FVs of an LoD signal using a fixed time window. Section 10.3 illustrates the potential of the GBM RP model to predict FVs of an LoD signal using a sliding time window. Section 10.4 illustrates the potential of the same model to predict the FHT for an LoD signal using a sliding time window. Section 10.5 illustrates the potential of the same model to predict the SP for an LoD signal using a sliding time window. Section 10.6 presents a reliable drowsiness-detection system based on the SP. Section 10.7 briefly alludes to the prediction results from Study C. Section 10.8 concludes the chapter.

10.1 Introduction

This chapter covers four main topics. First, we illustrate the potential of the GBM RP model to predict future values (FVs) of a LoD signal using (1) a fixed time window and (2) a sliding time window. Second, we illustrate the potential of the GBM RP model to predict the first hitting time (FHT) using a sliding time window. Third, we illustrate the potential of the GBM RP model to predict the survival probability (SP). Fourth, we present a drowsiness-detection system

based on the SP, and we present a graphical method to evaluate its detection performance.

10.2 Non-adaptive prediction of future values of a signal (for LoD signals)

In this section, we construct a unique RP model for each signal of interest. Specifically, we do not adapt the model as time evolves, such as at every time step. To construct this non-adaptive RP model, we use most of the samples of the signal. We do not use all of them, because we wish to test our ability to make predictions of FVs of the signal. In practice, the few last samples in each signal (in fact, exactly 4) are those where we wish to make predictions (of FVs), and these are thus not used to build the RPM model. Starting with Section 10.3, we exclusively use RP models that adapt, and, specifically, at each time step.

The next two sections respectively (1) illustrate the prediction of FVs of a signal using the GBM RP model, and (2) quantify the performance of the prediction both in terms of prediction error and computation speed, and for both the GBM RP model and conventional RP models.

10.2.1 Illustration of non-adaptive prediction of future values of a signal using GBM RP model (for one LoD signal from Study A)

We provide an illustrative example of predicting FVs of an example LoD signal from Study A up to 20 seconds in the future using a window of the past values with the length of 8.6 minutes (i.e., 105 samples).

In this experiment, all 105 samples observed up to and including the present sample are used to compute the parameters of the GBM RP model. The model is then used to predict the LoD signal values for 5, 10, 15, and 20 seconds in the future. Figure 10.1 shows the non-adaptive prediction of FVs (of signal) using the GBM RP model for one LoD signal from Study A.

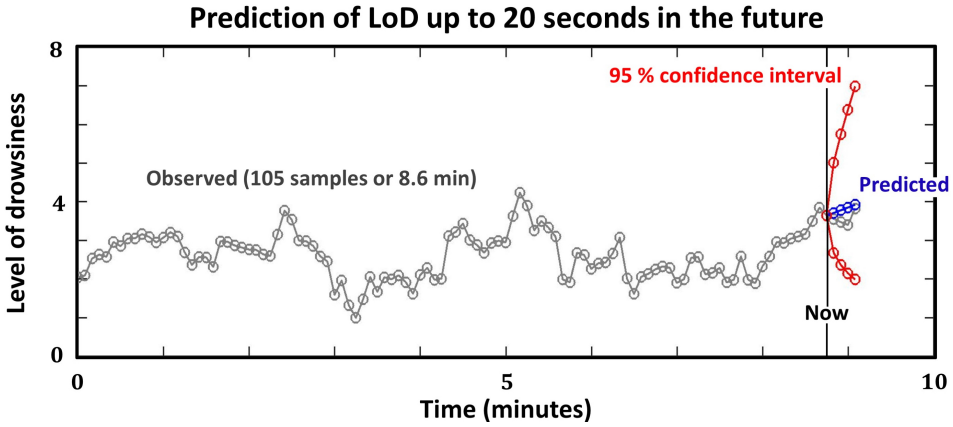

Figure 10.1: The graph illustrates for the GBM RP model, the prediction of the LoD signal values for 5, 10, 15, and 20 seconds in the future. In the particular experiment illustrated here, all 105 samples observed up to and including the present time/sample are used to compute the parameters of the GBM RP model. The model is then used to compute the four predicted values just mentioned. The graph also shows the 95% confidence interval for the predictions. (The fact that the upper bound grows in such a way as to exceed the upper limit (of 10) of the nominal range of values of LoD is not of concern.)

We could have similarly illustrated the operation of an appropriate conventional RP model, and produced a figure similar to Figure 10.1, but we elected not to do so. Although we do not illustrate here the operation of a conventional RP model, we made numerous such predictions, as will become clear in the next section on performance.

10.2.2 Performance in prediction error and computation time

10.2.2.1 Performance of *GBM RP model* for non-adaptive prediction of future values of a signal (for all 51 LoD signals from Study A)

We consider the task of predicting FVs of LoD signals for the 51 LoD signals from Study A.

We characterize the performance in prediction (1) in term of the mean prediction error and (2) in term of the computation time to predict FVs.

For each of the 51 LoD signals, we use a fixed window of 105 samples and we

predict FVs of the signals at 5, 10, 15 and 20 seconds in the future (as illustrated in Figure 10.1).

We characterize the error in prediction by computing, for all 51 LoD signals, the "mean of the mean squared errors (MMSE)" defined as

$$\text{MMSE} = \frac{\sum_{j=1}^{51} \text{MSE}_j}{51}, \tag{10.1}$$

where

$$\text{MSE}_j = \frac{\sum_{n=1}^{4} (x_{j,p+n} - \hat{x}_{j,p+n})^2}{4},$$

where p is the present time index, $x_{j,k}$ and $\hat{x}_{j,k}$ are the true and predicted values, respectively, of signal j at time index k.

We characterize the time necessary to predict four (4) future samples via the "mean of computation time (MCT)" defined as

$$\text{MCT} = \frac{\sum_{j=1}^{51} \text{CT4S}_j}{51}, \tag{10.2}$$

where CT4S_j is the computation time to predict the four (4) future samples of signal j.

The results obtained are shown in Table 10.1.

Model	Mean of mean squared errors	Mean of computation time (s)
GBM	0.6	0.0007

Table 10.1: The table shows the performance of the GBM RP model for predicting the FVs of a signal (for all 51 LoD signals from Study A), in terms of: (1) the mean of mean squared errors (MMSE) of predicted values for all 51 signals and (2) the mean of computation time (MCT) to produce these predicted values for all 51 signals (on Intel Core i7-5500U), where MMSE and MCT are given by Equations 10.1 and 10.2.

10.2.2.2 Performance of the *conventional RP models* for non-adaptive prediction of future values of a signal (for all 51 LoD signals from Study A)

We perform here a performance analysis similar to the one of the previous section. The only difference is that, instead of using the GBM RP model, we now use the conventional RP models built in Section 9.6.2 for the 51 LoD signals from Study A. For memory, the four models built are of the types AR(8), MA(5), ARIMA(2,1,2), and ARMA(2,2).

The performance results are given in Table 10.2. The results are listed for each of the four models. They were computed using all 51 LoD signals from Study A.

Model	Mean of mean squared errors	Mean of computation time (s)
AR(8)	0.6	0.82
MA(5)	1	0.66
ARIMA(2,1,2)	0.8	0.87
ARMA(2,2)	0.6	0.6

Table 10.2: The table is the counterpart, for the conventional RP models, of Table 10.1 related to GBM RP model. The table shows the performance of the four conventional RP models, i.e., AR(8), MA(5), ARIMA(2,1,2), and ARMA(2,2), for predicting FVs of a signal (for all 51 LoD signals from Study A), in terms of: (1) the mean of mean squared errors (MMSE) of these predicted values for all 51 signals and (2) the mean of computation time (MCT) to produce prediction for all 51 signals (on Intel Core i7-5500U), where MMSE and MCT are given by Equations 10.1 and 10.2.

10.2.2.3 Comparison of performance of the GBM and the conventional RP models

To enable to the comparison of the performance of the GBM RP model and the conventional RP models in predicting FVs of a signal (for all 51 LoD signals from Study A), we brought the entries from Table 10.1 and Table 10.2 together in Table 10.3.

Model	Mean of mean squared errors	Mean of computation time (s)
AR(8)	0.6	0.82
MA(5)	1	0.66
ARIMA(2,1,2)	0.8	0.87
ARMA(2,2)	0.6	0.6
GBM	0.6	0.0007

Table 10.3: The table shows jointly the information present in Table 10.1 and Table 10.2.

Table 10.3 shows that the GBM RP model provides the same MMSE as the best conventional RP models, but with a computation time reduced by a factor of around 1,000.

Given the low computational requirements of the GBM RP model, both for modeling and for prediction, it is feasible to use it in real-time applications. For this reason, we often say "in real time" in subsequent sections.

10.2.3 Discussion of results

Using a unique, fixed (thus non-adaptive) GBM RP model for a specific signal from Study A, we illustrated the capability of a GBM RP model to predict FVs of an LoD signal. This unique model is built from all the data samples except for the handful of samples (at the end of the signal) where we perform the predictions.

Still using a unique (non-adaptive) RP model, we quantified the performance—in terms of both prediction error and computation time—of both the GBM RP model and the conventional RP models, all fitted to each signal. The results show that the GBM RP model and the appropriate conventional RP model have similar prediction errors, but that the computation of each prediction with the GBM RP model is about one thousand (1000) faster than with a conventional RP model.

The experiments and results reported here, as well as many others not discussed in this section, lead us to the conclusion that the GBM RP model appears to be an excellent RP model for LoD signals, both in terms of prediction error and speed of computation of each prediction of a FV.

In Section 6.5, we already indicated the many advantages that the GBM RP model has, in general, over conventional RP models for modeling. The results reported in this section constitute a first confirmation of the potential of the GBM RP model to both model an LoD signal and enable the prediction of FVs of this signal.

The above conclusion leads us to focus exclusively on the the GBM RP model in future sections. At the time this research was performed, and still at the time of this writing, the advantages and potential of GBM RP model (for modeling and prediction) in the context of drowsiness monitoring and prediction indeed appear significant.

10.3 Adaptive prediction of future values (FVs) of a signal (for LoD signals)

Below, we progressively describe how to predict future values (FVs) of a signal using a sliding time window via an illustrative example using one LoD signal from Study A.

In Chapter 8, and in Section 9.5, we discussed (1) the need for using an RP model that adapts with time, and (2) the issue associated with the use of a sliding window with short signals, i.e., with a small number of samples. With respect to the second point, the number of samples in a window may be too small for the subsignal in the window to be GBM, even if the overall signal is GBM. Since the signals from Study A and Study B are short, the predictions performed below (with a sliding window) should be viewed as a proof of concept of what one would do in practice with longer signals (such as for a 2-h drive) and longer windows.

10.3.1 Illustration of adaptive prediction of FVs (for one signal from Study A)

Figure 10.2 illustrates the task of predicting FVs of an LoD signal (from Study A) using a GBM RP model that adapts/evolves with time. The adaptation is performed as described in Section 9.5. This involves a sliding time window.

The figure considers, as an illustrative example, the task of predicting, at each time step, the (yet unknown) value of the LoD signal 20 seconds into the future, which translates (for signals from Study A) into 4 time steps into the future. The lag/horizon of 20 seconds is an arbitrary choice, just for illustration purpose. (However, one should remember that, in driving, predicting just 6 seconds into the future can save human lives.)

The four successive subfigures/graphs correspond to four successive time steps. At each step, the window is moved one time step to the right. At each time step, and thus for each position of the window, one performs two tasks: (1) adaptation of the model and (2) prediction of the value of the signal 4 time steps ahead. Recall

that the adaptation of the GBM RP model means computing the new values of μ and σ.

In the present illustrative example, we predict, at each present instant, one sample into the future, namely, 4 time steps ahead. However, one could predict the values for any set of time instants into the future, including "all of them", up to ∞, at least in principle. It is important to note that the predicted sample is shown, in the graphs, at the future time of interest. We emphasize this point, because one could, alternatively, show this sample at the present time. If one showed the sample at the present time, the whole signal would simply be a time-shifted version of the signal showing the sample at the appropriate future time (as shown in Figure 10.2). Showing the sample at the present time leads, of course, to a display/presentation issue if one predicts the signal values at several instants in the future.

In the present case, after 4 time steps, one would have an opportunity to check how the predicted value (predicted four time steps earlier) relates to the true value that is now known. However, in Figure 10.2, we move the window only 3 times, i.e., by 3 time steps, which means that the blue and red sample do not yet overlap, but are just about to do so. Therefore, the figure does not allow one to see how well the first predicted value corresponds to the related, true value. In any case, even if we went one step further and allowed for the blue and red samples to start overlapping, their superposition would not make the comparison easy. However, we performed numerous experimental tests of prediction, and the visual comparison of the predicted and true values is generally quite good. A numerical assessment of the quality of prediction is given later.

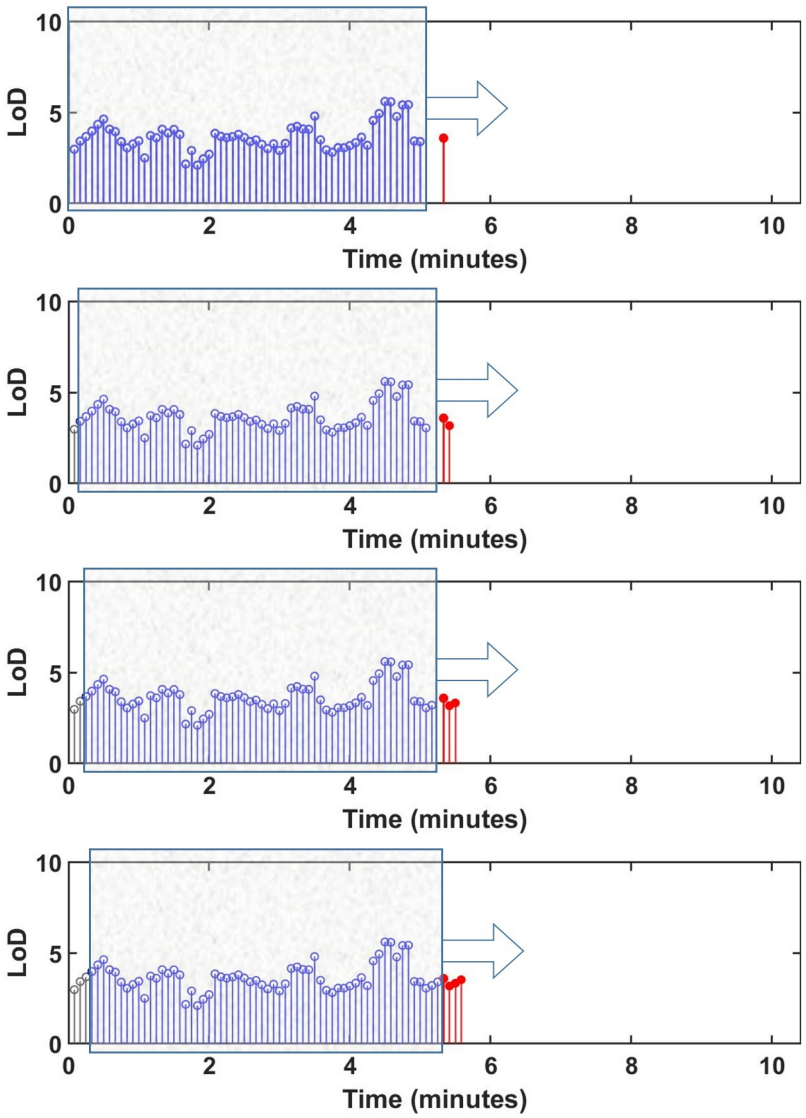

Figure 10.2: The figure illustrates the task of predicting future values of an LoD signal (from Study A) using a GBM RP model that adapts/evolves with time. The four successive graphs correspond to four successive positions of the window and, thus, of the present time. From one graph to the next, the window is moved by one time step, i.e., by 5 sec. In each graph, one uses all samples in the window shown to adapt the model (i.e., to compute the new μ and σ), and one then uses the adapted model to predict one single sample 4 time steps into the future, i.e., 20 sec into the future. The last graph corresponds to the case where the first predicted sample falls one time step ahead of the present time.

10.3.2 Discussion of results

In this section, we illustrated the potential of the GBM RP model to produce adaptive predictions of FVs for LoD signals via an illustrative example using an LoD signal from Study A.

Using a 5-minutes sliding time window, we illustrated that, at each time step, one can perform two tasks: (1) adaptation of the GBM RP model and (2) predict FVs of the signal.

Consequently, we illustrated (via an example) that the GBM RP model can readily adapt and predict FVs of an LoD signal, in real-time.

10.4 Adaptive prediction of first hitting time (FHT) (for LoD signals)

Below, we progressively describe how to predict the first hitting time (FHT) using a sliding time window via two illustrative examples using one signal from Study A and one signal from Study B, respectively.

10.4.1 First illustration of adaptive prediction of FHT (for one signal from Study A)

Figure 10.3 illustrates the task of predicting the first hitting time (FHT) for an LoD signal (from Study A) using a GBM RP model that adapts/evolves with time.

Although Figure 10.3 looks quite different from Figure 10.2, both figures are similar in spirit. First, whereas, in Figure 10.2, we show four (successive) position of the sliding time window, we only show one such window position in the present Figure 10.3. Second, since the prediction is now the FHT, we need to show one graph for the LoD signal and one separate graph for the FHT signal. Third, the FHT sample is shown at the present time (which is the simplest way of showing the FHT value). In terms of the terminology of Section 3.2, the two graphs corresponds to the (measurement) signal x_n and to the prediction signal y_n.

The pair of graphs in the present Figure 10.3 can be interpreted almost exactly in the same way as the four graphs of Figure 10.2. Of course, the difference is that we now predict the FHT rather than FVs of the signal at some time in the future, and precisely 4 time steps ahead in Figure 10.2. Note that the prediction of an FV involves specifying the time in the future where one wishes to make this prediction, whereas the FHT does not involve any such parameter. Also note that

the FHT implicitly says that one is interested in the first time where the signal "hits" the specified threshold level, and thus not the second time, third time, etc. The threshold level is shown in the figure.

At each time step, and thus for each position of the window, one performs two tasks: (1) adaptation of the model and (2) prediction of the FHT. Recall that the adaptation means computing the new values of μ and σ.

As in the case of Figure 10.2, one uses all the LoD-signal samples within the window to predict, at "each present time", the corresponding FHT. In Figure 10.3, the last FHT sample shown is thus computed based on the GBM RP model corresponding to the window shown. All other FHT samples shown corresponds to all previous positions of the present time and, thus, of the window. While we always indicate the FHT as the time (of first hitting) with respect to, i.e., relatively to, the present time, one could also envision expressing it in terms of the absolute time. Note that the FHT is expressed in minutes, and, thus, not in time steps.

The present Figure 10.3 is similar in spirit to Figure 9.9. Indeed, while Figure 10.3 shows the values of the FHT at the present time, Figure 9.9 shows the values of the parameters μ and σ at the present time. The sole reason for this last comment is to show that, in both cases, the value of interest (i.e., FHT, μ, and/or σ) are shown at the present time. The second graph of Figure 10.3 is thus similar in structure to the last two graphs of Figure 9.9.

Imagine that the predicted value of FHT at time n is t_n. Then, to determine how good the predicted value of FHT is, one needs to look at the LoD signal at time $n+\lfloor t_n/\Delta t \rfloor$, where Δt is the spacing (in minutes) between samples, and observe whether or not the LoD signal "goes through" the threshold level at that time index. Note that we only consider the cases where the signal crosses the threshold level coming from below it and going above it.

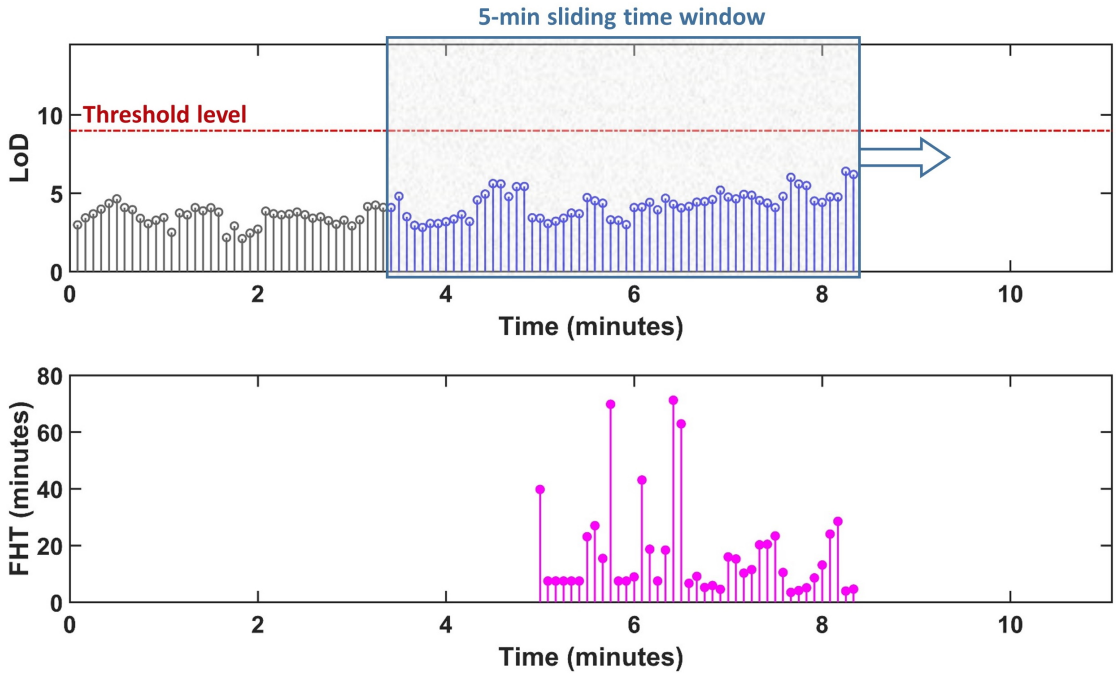

Figure 10.3: The figure illustrates the task of predicting the first hitting time (FHT) for an LoD signal (from Study A) using a GBM RP model that adapts/evolves with time. The adaptation of the model and the subsequent calculation of the FHT value is done at each time step, i.e., every 5 sec. The graphs successively show the LoD signal of interest and the corresponding FHT signal, which respectively correspond to the generic signals/notations x_n and y_n introduced in Section 3.2. The FHT predicted at each present instant n is shown as a sample at time n. The last FHT sample shown corresponds to the shown position of the window. Each FHT value at time index n indicates the time (in minutes) past n where the LoD signal is predicted to go through the threshold level for the first time, from below.

10.4.2 Second illustration of adaptive prediction of FHT (for one signal from Study B)

Figure 10.4 illustrates the task of predicting the first hitting time (FHT) for an LoD signal (from Study B) using a GBM RP model that adapts/evolves with time.

This figure is the counterpart, for Study B, of Figure 10.3, related to Study A. The main difference between the two figures is the sample separation, which is 5 sec for Study A (and, thus, for Figure 10.3) and 20 sec for Study B (and, thus, for

Figure 10.4).

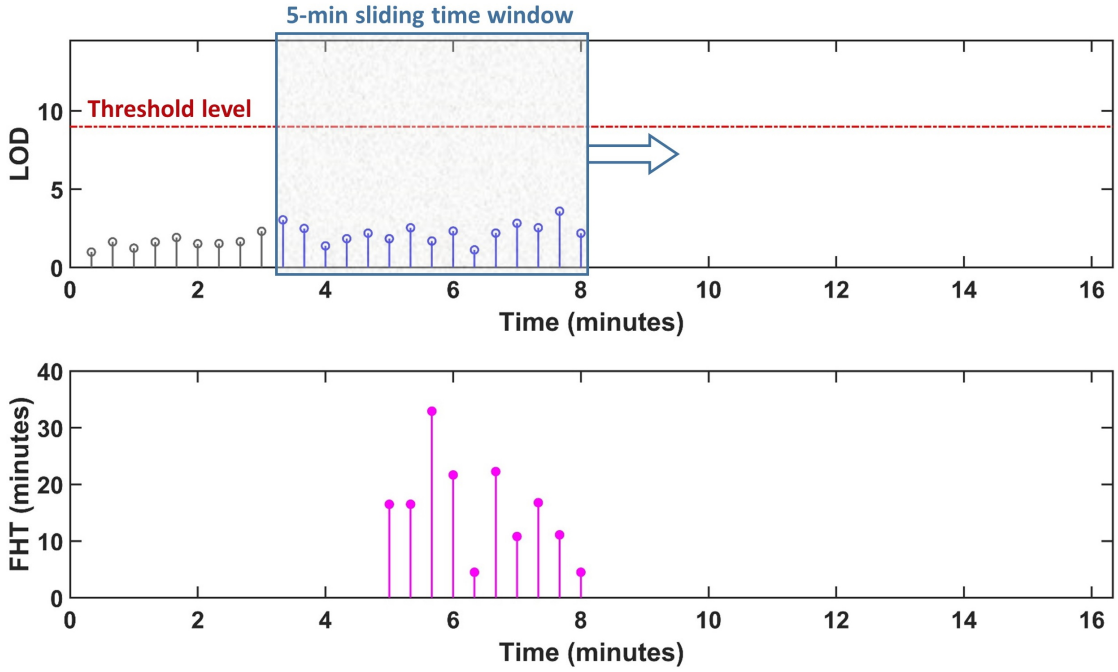

Figure 10.4: This figure is the counterpart, for Study B, of Figure 10.3, related to Study A. The adaption of the model and the subsequent calculation of the FHT value is done at each time step, i.e., every 20 seconds. All other comments made in the caption of Figure 10.3 apply here.

10.4.3 Discussion of results

In this section, we illustrated the potential of the GBM RP model to produce adaptive predictions of the FHT for LoD signals via two illustrative examples of LoD signals (one from Study A and one from Study B).

Using a 5-minutes sliding time window, we illustrated that, at each time step, one can perform two tasks: (1) adapt the GBM RP model and (2) predict the FHT.

Consequently, we illustrated (via two examples) that the GBM RP model can readily adapt and predict the FHT of an LoD signal, in real-time.

10.5 Adaptive prediction of survival probability (SP) (for LoD signals)

Below, we progressively describe how to predict the first hitting time (FHT) using a sliding time window via two illustrative examples using one signal from Study A and one signal from Study B, respectively.

The texts of the following three subsections are made, on purpose, as similar as possible to the texts of the corresponding sections in Section 10.4.

10.5.1 First illustration of adaptive prediction of SP (for one signal from Study A)

Figure 10.5 illustrates the task of predicting the survival probability (SP) for an LoD signal (from Study A) using a GBM RP model that adapts/evolves with time.

Although Figure 10.5 looks quite different from Figure 10.2, both figures are similar in spirit. First, whereas, in Figure 10.2, we show four (successive) position of the sliding time window, we only show one such window position in the present Figure 10.3. Second, since the prediction is now the SP, we need to show one graph for the LoD signal and one separate graph for the SP signal. Third, the SP sample is shown at the present time (which is the simplest way of showing the SP value). In terms of the terminology of Section 3.2, the two graphs corresponds to the (measurement) signal x_n and to the prediction signal y_n.

The pair of graphs in the present Figure 10.5 can be interpreted almost exactly in the same way as the four graphs of Figure 10.2. Of course, the difference is that we now predict the SP rather FV of the signal at some time in the future, and precisely 4 time steps ahead in Figure 10.2. Note that the prediction of a FV involves specifying the time in the future where one wishes to make this prediction, whereas the SP involves specifying two other parameters: (1) survival time and (ST) and (2) threshold level (TL). In this example, TL and ST are equal to 9 and one minute respectively.

At each time step, and thus for each position of the window, one performs two tasks: (1) adaptation of the model and (2) prediction of the SP. Recall that the adaptation means computing the new values of μ and σ.

Here, the SP is defined as the probability that FVs of the signal stay strictly below TL for the duration of the ST.

As in the case of Figure 10.2, one uses all the LoD-signal samples within the window to predict at "each present time" the corresponding SP. In Figure 10.5,

the last SP sample shown is thus computed based on the GBM RP model corresponding to the window shown. All other SP samples shown corresponds to all previous positions of the present time and, thus, of the window.

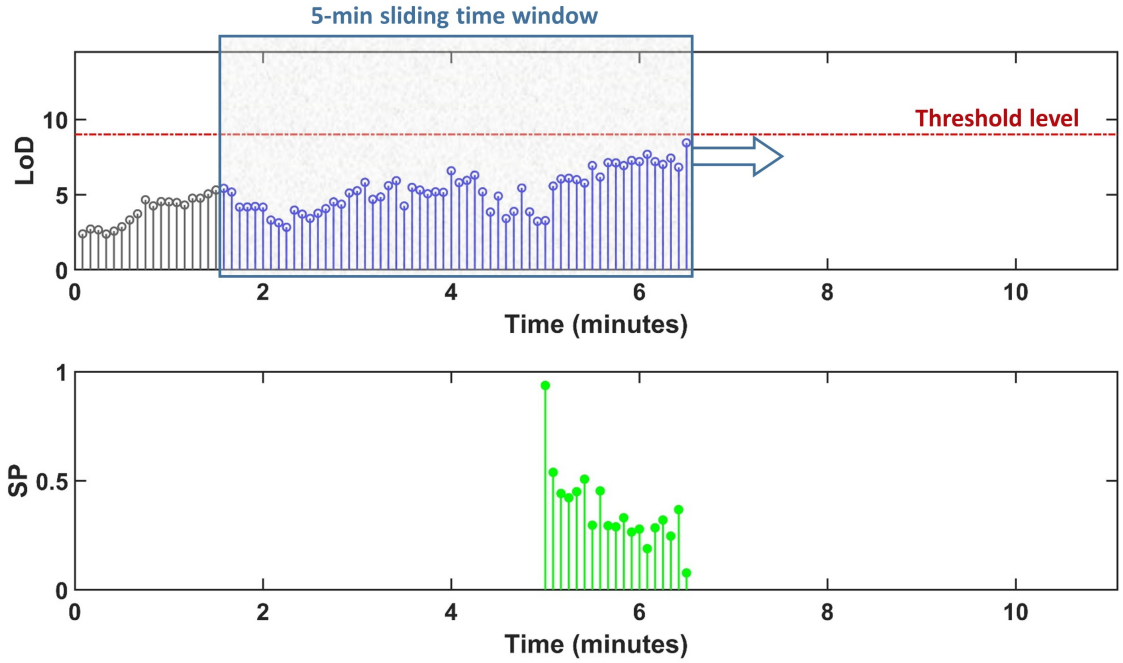

Figure 10.5: The figure illustrates the task of predicting the survival probability (SP) for an LoD signal (from Study A) using a GBM RP model that adapts/evolves with time. The present figure is the equivalent, for SP, of Figure 10.3, related to FHT. The adaptation of the model and the subsequent calculation of the SP value is done at each time step, i.e., every 5 sec. The graphs successively show the LoD signal of interest and the corresponding SP signal, which respectively correspond to the generic signals/notations x_n and y_n introduced in Section 3.2. The SP predicted at each present instant n is shown as a sample at time n. The last SP sample shown corresponds to the shown position of the window. Each SP value at time index n indicates the probability that the LoD signal will remain below the LoD threshold of 9 during a time of survival of 1 minute or more.

10.5.2 Second illustration of adaptive prediction of SP (for one signal from Study B)

Figure 10.6 illustrates the task of predicting the survival probability (SP) for an LoD signal (from Study B) using a GBM RP model that adapts/evolves with time.

This figure is the counterpart, for Study B, of Figure 10.5, related to Study A. The main difference between the two figures is the sample separation, which is 5 sec for Study A (and, thus, for Figure 10.5) and 20 sec for Study B (and, thus, for Figure 10.6).

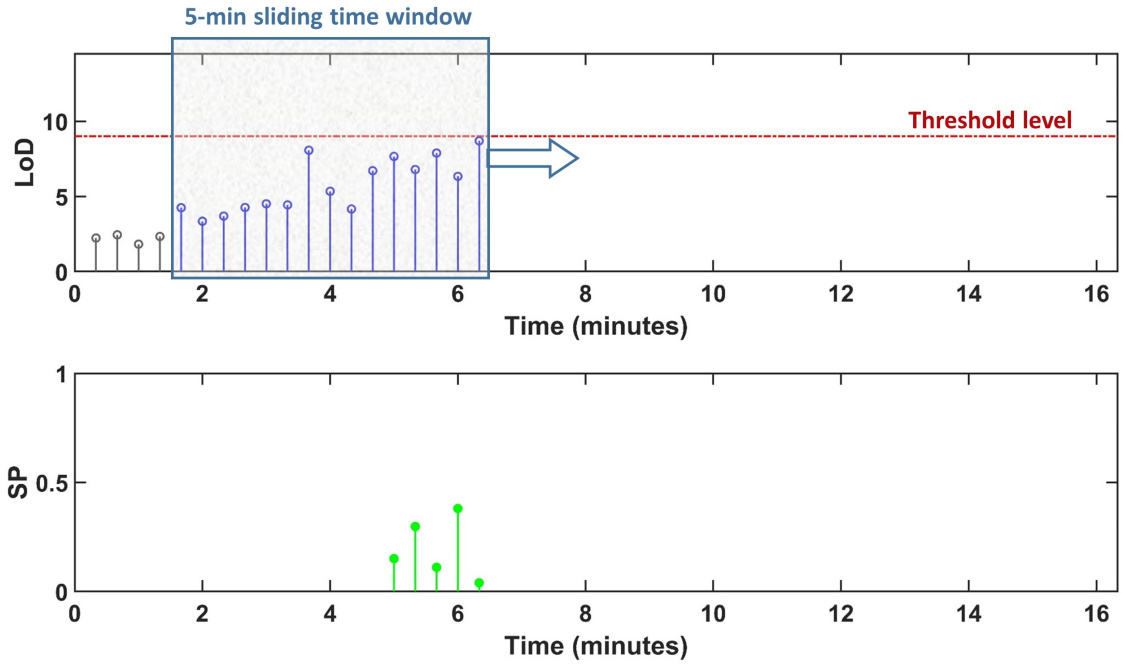

Figure 10.6: This figure is the counterpart, for Study B, of Figure 10.5, related to Study A. It indeed illustrates the task of predicting the survival probability (SP) for an LoD signal (from Study B) using a GBM RP model that adapts/evolves with time. The adaptation of the model and the subsequent calculation of the SP value is done at each time step, i.e., every 20 sec. All other comments made in the caption of Figure 10.5 apply here.

10.5.3 Discussion of results

In this section, we illustrated the potential of the GBM RP model to produce adaptive predictions of the SP for LoD signals via two illustrative examples of

LoD signals (one from Study A and one from Study B).

Using a 5-minutes sliding time window, we illustrated that, at each time step, one can perform two tasks: (1) adapt the GBM RP model and (2) predict the SP.

Consequently, we illustrated (via two examples) that the GBM RP model can readily adapt and predict the SP, in real-time.

10.6 Detection of drowsiness

10.6.1 General principle of detection using a threshold

Later, in the presentation of drowsiness detection systems, we consider signals and related thresholds, where the threshold is related to the values of the signal. Instead of just "threshold", we sometimes talk about a "threshold level", but the two terms are, for all practical purposes, equivalent.

Since the signals that we consider later are nonnegative, we can assume, for concreteness, that the signals considered in this section are nonnegative, but this assumption does not entail any loss of generality.

We assume that the signals of interest are DT signals. However, the whole discussion below is easily adapted for CT signals.

We consider a generic DT signal x_n and a threshold (level) a.

When one considers a signal x_n and a threshold a, there are two possibilities for the value of the signal x_n at any particular instant, say n_0, i.e., (1) $x_{n_0} \geqslant a$ and (2) $x_{n_0} < a$. Note that one could also consider the alternate pair of possibilities (1) $x_{n_0} > a$ and (2) $x_{n_0} \leqslant a$, where the equality has moved to the second case.

The two possibilities above, i.e., for a generic n, (1) $x_n \geqslant a$ and (2) $x_n \leqslant a$, can be viewed as corresponding to two classes, which we call Class 1 and Class 2, or C1 and C2 for short.

According to the view just presented, each instant n has a class associated with it, i.e., either C1 or C2.

In a traditional "target detection" problem (where "target" is used in a very broad sense), these two classes typically correspond to the cases "target" (or "target present") and "no target" (or "target absent"). Note that the terminology reflects the fact that a signal above threshold is assumed to indicate a target. However, it could very well be that the presence of a target corresponds to a signal value below the threshold. This will, in fact, be the case in the main drowsiness-detection systems considered later.

Since the comparison of a signal value to a threshold leads to two possible

classes C1 and C2, one can view this operation as effectively acting as a binary classifier.

Rather than talking about the dichotomy "target" vs "no target" or, even, "detection" vs "no detection", it is convenient to present the problem at hand in more general terms, i.e., to abstract it as much as possible.

In a binary classifier, one traditionally labels each outcome (or result) as being positive (p) or negative (n).

In the case where the binary classifier corresponds to the position of a signal value x_n with respect to a threshold a, one has the freedom of declaring that p corresponds to $x_n \geqslant a$ and n to $x_n < a$, or vice-versa. One must thus specify in a clear and precise way what p (and, thus, n) corresponds to. As a result, it could very well be that the presence of a "target" corresponds to p.

Still in the case of a signal x_n and a threshold a, the proper picture to have in mind is that, at each n, the classification process (i.e., the classifier) provides one (specific) outcome, i.e., p or n. One could even produce a DT binary outcome signal o_n that would have, e.g., a value of 1 for p, and of 0 for n. Conceptually, one can image a signal of labels p and n. The key point is that one has a p or n at each time index n. (This double use of "n" should not create any confusion.)

10.6.2 Ground truth for evaluation of performance

We indicated above that a system that performs "detection" using a threshold acts as a binary classifier.

In order to characterize the performance of a binary classifier, one must know the ground truth corresponding to each outcome. If the classifier outputs p, one should know whether the ground truth is p or n. Similarly, if the classifier outputs n, one should know whether the ground truth is p or n.

In the case of the signal x_n and threshold (as introduced above), we indicated that we should imagine that, at each time n, the classifier produces p or n. Therefore, the ground truth should tell us, for each n, what the true value is, either p or n.

It is convenient to imagine that the classifier produces a vector where the elements are p or n, and that the ground truth provides a similar vector, in perfect correspondence with the first one.

10.6.3 Key statistics describing the performance of a binary classifier

The description of the performance of a binary classifier involves a number of parameters and related terminology, which are introduced and defined below [35].

As indicated above, the binary classifier labels all outcomes/results (without exception) as one of the following:

- **positive (p)**
- **negative (n)**.

Assuming that we have access to the ground truth, each of the labels p and n can in turn be labelled as true (T) or false (F). As indicated above, it is useful to imagine (1) that all outcomes of interest (p or n) are placed in a vector, and (2) that the ground truth (or truth) is represented by a second vector (perfectly registered with the first one) also containing the (true) labels p or n.

This leads to the following four phrases describing each outcome/result

- **true positive (TP):**
  - both the classifier and the truth say p;
  - one also talks about "correct detection";
- **true negative (TN):**
  - both the classifier and the truth say n;
  - one also talks about "correct rejection";
- **false positive (FP):**
  - the classifier says p, but the truth says n;
  - one talks about "false alarm" or "type I error";
- **false negative (FN):**
  - the classifier says n, but the truth says p;
  - one talks about "miss" or "type II error".

For example, assuming that one knows the ground truth, one can say that a particular outcome/result is a true positive (TP).

However, one also uses the abbreviation TP to denote the total number of elements in the outcomes/results that are true positives (TPs). This is the case when TP appears in a mathematical formula, as we shall see below.

The above comments apply to all four abbreviations above, i.e., TP, TN, FP, and FN.

In the same vein, the two following parameters also give a total number of elements:

- **condition positives (P)** = total number of (real) p in ground truth
- **condition negatives (N)** = total number of (real) n in ground truth.

As we shall see below, these two numbers are generally used for normalization purposes.

Assuming that TP, TN, FP, and FN represent total numbers of elements (among the outcomes/results), one defines the following four important parameters:

- **True positive rate (TPR)**, aka sensitivity, recall, and hit rate:
  - $\mathrm{TPR} = \dfrac{\mathrm{TP}}{\mathrm{P}} = \dfrac{\mathrm{TP}}{\mathrm{TP+FN}} = 1\text{–FNR}$
- **True negative rate (TNR)**, aka specificity and selectivity:
  - $\mathrm{TNR} = \dfrac{\mathrm{TN}}{\mathrm{N}} = \dfrac{\mathrm{TN}}{\mathrm{TN\ +FP}} = 1\text{–FPR}$
- **False positive rate (FPR)**, aka fall-out and false alarm rate:
  - $\mathrm{FPR} = \dfrac{\mathrm{FP}}{\mathrm{N}} = \dfrac{\mathrm{FP}}{\mathrm{FP\ +TN}} = 1\text{–TNR}$
- **False negative rate (FNR)**, aka miss rate:
  - $\mathrm{FNR} = \dfrac{\mathrm{FN}}{\mathrm{P}} = \dfrac{\mathrm{FN}}{\mathrm{FP\ +TN}} = 1\text{–TPR}.$

Several other similar parameters can be defined in terms of the 10 parameters above.

10.6.4 Confusion matrix

The confusion matrix is a first, important tool for characterizing the performance of a binary classifier.

Figure 10.7 shows the structure of a confusion matrix.

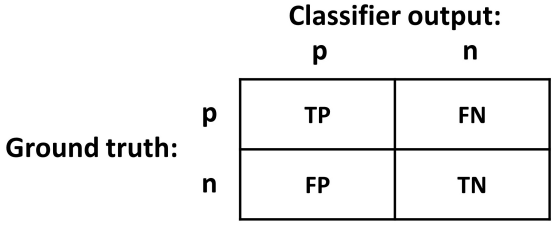

Figure 10.7: The figure shows the structure of a confusion matrix, which is a way to characterize the performance of a binary classifier.

10.6.5 Receiver operating characteristic (ROC) curve

The receiving operating characteristic (ROC) curve is a second, important tool for characterizing a binary classifier.

The ROC curve shows how the (value of) TPR varies as a function of (the value) of FPR. The curve consists in a set of points with coordinates (FPR, TPR), where each point corresponds to a particular value of a parameter. This parameter is typically a detection threshold (such as the threshold a introduced in Sect Section 10.6.1).

Figure 10.8 shows a conceptual example of ROC curve.

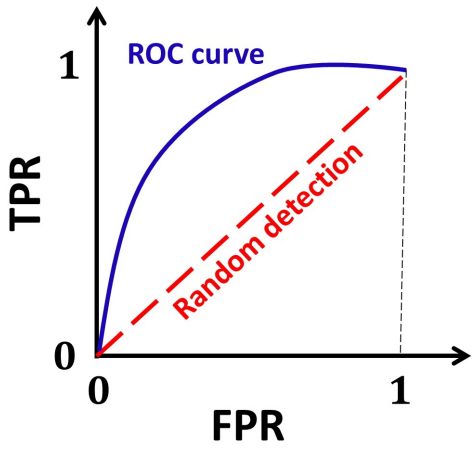

Figure 10.8: The figure shows a hypothetical example of a ROC curve, which is way to characterize the performance of a binary classifier. The diagonal line corresponds to random detection, and is shown just for reference.

Later, we use the ROC curve as the primary tool for evaluating the performance of drowsiness-detection systems.

10.6.6 Three adaptive drowsiness-detection systems using a threshold

In Chapter 3, we described the prediction of FVs of a signal, the first hitting time (FHT), and the survival probability (SP).

We indicated that, in operational conditions, it is paramount that one be able to adapt the RP process model that underlies the (measurement) signal of interest, i.e., an LoD signal in the context of this thesis.

In Chapter 9, we demonstrated that we could easily adapt the GBM RP model to track the evolution of an signal. In the present chapter, and specifically in Sections 10.3, 10.4, and 10.5, we demonstrated that we could perform all three types of predictions indicated above, and, furthermore, adaptively, using a sliding time window.

At this point, we can thus assume that we can easily produce, adaptively and in real-time, (1) FVs of a signal (at any specified time horizon), (2) an FHT signal, and (3) an SP signal. Examples of such signals of are found in Figures 10.2, 10.3, and 10.5, respectively.

It follows that we can place a threshold a on any of these signals y_n and, thereby, create three very different types of "drowsiness-detection" systems, which we now

briefly describe in high-level terms.

In accordance with the earlier development, the key is to declare at some time n that we have a "detection", i.e., a "positive" (or "p"). In the present application of drowsiness monitoring, this "detection" corresponds to a present time n where we detect "something" that is indicative that the drowsiness is about to evolve in a dangerous way. At the moment where we get such a "detection", i.e., "p", we will likely decide to activate an alarm of some sort. Describing the exact form/nature of this alarm is beyond the scope of this thesis.

The key point made in the last paragraph is that we must have some sort of "detection", i.e., "p" at the appropriate time.

A very interesting aspect of our work is that we have identified and described three distinct mechanisms that can be the basis for generating a detection, i.e., FVs of a signal, the FHT, and the SP. Furthermore, all three mechanisms could be called upon to produce a sophisticated, multi-mode detection and alarm system.

One important message from the above discussion is that we place the emphasis on some type of detection, and thus not on an alarm. While both are related, the detection comes, in our view, before the (issuing of an) alarm.

In the case of the prediction of FVs of the LoD signal, one could place an (LoD) threshold on FVs of the (LoD) signal, say, 20 sec in the future. The LoD threshold could be placed at 7, on a scale of 0 to 10. For this detection system, we can produce a confusion matrix and a ROC curve, using for parameter either the LoD threshold or the time horizon. One should emphasize that the various parameters of this system could be changed.

In the case of the prediction of the FHT, one could place a threshold on the FHT signal. For example, one would want to declare a "detection" if the LoD goes above some LoD threshold, say, in 60 sec. We can then compute the confusion matrix and ROC curve for such a system.

In the case of the prediction of the SP, one could place a threshold on the SP signal. For example, one could want to declare a "detection" if the SP goes below some SP threshold, say, of 0.3. Carefully note that we wish an SP that is as high as possible. It is this when the SP falls below the threshold that we want to have a detection. One would imagine that, when one starts driving, the SP would be 1. It would be catastrophic if it were 0!

Below, we consider in detail a drowsiness-detection system based on SP. We illustrate the operation of the system, and we quantify its performance in terms of a ROC curve.

We could do exactly the same for FVs of the LoD signal and for the FHT, but we decided not to do so in the present document.

We emphasize that the systems described could be optimized and fine-tuned in various ways. For example, the various thresholds involved could be adjusted/adapted dynamically as the drive progresses.

10.6.7 Illustration of adaptive detection of drowsiness based on SP

We describe, in a highly visual way, the operation of an adaptive drowsiness-detection system based on survival probability (SP). The next two sections describe the operation of the system on two different example signals, one from Study A and one from Study B. Recall that the adaptive nature of the system stems from the fact the underlying GBM RP process is periodically adapted and, in fact, here, at each time step (of 5 sec for the signal from Study A, and of 20 sec for the signal from Study B).

10.6.7.1 First illustration of adaptive detection of drowsiness based on SP (for one signal from Study A)

Figure 10.9 illustrates the operation, on one example signal from Study A, of an adaptive drowsiness-detection system based on SP. The signal is the same as the one considered in Section 10.5.1.

Figure 10.9 is an augmented version of Figure 10.5, and differs from it in three ways. First, we replaced the term "threshold level" by "LoD threshold". Second, we added a threshold on the SP signal, naturally called "SP threshold". Third, we added the first detection, which corresponds to the time index n where the SP signals falls below the SP threshold.

The SP threshold is arbitrarily set to 0.3. (Since the SP is a probability, the range of its values is from 0 to 1.) The idea is to declare a "detection" each time the SP signal falls below the SP threshold.

It is worth saying in words what the strategy is, and what the graphs show. In the present scenario, we wish to issue an alarm when the survival probability (SP) falls below 0.3, where the SP is the probability that the LoD signal will stay below the LoD threshold of 9 for at least a duration (the time of survival) of 1 minute.

Of course, the three parameters listed above can be changed. In the design of an actual driver monitoring system (DMS), one would need to decide how these parameters are selected or adjusted. Some parameters could be adjusted in real time, and these adjustments could be done either automatically by the DMS based on a variety of state-characterizing inputs (from vehicle, driver, and environment) or by the driver, or both. Designing an actual DMS is beyond the scope of the

present thesis.

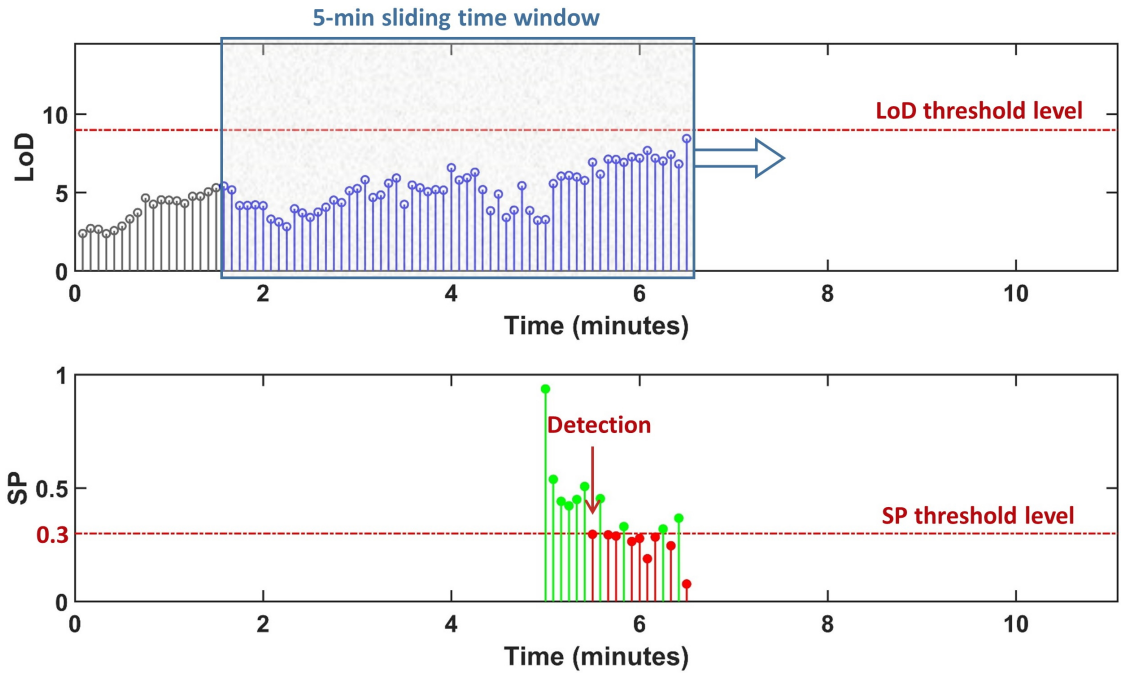

Figure 10.9: The figure uses Figure 10.5 as a basis. The first graph shows the example LoD signal (from Study A) and the selected LoD threshold (at 9). The second graph shows the corresponding survival probability (SP) signal. The GBM RP model that is used to compute the SP sample at each present time is adapted at each time step (of 5 sec) using the data within the sliding time window shown (which has a duration of 5 min, i.e., 60 samples). A main difference with respect to Figure 10.5 is that addition of the SP threshold (set to 0.3). The "detection" shown corresponds to the (first) time when the SP signal falls below the SP threshold. In practice, one might to issue an alarm at that moment.

10.6.7.2 Second illustration of adaptive detection of drowsiness based on SP (for one signal from Study B)

Figure 10.10 illustrates the operation, on one example signal from Study B, of an adaptive drowsiness-detection system based on SP The signal is the same as the one considered in Section 10.5.2. All comments made in the previous section apply here, except for the fact the present time step is of 20 sec.

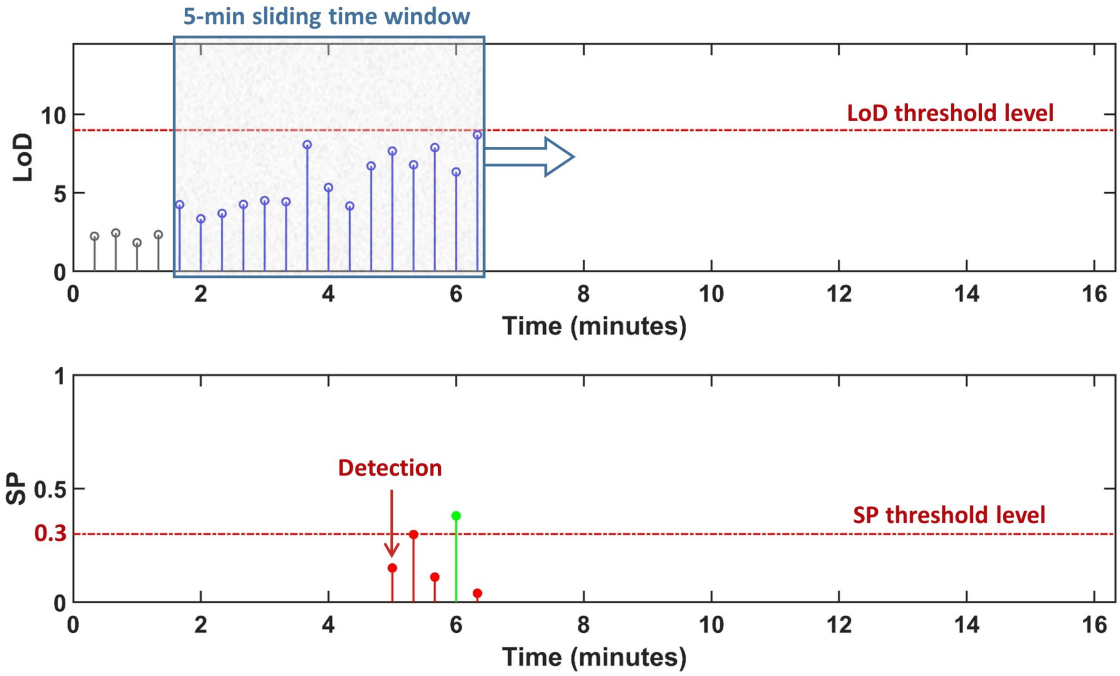

Figure 10.10: This figure is the counterpart, for Study B, of Figure 10.9, related to Study A. The figure uses Figure 10.6 as a basis. The first graph shows the example LoD signal (from Study B) and the selected LoD threshold (at 9). The second graph shows the corresponding survival probability (SP) signal. The GBM RP model that is used to compute the SP sample at each present time is adapted at each time step (of 20 sec) using the data within the sliding time window shown (which has a duration of 5 min, i.e., 15 samples). A main difference with respect to Figure 10.6 is that addition of the SP threshold (set to 0.3). The "detection" shown corresponds to the (first) time when the SP signal falls below the SP threshold. In practice, one might want to issue an alarm at that moment.

10.6.8 Performance of adaptive drowsiness detection system based on SP

10.6.8.1 Principle of detection

We describe here a detection system based on the use of survival probability (SP). The principle of such a system is already touched upon in Section 10.6.6. Figures 10.9 and 10.10 provide a visual support for the description of the system, which follows.

The three key parameters of the detection system are:

1. Level of drowsiness (LoD) threshold
2. Survival time (ST)
3. Survival probability (SP) threshold.

The specific values used in the two figures are 9, 1 minute, and 0.3, respectively.

The basic principle of our detection system based on SP is as follows. Each time the survival probability (SP) signal, or SP signal, falls strictly below the specified SP threshold (i.e., SP signal/sample $<$ SP threshold), we issue a detection.

For a given signal (such as any of the signals from Study A and Study B), there can be no detection, one detection, or several detections. (Once again, each detection corresponds to an SP sample falling strictly below the SP threshold.)

For a long drive, one would, of course, consider all detections that occur. By contrast, in the present work, given that all signals in Study A and Study B are relatively short, we consider at most one detection per signal in the evaluation of the performance of the present detection system. This means that, as soon as the first detection (if any) is issued, the rest of the potentially-remaining detections are ignored.

It is worth repeating that the SP at each instant n is the probability, computed at n, that the LoD signal will remain strictly below the LoD threshold for a duration of time that is at least equal to the specified survival time (ST).

10.6.8.2 Key detection statistics

To compute the performance of our drowsiness-detection system based on SP, we have to specify what we mean by "true positives (TP)", "true negatives (TN)", "false positive (FP)", and "false negative (FN)". Based upon the discussion in the previous section, for each signal x_n, we define TP, TN, FP, and FN as follows:

- **true positives (TP)**: the signal passed the LoD threshold (i.e., $x_n \geqslant$ LoD threshold) and at least one detection (i.e., $y_n <$ SP threshold, where y_n is the SP signal) was issued before the passage;
- **true negative (TN)**: the signal did not pass the LoD threshold and no detection was issued;
- **false positives (FP)**: the signal did not pass the LoD threshold, but at least one detection was issued;

- **false negative (FN)**: the signal passed the LoD threshold, but no detection was issued before the passage.

Above, "passage" refers, of course, to the passage of the LoD signal x_n through the LoD threshold level.

In the next two sections, we use these four parameters, to construct the ROC curve describing the drowsiness-detection system, this for all signals from Study A and for all signals from Study B. Here, we produce two distinct ROC curves.

Any ROC curve involves a "detection parameter". It is by varying this parameter that one obtains a set of pairs of values of TPR and FPR. In the present case, this parameter is the SP threshold. It should be clear that (1) if one lowers the SP threshold, one will increase the number of TPs (correct detections) and also increase the number of FPs (false alarms), and that (2) if one raises the SP threshold, one will decrease the number of TPs (correct detections) and also decrease the number of FPs (false alarms), This means (1) that, as one decreases the SP threshold, one moves toward the upper-right corner of the ROC "frame", and (2) that, as one increases the SP threshold, one moves toward the lower-left corner of the ROC "frame".

In the ROC curves shown below, we use 200 values of the SP threshold that divide the [0,1] interval (of probabilities) in intervals of equal lengths. This mean that each ROC curve is built from 200 points, i.e., pairs of TPR and FPR.

We now show the two ROC curves obtained for the detection system described above.

10.6.8.3 ROC curve with SP as parameter (for all 51 signals from Study A)

The first ROC curve corresponds to all 51 signals from Study A; it is called "ROC curve A" and is shown in Figure 10.11.

Even though 200 points—corresponding to 200 equispaced values of the SP threshold—are used to construct each ROC curve, one only sees about 30 points (solid dots) in each graph. This is due to fact that some of the points/dots shown correspond to several identical pairs (TPR, FPR).

The graph shows the line at 45°, which corresponds to the random issuance of a detection.

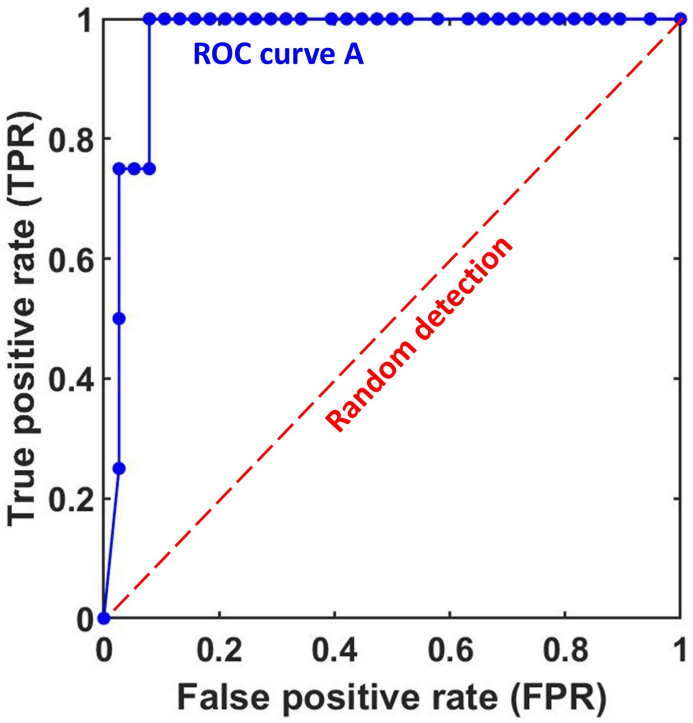

Figure 10.11: The figure shows the ROC curve describing the performance of the detection system described in the text, for all 51 signals from Study A. For each signal, only the first alarm (if any) is taken into account. The parameter that is varied to produce the ROC curve is the SP threshold. The lower-left end of the curve corresponds to an SP threshold of 0 (minimum value), and the upper-right end of the curve to an SP threshold of 1 (maximum value). While 200 equispaced values of the SP threshold are used, not all points appear distinctly in the figure as a result of the existence of pairs (TPR,FPR) that are identical. The diagonal line corresponds to the random issuance of a detection, and is shown just for reference.

10.6.8.4 ROC curve with SP as parameter (for all 39 signals from Study B)

The second ROC curve corresponds to all 39 signals from Study B; it is called "ROC curve B" and is shown in Figure 10.12.

All the comments above for ROC curve A apply to ROC curve B.

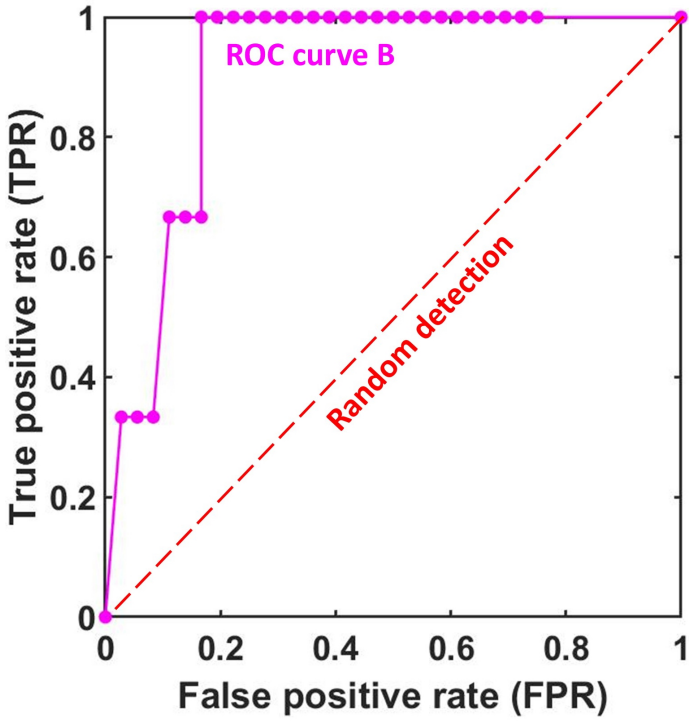

Figure 10.12: This figure is the counterpart, for Study B, of Figure 10.11, related to Study A. The figure thus shows the ROC curve describing the performance of the detection system described in the text, for all 39 signals from Study B. Most comments made for Figure 10.11 apply to the present figure.

10.6.8.5 Comparison of ROC curves for Study A and Study B

Figure 10.13 shows both ROC curves jointly in the same axes.

The curves show that the (drowsiness) detection system performs better on the signals from Study A than on the signals from Study B. This may be due to the fact that that the sampling rate of the signals is four times higher in Study A than in Study B (i.e., 5 sec vs 20 sec).

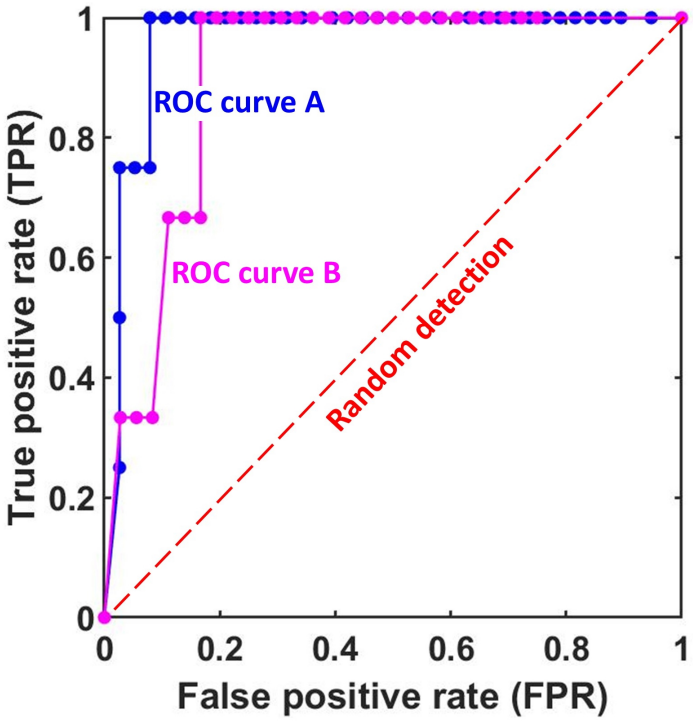

Figure 10.13: The figure shows, in the same axes, the two ROC curves of Figures 10.11 and 10.12. For memory, ROC curve A is obtained using all 51 signals from Study A, and ROC curve B is obtained using all 39 signals from Study B. The curves show that the detection system performs better on the signals from Study A that on the signals from Study B. This may be due to the fact that that the sampling rate of the signals is four times higher in Study A than in Study B.

10.6.9 Discussion of results

We indicated that comparing a signal to a threshold effectively leads to a binary classifier.

We reviewed the various parameters that describe the performance of a binary classifier, and we reviewed briefly the two main tools that are typically used to describe the classification performance of a binary classifier, i.e., the confusion matrix and the ROC curve.

We indicated that we could define thresholds on the three types of predictions of interest, i.e., FVs, the FHT, and the SP. This allows us to construct simple drowsiness-detection systems. These systems declare a "detection" when the corresponding value/signal crosses the threshold.

We examined in detail the performance of a drowsiness-detection system based on SP, both for all 51 signals from Study A and all 39 Signals from Study B.

The ROC curves indicate, at a glance, that the drowsiness-detection system based on SP exhibits excellent performance, this for two distinct datasets.

10.7 About prediction for signals from Study C

We performed, on all signals from Study C, the same prediction exercise as the ones described above for Study A and Study B. Furthermore, using the signals from Study C, we found the optimal values of the following four parameters: (1) sampling period, (2) size of the window, (3) LoD threshold level, and (4) SP threshold level. However, as already indicated the results linked to Study C are protected by a non-disclosure agreement.

10.8 Conclusion

While Chapter 9 is dedicated to modeling, the present chapter is dedicated to prediction.

We presented progressively experimental results for the three types of predictions of interest, i.e., future values (FVs), the first hitting time (FHT), and the survival probability (SP).

The first set of experiments was performed using a fixed RP model for each signal of interest and we focused on predicting FVs (of a signal). This allowed us to use more samples to built the model. For all signals from Study A, we considered both the GBM RP model and the conventional RP models, and we reported on the performance of prediction, both in terms of prediction error and computation time. We also showed a graph illustrated the process of prediction for one signal, using a GBM RP model.

For all subsequent experiments we used only the GBM RP model and we used it in an adaptive way, meaning that the model is adapted at each time step (of 5 or 20 seconds) using a sliding time window of 5 minutes in duration.

Using such an adaptive GBM RP model, we illustrated the prediction of the quantities of interest, i.e., FVs, the FHT, and the SP.

We described a drowsiness-detection system using any of the three types of predictions together with a threshold. We examined in detail the operation and performance of a drowsiness-detection system based on SP.

The modeling and detection experiments described in the present chapter and

the previous chapter, demonstrate the definite and high potential of the GBM RP model to make various types of prediction concerning the evolution of the level of drowsiness of a person such as a driver.

Chapter 11

Conclusion

Drowsiness is a major cause of accidents in many areas of human activity, and transportation is probably the single most important source of drowsiness-related accidents. It is thus critical to monitor a driver's level of drowsiness (LoD), and to devise in-car safety systems to help prevent related accidents.

For road vehicles, we distinguished between three categories of in-vehicle systems for monitoring drowsiness, which respectively monitor the car behavior, the driver behavior, and the driver physiology. We explained that the systems in the last category are the only ones that can truly measure the state of drowsiness of a person, and that they are application-independent and "universal".

As indicated in Chapter 2, all significant drowsiness monitoring systems that reasonably claim to estimate and produce the LoD of an operator in real-time do, in fact, produce an LoD that is representative of the recent past and not of the present time. Therefore, there is an imperative need to estimate how the LoD will evolve past the present time and to make LoD-related predictions. The main objective of this thesis is to produce such LoD-related predictions.

In Chapter 3, we presented two main prediction frameworks, i.e., prediction using random processes (RP) models, and prediction using machine learning (ML) techniques. Each framework can produce the three types of predictions of interest, i.e., predicting futures values (FVs) (of the signal of interest), the first hitting time (FHT), and the survival probability (SP).

We selected the first framework (i.e., prediction using RP models) to produce LoD-related predictions, and we justified our selection.

In Chapter 4, we first precisely defined the concept of RP, which is the building block of the first framework, and we then presented conventional RP models and the geometric Brownian motion (GBM) RP model. The GBM RP model is the

cornerstone of this thesis.

We indicated that the GBM RP model is frequently used in finance to produce different types of predictions, and that this application led to two Nobel prizes in Economic Sciences. However, it is generally unknown in other important domains, such as in engineering.

In Chapter 5 and Chapter 6, we described in detail how to produce the three types of predictions of interest, i.e., predicting FVs, the FHT, and the SP using the RP models presented in Chapter 4. At the end of Chapter 6, we presented a very important flowchart that should be considered as a "must" when dealing with the positive-valued signals. According to this flowchart, when dealing with positive-valued signals, the GBM RP model should be considered as the first choice of RP model. Consequently, once the GBM conditions are verified for positive signals, further investigation of other RP models is, for all practical purposes, useless.

In order to obtain experimental data, our team carefully designed and performed two laboratory-based studies, called Study A and Study B. Chapter 7 describes the details of each study, e.g., the applied protocols, the general characteristics of participants, and the measurements setup. From Study A and Study B, we obtained, in total, 90 LoD signals from 30 subjects in 3 progressively increasing levels of sleep deprivation. Beside these, as part of a contract with a Belgian company, we had access to experimental data from another study, referred to as Study C. However, since the work was done under non-disclosure confidentiality agreement, we cannot report here on the experimental setup and the nature of data collected.

In Chapter 8, we indicated that to model long signals that most likely exhibit several instances of growing, steady-state, and decaying behaviors, it is crucial to adapt the GBM RP model (and in fact any RP model) with time. Indeed, a given GBM RP model can only model a single of these behaviors at any one time. On the one hand, we studied the question theoretically (as far as we could possibly go). On the other hand, we presented a pragmatic solution, which consists in using a sliding time window, and in computing/adapting the two parameters of the GBM RP model using only the samples within each window.

We also discussed the issue that we are facing with the short signals from Study A and Study B. Indeed, if one wishes to perform adaptation using a sliding window, each subsignal defined by such a window is relatively short, so that this subsignal may not obey the two conditions of normality and independency for it to be GBM. We also pointed out that, in actual conditions (for a long drive, or a long period of observation of stock price), one will be able to use longer windows. We performed an experiment on a long synthetic GBM signal and showed that both the whole signal was GBM (as it should) and all subsignals considered were

also GBM.

In Chapter 9, we discussed the modeling of the level of drowsiness (LoD) signals using RP models. We considered two types of RP models, i.e., the GBM RP model and the conventional RP models (such as AR, MA, ARMA, and ARIMA).

We examined whether the GBM RP model could model the LoD signals from Study A, Study B, and Study C. We showed that all 51 signals from Study A and all 39 signals from Study B can be successfully modeled by a GBM RP model.

We showed that the GBM RP model can easily be adapted, even at every time step, and track the three possible trends of the evolution of (the level of) drowsiness, i.e., increasing, constant, decreasing.

Even though we were convinced of the potential power of the GBM RP model to model drowsiness, we also modeled the LoD signals from Study A using conventional RP models. We found, without surprise, that using these models is much more cumbersome and much more demanding in terms of computational power.

From the standpoint of modeling, we concluded that the GBM RP model is an excellent candidate for modeling LoD signals, as well as related biological signals, such as the PERCLOS signal.

In Chapter 10, we performed the task of prediction for the three types of predictions, i.e., FVs, the FHT, and the SP, for LoD signals using RP models.

We performed the task of non-adaptively predicting FVs a signal using both the GBM RP model and the conventional RP models, for all 51 LoD signals from Study A. We then compare the performance of these RP models in predicting FVs of a signal (for all 51 LoD signals from Study A). We observe that the GBM RP model provides the same accuracy as the best conventional RP models, but with a computation time reduced by a factor of 1,000.

We provided an illustrative example of adaptive prediction of FVs of an LoD signal (from Study A) using the GBM RP model.

We provided two illustrative examples of adaptive prediction of the FHT for two LoD signals (one from Study A and one Study B) using the GBM RP model.

We provided two illustrative examples of adaptive prediction of the SP for two LoD signals (one from Study A and one Study B) using the GBM RP model.

We finally presented a reliable drowsiness-detection system based on the SP. We illustrated its application on two example signals from Study A and Study B. Using ROC curves, we quantified its performance on all 51 LoD signals from Study A and all 39 LoD signals from Study B.

The above results show that the GBM RP model is an excellent RP model (1) to model short LoD (and PERCLOS) signals and (2) to model locally longer LoD signals. For long signals, the key is to adapt the parameters of the GBM RP

model locally, e.g., by using a sliding time window.

This concludes the descriptions of the individual chapters.

Before being sure that an adaptive GBM RP model can be used to model all, or most, LoD signals to be encountered in practice, it will be necessary to conduct studies on more subjects and in actual operational conditions such as driving on a real road.

In addition, the work reported here can provide a strong motivation for researchers interested in modeling the physiological and biological processes to examine whether—starting from the physiological and biological mechanisms involved in the evolution of drowsiness, and using appropriate mathematical models and techniques—they can possibly show that an LoD signal should in fact naturally be a realization of an underlying GBM RP model. In this approach, one would model the real world, which is quite different from modeling the signals that emanate from it, as we did in this thesis.

Publications

Peer-reviewed abstracts in journals:

- Ebrahimbabaie, P. and Verly, J. G., 2017. Geometric Brownian motion (GBM) random process model appears to be an excellent choice for modeling realizations of PERCLOS signals. *Sleep Medicine*, Volume 40 (1), e86, DOI: http://dx.doi.org/10.1016/j.sleep.2017.11.246.

- Ebrahimbabaie, P. and Verly, J. G., 2017. Prediction of level of drowsiness using an adaptive geometric Brownian motion model, with application to drowsy driving accident prevention. *Sleep Medicine*, Volume 40 (1), e86, DOI: http://dx.doi.org/10.1016/j.sleep.2017.11.247.

- Kermi, S., Ebrahimbabaie Varnosfaderani, P. and Verly, J. G., 2017. Preliminary investigation of the applicability of geometric Brownian motion (GBM) to model the evolution with time of the level of drowsiness of narcoleptic subjects. *Sleep Medicine*, 40(1), e156. DOI: https://doi.org/10.1016/j.sleep.2017.11.457.

Peer-reviewed papers in books and proceedings:

- Ebrahimbabaie Varnosfaderani, P. and Verly, J. G., 2018. Excellent potential of geometric Brownian motion (GBM) as a random process model for level of drowsiness signals. In Proceedings of the *11th International Joint Conference on Biomedical Engineering Systems and Technologies*, Funchal, Madeira, Portugal. 19-21 January. SciTePress.

Peer-reviewed presentations:

- Ebrahimbabaie Varnosfaderani, P. and Verly, J. G., 2018. Excellent potential of geometric Brownian motion (GBM) as a random process model for level of drowsiness signals. Paper presented at the *11th International Joint*

Conference on Biomedical Engineering Systems and Technologies, Funchal, Madeira, Portugal. 19-21 January.

- Ebrahimbabaie, P. and Verly, J. G., 2017. Prediction of level of drowsiness using an adaptive geometric Brownian motion model, with application to drowsy driving accident prevention. Paper presented at the *Joint Congress of Association of Sleep Medicine and World Sleep Federation (World Sleep)*. Prague, Czech Republic, 7-11 October.

- Ebrahimbabaie, P. and Verly, J. G., 2017. Geometric Brownian motion (GBM) random process model appears to be an excellent choice for modeling realizations of PERCLOS signals. Poster presented at the *Joint Congress of Association of Sleep Medicine and World Sleep Federation (World Sleep)*. Prague, Czech Republic, 7-11 October.

- Kermi, S., Ebrahimbabaie Varnosfaderani, P. and Verly, J. G., 2017. Preliminary investigation of the applicability of geometric Brownian motion (GBM) to model the evolution with time of the level of drowsiness of narcoleptic subjects. Poster presented at the *Joint Congress of Association of Sleep Medicine and World Sleep Federation (World Sleep)*. Prague, Czech Republic, 7-11 October.

- Ebrahimbabaie, P. and Verly, J. G., 2017. Discovery that a person's level of drowsiness appears to evolve in time according to a geometric Brownian motion (GBM) random process model. Paper presented at the *10th International Conference on Managing Fatigue*. San Diego, CA, USA, 20-23 March.

- Ebrahimbabaie, P. and Verly, J. G., 2016. Prediction of future values of a level of drowsiness derived from images of an eye based on its past values, with application to drowsy driving. Paper presented at the *International Symposium on Somnolence, Vigilance, and Safety (SomnoSafe)*. Brussels, Belgium. 21-23 February.

- Ebrahimbabaie, P. and Verly, J. G., 2016. Prediction of future values of the eye PERCLOS based on its past values, with application to drowsiness monitoring. Paper presented at the *International Symposium on Somnolence, Vigilance, and Safety (SomnoSafe)*. Brussels, Belgium. 21-23 February.

Non-peer-reviewed presentations:

- Ebrahimbabaie, P. and Verly, J. G., 2017. Geometric Brownian motion (GBM) as a promising random process model of the time evolution of the level of

drowsiness. Paper presented at the *Annual Meeting of the IEEE-EMBS Benelux Chapter, jointly with 16th Belgian National Day on Biomedical Engineering*. Brussels, Belgium. 30 November.

- Ebrahimbabaie, P. and Verly, J. G., 2017. Geometric Brownian motion (GBM) as a promising random process model of the time evolution of the level of drowsiness. Poster presented at the *Annual Meeting of the IEEE-EMBS Benelux Chapter, jointly with 16th Belgian National Day on Biomedical Engineering*. Brussels, Belgium. 1 December.

- Ebrahimbabaie, P. and Verly, J. G., 2015. Random process modeling of an optooculography-based level of drowsiness, with application to drowsy driving. Poster presented at the Joint Meeting of the *IEEE-EMBS Benelux Chapter and the 14th Belgian National Day on Biomedical Engineering*. Brussels, Belgium. 26-27 October.

Patents:

Granted:

- Verly, J. G. and Ebrahimbabaie, P., 2020. *Real time prediction device*, JP. Patent: JP 66,60,405.

- Verly, J. G. and Ebrahimbabaie, P., 2019. *Real time prediction device*, U.S. Patent: US 10,457,144 B2.

Pending:

- Verly, J. G. and Ebrahimbabaie, P., 2020. *A real time prediction device*, Australian Patent Application: 2016310035. Australian Government: IP Australia.

- Verly, J. G. and Ebrahimbabaie, P., 2017. *A prediction device*, European Patent Application: EP 3 131 038 A1. European Patent Office.

- Verly, J. G. and Ebrahimbabaie, P., 2017. *A real time prediction device*, WIPO International Patent Application: WO 2017/029068 A1. World International Property Organization (WIPO).

Bibliography

[1] T. Åkerstedt and M. Gillberg. Subjective and Objective Sleepiness in the Active Individual. *International Journal of Neuroscience*, 52(1-2):29–37, January 1990. ISSN 0020-7454. doi: 10.3109/00207459008994241. URL http://www.tandfonline.com/doi/full/10.3109/00207459008994241.

[2] C. Anderson, A.-M. Chang, J. P. Sullivan, J. M. Ronda, and C. A. Czeisler. Assessment of drowsiness based on ocular parameters detected by infrared reflectance oculography. *Journal of Clinical Sleep Medicine*, 9(09):907–920, 2013. ISSN 1550-9389.

[3] T. Areerak. Mathematical model of stock prices via a fractional Brownian motion model with adaptive parameters. *International Scholarly Research Notices*, 2014, 2014.

[4] J. S. Armstrong. *Long-range forecasting*. Wiley New York ETC., 1985. ISBN 0471823600.

[5] A. P. Association. *Diagnostic and statistical manual of mental disorders (DSM-5®)*. American Psychiatric Pub, 2013. ISBN 0890425574.

[6] Association des Sociétés Françaises d'Autoroutes. Somnolence au volant, 2010. URL http://www.autoroutes.fr/FCKeditor/UserFiles/File/Publications/ASFA{_}-{_}Somnolence{_}p-p2.pdf.

[7] G. K. Basak. First passage time and level crossing probabilities for linear processes. *Advances in Applied Probability*, 36(2):643–666, 2014. doi: 10.1239/aap/1086957589.

[8] N. H. Bingham and R. Kiesel. *Risk-neutral valuation: Pricing and hedging of financial derivatives*. Springer Science & Business Media, 2013. ISBN 1447138562.

[9] A. A. Borbély. A two-process model of sleep regulation. *Hum Neurobiol*, 1 (3):195–204, 1982. ISSN 0721-9075.

[10] A. A. Borbély, S. Daan, A. Wirz-Justice, and T. Deboer. The two-process model of sleep regulation: a reappraisal. *Journal of Sleep Research*, 25(2): 131–143, 2016. ISSN 0962-1105.

[11] G. E. P. Box, G. M. Jenkins, G. C. Reinsel, and G. M. Ljung. *Time Series Analysis: Forecasting and Control*. John Wiley & Sons, 2015. ISBN 1118674928.

[12] P. Brandimarte. *Handbook in Monte Carlo simulation: applications in financial engineering, risk management, and economics*. John Wiley & Sons, 2014. ISBN 1118593642.

[13] P. J. Brockwell and R. A. Davis. *Introduction to time series and forecasting*. Springer, 2016. ISBN 3319298542.

[14] I. D. Brown. Driver fatigue. *Human Factors*, 36(2):298–314, 1994. ISSN 0018-7208.

[15] J. Brownlee. *Deep Learning for Time Series Forecasting: Predict the Future with MLPs, CNNs and LSTMs in Python*. Machine Learning Mastery, 2018.

[16] M. Capinski and P. E. Kopp. *Measure, integral and probability*. Springer Science & Business Media, 2013. ISBN 1447106458.

[17] Centres for Disease Control and Prevention (CDC). Drowsy Driving: Asleep at the Wheel. URL https://www.cdc.gov/features/dsdrowsydriving/index.html. Accessed 25 June 2020.

[18] H. Chang, E. Charbon, U. Choudhury, A. Demir, E. Felt, E. Liu, E. Malavasi, A. Sangiovanni-Vincentelli, and I. Vassiliou. *A Top-Down, Constraint-Driven Design Methodology for Analog Integrated Circuits*. Springer Science & Business Media, 2011. ISBN 1441987525.

[19] C. Chatfield. *Time-series forecasting*. CRC press, 2000. ISBN 1420036203.

[20] B. Chevalier-Roignant and L. Trigeorgis. *Competitive Strategy: Options and Games*. MIT Press, 2011. ISBN 0262015994.

[21] C.-L. Chi, W. N. Street, and W. H. Wolberg. Application of artificial neural network-based survival analysis on two breast cancer datasets. *AMIA Annual Symposium Proceedings. AMIA Symposium*, 2007:130–134, Oct 2007. ISSN 1942-597X. URL https://pubmed.ncbi.nlm.nih.gov/18693812https://www.ncbi.nlm.nih.gov/pmc/articles/PMC2813661/.

[22] G. H. Choe. *Stochastic analysis for finance with simulations*. Springer, 2016. ISBN 3319255878.

[23] S. Chokroverty and L. Ferini-Strambi. *Oxford textbook of sleep disorders*. Oxford University Press, 2017. ISBN 0199682003.

[24] E. C.-P. Chua, W.-Q. Tan, S.-C. Yeo, P. Lau, I. Lee, I. H. Mien, K. Puvanendran, and J. J. Gooley. Heart rate variability can be used to estimate sleepiness-related decrements in psychomotor vigilance during total sleep deprivation. *Sleep*, 35(3):325–334, 2012. ISSN 0161-8105.

[25] T. Deboer. Sleep homeostasis and the circadian clock: Do the circadian pacemaker and the sleep homeostat influence each other's functioning? *Neurobiology of Sleep and Circadian Rhythms*, 5:68–77, 2018. ISSN 2451-9944.

[26] D. Dinges. What is drowsy driving and what causes it?, 2014. Paper presented at the first panel of the National Transportation Safety Board (NTSB) Conference: Overcoming the Dangers of Drowsy Driving. Washington, D.C, 21 October.

[27] D. F. Dinges and R. Grace. PERCLOS: A valid psychophysiological measure of alertness as assessed by psychomotor vigilance. *US Department of Transportation, Federal Highway Administration, Publication Number FHWA-MCRT-98-006*, 1998.

[28] M. A. Djauhari, L. S. Li, and R. M. Salleh. Modeling Positive Time Series Data: A Neglected Aspect in Time Series Courses. *American Journal of Applied Sciences*, 13(7):860–869, Jul 2016. ISSN 1546-9239. doi: 10.3844/ajassp.2016.860.869. URL http://thescipub.com/abstract/10.3844/ajassp.2016.860.869.

[29] J. F. Duffy, K.-M. Zitting, and C. A. Czeisler. The case for addressing operator fatigue. *Reviews of Human Factors and Ergonomics*, 10(1):29–78, 2015. ISSN 1557-234X.

[30] P. Ebrahimbabaie and J. G. Verly. Excellent Potential of Geometric Brownian Motion (GBM) as a Random Process Model for Level of Drowsiness Signals. In *Proceedings of the 11th International Joint Conference on Biomedical Engineering Systems and Technologies*, pages 105–112. SCITEPRESS - Science and Technology Publications, 2018. ISBN 978-989-758-279-0. doi: 10.5220/0006545101050112. URL http://www.scitepress.org/DigitalLibrary/Link.aspx?doi=10.5220/0006545101050112.

[31] Encyclopedia of Mathematics (The European Mathematical Society). Itô process, 2011. URL https://encyclopediaofmath.org/wiki/It%C3%B4_process.

[32] Encyclopedia of Mathematics (The European Mathematical Society). Chi-squared distribution, 2011. URL https://encyclopediaofmath.org/wiki/Chi-squared_distribution.

[33] Z. Fang and H. Rao. Imaging homeostatic sleep pressure and circadian rhythm in the human brain. *Journal of Thoracic Disease*, 9(5):E495, 2017.

[34] D. Faraggi and R. Simon. A neural network model for survival data. *Statistics in Medicine*, 14(1):73–82, 1995. ISSN 0277-6715.

[35] T. Fawcett. An introduction to ROC analysis. *Pattern recognition letters*, 27 (8):861–874, 2006. ISSN 0167-8655.

[36] A. Field. *Discovering statistics using IBM SPSS statistics*. sage, 2013. ISBN 1446274586.

[37] H. Föllmer and M. Schweizer. A microeconomic approach to diffusion models for stock prices. *Mathematical Finance*, 3(1):1–23, 1993. ISSN 0960-1627.

[38] C. François. Development and validation of algorithms for automatic and real-time characterization of drowsiness, 2018. Doctoral dissertation, University of Liège, Liège, Belgium.

[39] C. François, J. Wertz, and J. Verly. Validation of a new automatic drowsiness quantification system for drivers, 2014. Poster presented at the 5th International Conference on Applied Human Factors and Ergonomics (AHFE), Krakow, Poland, 19-23 July.

[40] C. François, T. Hoyoux, T. Langohr, J. Wertz, and J. Verly. Test of a New Drowsiness Monitoring System Based on Ocular Parameters. 2015. Paper presented at the 6th International Conference on Applied Human Factors and Ergonomics, Las Vegas, USA, 26-30 July.

[41] C. François, T. Hoyoux, T. Langohr, J. Wertz, and J. Verly. Tests of a New Drowsiness Characterization and Monitoring System Based on Ocular Parameters. *International Journal of Environmental Research and Public Health*, 13(2):174, Jan 2016. ISSN 1660-4601. doi: 10.3390/ijerph13020174. URL http://www.mdpi.com/1660-4601/13/2/174.

[42] L. H. Gilpin, D. Bau, B. Z. Yuan, A. Bajwa, M. Specter, and L. Kagal. Explaining explanations: An overview of interpretability of machine learning. In *2018 IEEE 5th International Conference on Data Science and Advanced Analytics (DSAA)*, pages 80–89. IEEE, 2018. ISBN 1538650908.

[43] N. Goel, M. Basner, H. Rao, and D. F. Dinges. Circadian rhythms, sleep deprivation, and human performance. In *Progress in Molecular Biology and Translational Science*, volume 119, pages 155–190. Elsevier, 2013. ISBN 1877-1173.

[44] R. Gräfin von Thun und Hohenstein. Type-approval requirements for motor vehicles and their trailers, and systems, components and separate technical units intended for such vehicles, as regards their general safety and the protection of vehicle occupants and vulnerable road users. Technical report, European Parliament, 2019. URL http://www.europarl.europa.eu/doceo/document/A-8-2019-0151-AM-110-110{_}EN.pdf?redirect.

[45] C. Guilleminault and V. C. Abad. Polysomnographic Evaluation of Sleep Disorders. In *Electrodiagnosis in Clinical Neurology*, pages 701–731. Elsevier, 2005.

[46] M. L. Gumz. *Circadian Clocks: Role in Health and Disease*. Springer, 2016. ISBN 1493934503.

[47] S. Guo. *Survival Analysis*. Oxford University Press, 2010. ISBN 0199713979.

[48] M. H. Hayes. *Statistical digital signal processing and modeling*. John Wiley & Sons, 2009. ISBN 8126516100.

[49] Investopedia. Stochastic Volatility, 2020. URL https://www.investopedia.com/terms/s/stochastic-volatility.asp.

[50] M. L. Jackson, S. Raj, R. J. Croft, A. C. Hayley, L. A. Downey, G. A. Kennedy, and M. E. Howard. Slow eyelid closure as a measure of driver drowsiness and its relationship to performance. *Traffic Injury Prevention*, 17(3):251–257, apr 2016. ISSN 1538-9588. doi: 10.1080/15389588.2015.1055327. URL https://doi.org/10.1080/15389588.2015.1055327.

[51] M. Jeanblanc, M. Yor, and M. Chesney. *Mathematical methods for financial markets*. Springer Science & Business Media, 2009. ISBN 1846287375.

[52] V. Jobin, A. Mathieu, P. Rompré, M. P. Brillon, and G. Rondeau. Accuracy of the Oxford Sleep Resistance Test versus Simultaneous Electroencephalography to Detect Sleep Onset. *J Sleep Disord Ther*, 6(257):277–2167, 2017.

[53] M. W. Johns. A New Method for Measuring Daytime Sleepiness: The Epworth Sleepiness Scale. *Sleep*, 14(6):540–545, 1991. ISSN 0161-8105.

[54] M. W. Johns. Sensitivity and specificity of the multiple sleep latency test (MSLT), the maintenance of wakefulness test and the Epworth sleepiness scale: failure of the MSLT as a gold standard. *Journal of Sleep Research*, 9 (1):5–11, 2000. ISSN 0962-1105.

[55] M. W. Johns. Assessing the drowsiness of drivers. *Melbourne: VicRoads*, 2001.

[56] M. W. Johns. A new perspective on sleepiness. *Sleep and Biological Rhythms*, 8(3):170–179, 2010. ISSN 1446-9235.

[57] K. Kaida, T. Åkerstedt, G. Kecklund, J. P. Nilsson, and J. Axelsson. Use of subjective and physiological indicators of sleepiness to predict performance during a vigilance task. *Industrial Health*, 45(4):520–526, 2007. ISSN 0019-8366.

[58] E. S. Katz and C. L. Marcus. Diagnosis of obstructive sleep apnea syndrome in infants and children. *Principles and Practice of Pediatric Sleep Medicine. Elsevier Saunders*, pages 197–210, 2005.

[59] W. D. S. Killgore. Effects of sleep deprivation on cognition. In *Progress in Brain Research*, volume 185, pages 105–129. Elsevier, 2010. ISBN 0079-6123.

[60] D. G. Kleinbaum and M. Klein. *Survival analysis*, volume 3. Springer, 2010.

[61] P. E. Kloeden and E. Platen. *Numerical solution of stochastic differential equations*, volume 23. Springer Science & Business Media, 2013. ISBN 3662126168.

[62] R. F. Knipling and W. W. Wierwille. Vehicle-based drowsy driver detection: Current status and future prospects, 1994. Paper presented at the Intelligent Vehicle Highway Systems (IVHS) America Fourth Annual Meeting, Atlanta, GA, USA, 17-20 April.

[63] A. Kozak, R. Kozak, S. Watts, and C. Staudhammer. *Introductory probability and statistics*. CABI, 2007. ISBN 1780640528.

[64] V. Krishnan. *Probability and Random Processes*. John Wiley & Sons, 2015.

[65] V. Kumar. Eye is the Window to the Brain Pathology. *Current Advances in Ophthalmology*, 1(1):3, 2018.

[66] M. L. Lee, M. E. Howard, W. J. Horrey, Y. Liang, C. Anderson, M. S. Shreeve, C. S. O'Brien, and C. A. Czeisler. High risk of near-crash driving events following night-shift work. *Proceedings of the National Academy of Sciences*, 113(1):176–181, 2016. ISSN 0027-8424.

[67] S. L. Lee, M. A. Djauhari, and I. Mohamad. Modeling autocorrelated process control with industrial application. In *IEEE International Conference on Industrial Engineering and Engineering Management (IEEM)*, pages 127–131. IEEE, 2014. ISBN 1479964107.

[68] Y. Liang, W. J. Horrey, M. E. Howard, M. L. Lee, C. Anderson, M. S. Shreeve, C. S. O'Brien, and C. A. Czeisler. Prediction of drowsiness events in night shift workers during morning driving. *Accident Analysis and Prevention*, 126: 105–114, 2019. ISSN 0001-4575.

[69] D. Machin, Y. B. Cheung, and M. Parmar. *Survival analysis: a practical approach*. John Wiley & Sons, 2006. ISBN 0470870419.

[70] R. K. Malhotra. *Sleepy or sleepless: Clinical approach to the sleep patient*. Springer, 2015. ISBN 3319180541.

[71] R. R. Marathe and S. M. Ryan. On the validity of the geometric Brownian motion assumption. *The Engineering Economist*, 50(2):159–192, 2005. ISSN 0013-791X.

[72] Q. Massoz. Non-invasive, automatic, and real-time characterization of drowsiness based on eye closure dynamics, 2019. Doctoral dissertation, University of Liège, Liège, Belgium.

[73] Q. Massoz, J. G. Verly, and M. Van Droogenbroeck. Multi-timescale drowsiness characterization based on a video of a driver's face. *Sensors*, 18(9):2801, 2018.

[74] A. V. Metcalfe and P. S. P. Cowpertwait. *Introductory time series with R*. Springer, 2009. ISBN 0387886982.

[75] T. Mikosch. *Elementary stochastic calculus, with finance in view*, volume 6. World Scientific Publishing Company, 1998. ISBN 9813105291.

[76] P. Mota. Normality assumption for the log-return of the stock prices. *Discussiones Mathematicae Probability and Statistics*, 32(1-2):47–58, 2012. ISSN 1509-9423.

[77] T. Nakamura, A. Maejima, and S. Morishima. Detection of driver's drowsy facial expression. In *2013 2nd IAPR Asian Conference on Pattern Recognition*, pages 749–753. IEEE, 2013. ISBN 1479921904.

[78] National Highway Traffic Safety Administration (NHTSA). Research on Drowsy Driving. URL https://one.nhtsa.gov/Driving-Safety/Drowsy-Driving/Research-on-Drowsy-Driving. Accessed 25 June 2020.

[79] G. Padmavathi. *Handbook of Research on Machine and Deep Learning Applications for Cyber Security*. IGI Global, 2019.

[80] A. Papoulis. *Probability, random variables, and stochastic processes*. McGraw-Hill, 1965.

[81] J. N. Parker and P. M. Parker. *The Official Patient's Sourcebook on Narcolepsy*. Icon Health Publications, 2002. ISBN 0585430578.

[82] P. S. PeopIe, D. F. Dinges, and G. Maislin. Evaluation of techniques for ocular measurement as an index of fatigue and the basis for alertness management (DOT HS 808 762), 1998. Technical report by the National Highway Traffic Safety Administration (NHTSA), Washington, D.C., USA.

[83] H. F. Posada-Quintero and K. H. Chon. Innovations in Electrodermal Activity Data Collection and Signal Processing: A Systematic Review. *Sensors*, 20(2): 479, 2020.

[84] G. Rodríguez. Lecture notes on generalized linear models. *URL: http://data. princeton. edu/wws509/notes/c4. pdf*, 2007. Accessed 20 June 2020.

[85] S. M. Ross. *An elementary introduction to mathematical finance*. Cambridge University Press, 2011. ISBN 1139498037.

[86] A. Shahid, K. Wilkinson, S. Marcu, and C. M. Shapiro. *STOP, THAT and one hundred other sleep scales*. Springer Science & Business Media, 2012. ISBN 1441998934.

[87] J. G. Underhill. Clinical Neurophysiology: Basis and Technical Aspects. Cambridge, MA, Elsevier, 2020, ISBN: 0444640320.

[88] V. V. Vyazovskiy, U. Olcese, Y. M. Lazimy, U. Faraguna, S. K. Esser, J. C. Williams, C. Cirelli, and G. Tononi. Cortical firing and sleep homeostasis. *Neuron*, 63(6):865–878, 2009. ISSN 0896-6273.

[89] P. Wang, Y. Li, and C. K. Reddy. Machine learning for survival analysis: A survey. *ACM Computing Surveys (CSUR)*, 51(6):1–36, 2019. ISSN 0360-0300.